

Motor Learning and Preparatory Neural Dynamics in Parkinson's Disease


by  
Kara Nicole Presbrey

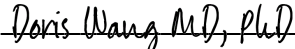
DISSERTATION  
Submitted in partial satisfaction of the requirements for degree of  
DOCTOR OF PHILOSOPHY


in  
Neuroscience

in the  
GRADUATE DIVISION  
of the  
UNIVERSITY OF CALIFORNIA, SAN FRANCISCO

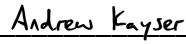
Approved:

DocuSigned by:  
  
12024A1A01564EB...  
Alexandra Nelson  
Chair

DocuSigned by:  
  
Doris Wang MD, PhD

DocuSigned by:  
  
Dr. Philip Starr

DocuSigned by:  
  
Felice A. Dunn

DocuSigned by:  
  
A8BA24710C93470...  
Andrew Kayser  
Committee Members

Copyright 2024

by

Kara Nicole Presbrey

*To Ama and to my parents, Laurie and Tom.  
With your help, Mom, we finished what you started.*

## Acknowledgments

I was fortunate to have access to engaging neuroscience opportunities in high school and college, without which I may not have discovered this passion. Mike Christensen introduced me to the study of the mind and sparked my initial curiosity. Jeremy Nathans and Stewart Hendry nurtured this curiosity with captivating conversation and a narrative teaching style. Mark Shelhamer and David Zee introduced me to the joy of the neuroscientific pursuit and offered a glimpse of clinical neuroscience. To all the other teachers and professors who held me to a high standard and challenged me with complex ideas, thank you, too. The professors who led my undergraduate education at MIT contributed to my love for neuroscience and prepared me exceptionally well for graduate school. Finally, the ongoing mentorship and generosity of Kay Tye and Edward Nieh over the past 12 years has been instrumental in my academic journey and development as a scientist—from providing my first four years of intensive research training to providing critical support and direction at key junctures along the way to both my undergraduate and graduate degrees.

My thesis would not have been possible without the support I have received from a wide range of teams and individuals at UCSF. My colleagues and collaborators in Abbasi Lab, Wang Lab, Starr Lab, Little Lab, the Department of Neurological Surgery and the OpenMind Consortium have fostered an active community of intellectual discussion and collaboration, enriching my research experience. The guidance and insights from my mentors and thesis committee members, Doris Wang, Reza Abbasi-Asl, Philip Starr, Rich Ivry, Alexandra Nelson, Felice Dunn and Andrew Kayser, have been indispensable



in my scientific growth and the completion of this study. I am immensely grateful for the opportunities, time, resources and thoughtfulness these mentors have granted me. Beyond my immediate lab and committee vicinity, Karunesh Ganguly, David Kastner, Noelle L'Etoile, Sam Pleasure and John Rubenstein each played a key role in helping me navigate and persevere through some of the most challenging moments of my PhD experience. Thank you all for helping to make this thesis a reality.

The support of my family and friends over the years has buoyed me through my academic journey and has shaped my science by helping to shape me into the determined, resilient and unrelentingly curious person that I am today. My parents, Tom and Laurie, made innumerable sacrifices to consistently provide me with opportunities, encouraged me to pursue STEM, pushed me to excel and never doubted my abilities. My siblings, Scott and Joe, paved the way by providing examples of strength and initiative in pursuing one's passions. My grandparents, Betty, Wayne, Lucille and George, instilled in us the strong values and ambitions that grew the person and scientist I am today. Last but not least, my chosen family, near and far, has provided a loving community, patience, advice, stability, listening ears and deep friendship—through thick and thin. Thank you.

Finally, I extend my deepest gratitude to our patients. They welcomed me into their homes and trusted me not only to interface with their neural implants but also to prioritize their COVID safety during the peak of the pandemic. Their kindness, humor and strong work ethic made my work with them a truly rewarding experience—the most fulfilling part of my PhD.

## Contributions

*Chapter 2* is adapted from Presbrey, K. N., Wozny, T. A., Louie, K. H., Little, S., Starr, P. A., Abbasi-Asl, R., Wang, D. D. Learning-related oscillatory dynamics in the human cortico-basal ganglia network during motor sequence initiation in Parkinson's Disease. bioRxiv 2024.09.13.612783 (2024). doi:10.1101/2024.09.13.612783.

# Motor Learning and Preparatory Neural Dynamics in Parkinson's Disease

Kara Nicole Presbrey

## Abstract

Parkinson's Disease (PD) is among the most common movement disorders. In addition to its hallmark motor symptoms of shaking, rigidity, slowness and imbalance, PD can involve a progressive decline in the ability to learn and execute precise hand and finger movements. Impairment of these fine motor skills can substantially reduce autonomy and quality of life and may relate to impaired optimization of motor preparation and initiation. However, neither pre-movement neural activity nor its optimization is well understood, particularly for fine motor sequences, which involve multiple movements strung into a single cohesive action. This thesis aims to describe a functional model of learning-related pre-movement neural activity in the motor control network for fine motor sequences in PD. *Chapter 1* provides a background of motor control and learning in the healthy state and Parkinson's Disease. *Chapter 2* presents research into the individual and collective involvement of cortical and basal ganglia regions in fine motor sequence planning and initiation in PD, highlighting how the characteristics of this involvement vary with skill development. Local pre-movement activity in the cortex and basal ganglia was specific to each motor sequence, was increasingly specific with learning and was linked to a framework of coordinated network activity. Learning deficits were associated with a functional disconnect between cortex and basal ganglia and a lack of

learning-related enhancement of pre-movement local and network activity. These results suggest that both cortical and basal ganglia areas plan multiple sequence elements before movement and that cortico-basal ganglia communication is critical to learning-driven optimization of motor preparation. *Chapter 3* concludes by discussing future research directions to achieve therapeutic restoration of fine motor learning and control in PD.

# Table of Contents

<b>Chapter 1: An Introduction to the Neurophysiology of Fine Motor Control.....</b>	<b>1</b>
Figures.....	16
<b>Chapter 2: Low-Frequency Cortico-Basal Ganglia Network Synchrony Organizes Motor Learning-Driven Patterns of Preparatory High-Frequency Activity in Parkinson's Disease.....</b>	<b>17</b>
Abstract.....	18
Introduction.....	19
Methods.....	21
Results.....	34
Discussion.....	43
Figures.....	55
Tables.....	79
<b>Chapter 3: Recommendations for Future Work and the Restoration of Fine Motor Control.....</b>	<b>112</b>
<b>References.....</b>	<b>119</b>

# List of Figures

## Chapter 1

Figure 1.1. A simple model of the motor control circuit.....	16
Figure 1.2. The classical circuit model of Parkinson’s Disease.....	17

## Chapter 2

Figure 2.1. Predicted learning-related cortico-basal ganglia activity during motor sequence initiation.....	55
Figure 2.2. Cortical and subcortical lead reconstructions.....	56
Figure 2.3. Experimental design and behavioral data collection.....	57
Figure 2.4. Behaviorally distinguishing improvers and nonimprovers.....	58
Figure 2.5. Block average performance data.....	59
Figure 2.6. Single-trial performance data.....	60
Figure 2.7. Pre-movement sequence-specific $\gamma$ activity, present in all brain regions, demonstrates practice-driven increases and decreases in discriminability in improvers and nonimprovers, respectively.....	61
Figure 2.8. Features selected prior to lasso regularization.....	62
Figure 2.9. On Days 1–3, overall sequence performance was comparable between S1 and S2.....	63
Figure 2.10. Correlations between features after grouping by canonical frequency band and signal property.....	64
Figure 2.11. Absolute decoding accuracy decreases for features grouped by	

canonical frequency band and signal property.....	65
Figure 2.12. Correlations between features after grouping into 1) $\delta$ through $\beta$ and 2) low $\gamma$ through high $\gamma$ .....	66
Figure 2.13. Single-trial $\delta$ time domain data.....	67
Figure 2.14. Day 3 single-trial $\delta$ phase.....	68
Figure 2.15. Improvement is associated with cortically-led network $\delta$ phase synchrony, to which sequence learning and task exposure add distinct effects, while lack of improvement is associated with highly synchronous BG $\delta$ .....	69
Figure 2.16. Intraregional $\delta$ - $\gamma$ coupling.....	71
Figure 2.17. High $\gamma$ amplitude distributions.....	72
Figure 2.18. Sequence learning is associated with specific corticocortical, cortico-basal ganglia and inter-basal ganglia $\delta$ - $\gamma$ couplings.....	73
Figure 2.19. $\beta$ amplitude distributions.....	74
Figure 2.20. Intraregional $\delta$ - $\beta$ coupling.....	75
Figure 2.21. Striatocortical $\delta$ - $\beta$ coupling increases with sequence learning, while task exposure brings a range of $\delta$ - $\beta$ couplings in improvers mostly absent in nonimprovers.....	76
Figure 2.22. Observed learning-related cortico-basal ganglia activity during motor sequence initiation.....	77
Figure 2.23. Coordinated $\delta$ activity supports a hierarchical functional network that reflects the specialized roles of cortico-basal ganglia regions in motor learning.....	78

# List of Tables

## Chapter 2

Table 2.1. Subject demographic and clinical information.....	79
Table 2.2. Sequences.....	80
Table 2.3. Supplementary data collection.....	81
Table 2.4. Behavioral comparison within sequences across days (Day 1 vs. Day 3): $p$ -values.....	82
Table 2.5. Behavioral comparison of pooled sequences across days (Day 3 vs. Day 4): $p$ -values.....	83
Table 2.6. Within-day across-sequence comparison of performance index: $p$ -values.....	84
Table 2.7. Baseline testing of model performance in single-trial classification: $p$ -values.....	85
Table 2.8. Across-day testing of model performance in single-trial classification: $p$ -values.....	86
Table 2.9. Across-day testing of feature importance (high frequencies): $p$ -values....	87
Table 2.10. Across-day testing of feature importance (low frequencies): $p$ -values...	88
Table 2.11. Baseline testing of local cue-related $\delta$ phase locking value: $p$ -values....	89
Table 2.12. Across-day testing of local cue-related $\delta$ phase locking value: $p$ -values.....	90
Table 2.13. Baseline testing of $\delta$ PPC: $p$ -values.....	91



Table 2.14. Across-day testing of $\delta$ PPC: $p$ -values.....	92
Table 2.15. Baseline testing of $\delta$ PSI: $p$ -values.....	93
Table 2.16. Across-day testing of session-wide null PPC: $p$ -values.....	94
Table 2.17. Baseline testing of intraregional $\delta$ - $\gamma_h^\delta$ PPC: sequence learning-related $p$ -values.....	95
Table 2.18. Across-day testing of intraregional $\delta$ - $\gamma_h^\delta$ PPC: sequence learning-related $p$ -values.....	96
Table 2.19. Baseline testing of intraregional $\delta$ - $\gamma_h^\delta$ PSI: sequence learning-related $p$ -values.....	97
Table 2.20. Baseline testing of movement-related $\gamma$ amplitude synchronization: $p$ -values.....	98
Table 2.21. Baseline testing of interregional $\delta$ - $\gamma_h^\delta$ PPC: sequence learning-related $p$ -values.....	99
Table 2.22. Across-day testing of interregional $\delta$ - $\gamma_h^\delta$ PPC: sequence learning-related $p$ -values.....	100
Table 2.23. Baseline testing of interregional $\delta$ - $\gamma_h^\delta$ PSI: sequence learning-related $p$ -values.....	101
Table 2.24. Baseline testing of movement-related $\beta$ amplitude desynchronization: $p$ -values.....	102
Table 2.25. Baseline testing of intraregional $\delta$ - $\beta^\delta$ PPC: sequence learning-related $p$ -values.....	103

Table 2.26. Across-day testing of intraregional $\delta$ - $\beta^{\delta}$ PPC:	
sequence learning-related $p$ -values.....	104
Table 2.27. Baseline testing of intraregional $\delta$ - $\beta^{\delta}$ PSI:	
sequence learning-related $p$ -values.....	105
Table 2.28. Baseline testing of interregional $\delta$ - $\beta^{\delta}$ PPC:	
sequence learning-related $p$ -values.....	106
Table 2.29. Across-day testing of interregional $\delta$ - $\beta^{\delta}$ PPC:	
sequence learning-related $p$ -values.....	107
Table 2.30. Baseline testing of interregional $\delta$ - $\beta^{\delta}$ PSI:	
sequence learning-related $p$ -values.....	108
Table 2.31. Baseline testing of interregional $\delta$ - $\beta^{\delta}$ PPC:	
task exposure-related $p$ -values.....	109
Table 2.32. Across-day testing of interregional $\delta$ - $\beta^{\delta}$ PPC:	
task exposure-related $p$ -values.....	110
Table 2.33. Baseline testing of interregional $\delta$ - $\beta^{\delta}$ PSI:	
task exposure-related $p$ -values.....	111

## List of Abbreviations

Basal Ganglia	BG
Cross-Frequency Coupling	CFC
Deep Brain Stimulation	DBS
Dorsal Subthalamic Nucleus	dSTN
Electrocorticography	ECoG
Globus Pallidus	GP
Globus Pallidus Externus	GPe
Globus Pallidus Internus	GPI
Local Field Potential	LFP
Montreal Cognitive Assessment	MoCA
Movement Disorders Society Unified Parkinson's Disease Rating Scale	MDS-UPDRS
Pairwise Phase Consistency	PPC
Parietal Cortex	Par
Parkinson's Disease	PD

Phase Locking Value	PLV
Phase Slope Index	PSI
Premotor Cortex	PM
Primary Motor Cortex	M1
Putamen	Put
Reaction Time	RT
Sequence 1 or Primary Somatosensory Cortex	S1
Sequence 2	S2
Sequence 3	S3
Sequence 4	S4
Striatum	Str
Subthalamic Nucleus	STN
Superior Parietal Lobule	SPL
Ventral Subthalamic Nucleus	vSTN

## List of Symbols

Alpha	$\alpha$
Beta	$\beta$
Delta	$\delta$
Gamma	$\lambda$
Theta	$\theta$

# Chapter 1: An Introduction to the Neurophysiology of Fine Motor Control

Parkinson's Disease (PD) is among the most prevalent neurodegenerative disorders and exhibits one of the most rapidly increasing prevalence rates of all neurological conditions. PD currently affects an estimated 8.5 million individuals globally—a figure projected to reach 17 million by 2040<sup>1,2</sup>. PD impairs motor function, leading to a gradual decline in mobility. Hallmark symptoms include tremor (rhythmic shaking of a part of the body), rigidity (high muscle tone resulting in stiffness), bradykinesia (movement slowness) and postural instability<sup>3</sup>. These symptoms predominantly affect the upper and lower limbs and can impact the initiation of movements and the adaptation of ongoing movements to situational demands<sup>4</sup>. In addition to these core motor symptoms, PD may disrupt the learning of new motor skills and the memory of previously learned motor skills, ultimately compounding the effect of PD on motor control<sup>5-7</sup>.

The impact of these symptoms on fine motor skills, which involve precise hand and finger movements, can be particularly debilitating. High quality of life relies on autonomy, which critically involves tasks employing complex hand movements that are highly refined through practice, such as feeding oneself and getting dressed<sup>8,9</sup>. Loss of autonomy can lead to social isolation and feelings of helplessness, which can, in turn, contribute to the development of depression and anxiety that can worsen other PD symptoms<sup>10,11</sup>. This underscores the importance of understanding fine motor control dysfunction to improving the lived experience of individuals with PD.

To frame dysfunction, one must define function. Thus, this chapter begins with an overview of motor control and learning in the healthy state before turning to Parkinson's Disease. Particular focus is granted to neural activity preceding movement initiation, one of the core motor functions impaired with disease progression.

### *Motor control in the healthy state*

Motor control is the complex process by which the nervous system plans and executes movements. It encompasses a multifaceted interplay of neural, muscular and skeletal systems, working in concert to generate coordinated, purposeful and adaptable movements. Motor planning begins with the conception of the movement based on goals, environmental variables and available resources and results in the eventual creation of a motor plan. The motor plan specifies the sequence, timing and force of the planned muscle activations and is triggered to initiate movement. Motor neurons then coordinate the necessary sequence of muscle contractions and relaxations to execute the planned movement. During ongoing movement and possibly changing environmental conditions, sensory information is integrated to adjust the movement parameters as needed to ensure accurate and efficient motor performance. With practice, motor learning refines motor control by improving the ability to plan and execute movements, resulting in motor skills that are faster, more accurate and less variable<sup>12</sup>.

These motor functions are orchestrated by a complex network of brain regions, most notably the prefrontal cortex, parietal cortex, motor cortex, cerebellum, thalamus and basal ganglia, the lattermost of which is a group of interconnected subcortical nuclei (**Figure 1.1**). The following general roles are typically ascribed to these regions in the control of individual movements<sup>12</sup>. The prefrontal cortex develops a high-level, goal-oriented strategy and influences the secondary motor cortex, which begins developing a motor plan. In parallel, the prefrontal cortex also influences the parietal cortex, which integrates relevant sensory information (e.g., visual and proprioceptive information) in the context of this goal. Parietal cortex communicates with secondary motor cortex to better inform the motor plan under development, ensuring that the motor plan aligns with real-time sensory context. As the motor plan develops, it is processed through the cortico-basal ganglia-thalamic loop. The basal ganglia help to select and initiate appropriate movements while inhibiting competing or unwanted movements, ultimately constraining and refining the motor plan. Once the motor plan is finalized, the primary motor cortex generates the motor commands, sending signals down the spinal cord to activate spinal neurons that directly control muscle contractions to produce movement. During movement execution, the cerebellum monitors sensory feedback and helps to correct errors in movement trajectory, while ongoing inputs from the parietal cortex and basal ganglia further ensure accuracy, timing, and adaptability.

In the consideration of more complex hand movements, this descriptive model of motor control becomes more complicated. A crucial component of fine motor control is the ability to learn and perform fine motor sequences. Humans string together elementary movements (motor primitives) to perform a single sequential movement, such as



shoe-tying or instrument-playing, that becomes fluid and efficient with practice. This may be implemented by a motor sequence control hierarchy that orchestrates not only the individual movements but also learns more abstract sequence properties to optimize fluid sequential movements<sup>13-17</sup>. This prevalent hierarchical model proposes that, during initial sequence learning, each elementary movement is explicitly selected by the activation of a stable dynamical neural network. With practice, intermediate-level binding of motor primitives develops through the encoding of abstract properties such as sequence boundaries, serial order of sequence elements and groupings of multiple movements called chunks. This allows the preselection of multiple sequence elements simultaneously. Neurons at the top of the hierarchy can then trigger sequence production by activating a single dynamical control network at the intermediate level governing the execution of the entire sequence.

In the context of this motor sequence encoding hierarchy, the initially proposed model of the motor network requires clarification. Primary and secondary motor cortices and striatum (the main input nucleus of the basal ganglia) are among the most well-studied brain regions in the motor network. Focusing first on research in animal models—While evidence remains inconclusive on the role of primary motor cortex beyond motor primitive encoding, it strongly indicates intermediate- and higher-level sequence property encoding in striatum and secondary motor cortex, respectively. Striatal neuron firing in rodents encodes motor chunk initiation, serial order and sequence start/stop boundaries—all of which are intermediate-level spatiotemporal properties<sup>18-20</sup>. Secondary motor cortex is tuned to sequence identity and motor chunks in monkeys<sup>21,22</sup>, and it drives sequence production through input to striatum in rodents<sup>23</sup>. Finally, the

refinement of motor skills relies on plasticity within and between basal ganglia and motor cortex in rodents<sup>24</sup>. However, the contributions of different brain regions to fine motor control may considerably diverge between humans and animal models. Human hand dexterity greatly surpasses that of any other animal and often involves highly rapid sequencing of individuated finger movements (not observed in nonhuman primates or rodents). Among mammals, dexterity positively correlates with the proportion of primary motor cortex dedicated to the hand, the complexity of cortico-basal ganglia and fronto-parietal local and network connectivity and the number of projections from primary motor cortex to spinal motor neurons<sup>25–33</sup>. This indicates uniquely specialized human neuroanatomy, highlighting the importance of studies of fine motor control in humans to understanding our mechanistic neurophysiology.

In healthy humans, decades of extensive research have begun to describe fine motor control, but the encoding of sequence properties when dexterous movements are strung into a sequence is less well understood. Human electrophysiology and neuroimaging work have shown that cortical contribution to the control of individual dexterous movements involves a large distributed network spanning primary sensorimotor (primary motor and primary somatosensory) cortex and secondary motor and parietal cortices<sup>34–36</sup>. In the basal ganglia and cerebellum, neuroimaging demonstrates activation changes with finger movements, possibly related to local somatotopy<sup>37–42</sup>. In hierarchical finger sequences, the role of primary motor cortex beyond motor primitive encoding remains debated<sup>43–45</sup>, but basal ganglia, secondary motor cortex and parietal cortex appear to participate in motor chunking<sup>46–48</sup>. However, the inherent temporal overlap of

activity related to higher-level sequence properties and individual finger movements remains a challenging confound in the interpretation of these studies.

As subjects become proficient with days of sequence practice, learned neural activity involved in the production of the sequence stabilizes to form a lasting memory. Neuroimaging suggests that, over days or weeks of practice, the motor and parietal cortices remain involved, but striatal involvement shifts from the associative (or cognitive) to the motor area<sup>49,50</sup>. A widely held view is that motor skill learning drives or results from interregional coordinated activity during motor skill acquisition (initial learning of the skill) and memory retrieval (reactivation of the stored motor memory) during later motor execution. During skill acquisition, functional connectivity increases from rest within the basal ganglia and between primary sensorimotor and secondary motor cortex<sup>51,52</sup>. With multiple days of practice, the retrieval and execution of a previously learned skill are associated with increased cortico-cortical and corticostriatal connectivity<sup>53,54</sup>. However, limited noninvasive spatiotemporal recording resolution impacts our ability to interpret both functional connectivity and movement-related local activation patterns in these studies.

The consequences of limited spatiotemporal recording resolution are particularly pronounced in studies of pre-movement motor planning and motor initiation. To fully differentiate preparatory neural activity from execution-related neural activity, the neural recording method should employ a temporal sampling rate that surpasses the rate of change of the behavior and a spatial sampling rate capable of resolving relevant spatial patterns of neural activity. While recent advances in imaging technology have enabled

higher spatial resolution of subcortical activity with functional magnetic resonance imaging, the temporal resolution undersamples motor reaction time (which is about 200ms long in response to visual stimulus)<sup>55</sup>. While noninvasive electrophysiological methods such as electroencephalography and magnetoencephalography have excellent temporal resolution, they have poor spatial resolution and cannot adequately capture basal ganglia activity or cortico-basal ganglia interactions. No currently available noninvasive recording methods can achieve resolution in both the spatial and temporal domains sufficient to fully clarify motor planning-related neural activity.

To work around this limitation, noninvasive studies of motor planning and initiation have relied on clever task designs to separate motor preparation from motor execution, but interpretation of these studies remains confounded. In one common paradigm, subjects are taught to expect a simple visual “go” cue that instructs them to perform a motor sequence. In some variations of this paradigm, the go cue is preceded by a planning cue that instructs the subject to begin preparing to move<sup>56</sup>. On a subset of trials, subjects are told not to respond to the go cue, or the go cue does not appear at all. The presumption is that, on trials in which cues are omitted or in which subjects are instructed not to respond, motor planning still occurs, allowing observation of neural correlates of preparation in the absence of movement. However, in these task designs, neural activity may also reflect anticipation of the cue, active suppression of the planned response or strategy adjustment<sup>57–60</sup>. These issues are compounded by the fact that most fine motor sequence studies have leveraged typing as a model behavior and have used standard typing devices that fail to accurately capture the onset of movement when the finger starts from a hovering position. Thus, without high spatiotemporal

resolution in both behavioral and neural recordings, fundamental questions about pre-movement neural activity will remain unanswered.

Overcoming these limitations and clarifying pre-movement neural activity is essential to understanding the performance and mastery of complex fine motor sequences. The hierarchical model of fine motor sequence control proposes that humans can preselect and preplan multiple sequence elements. Behavioral studies further indicate that improvements in multi-element pre-movement motor planning (i.e., preplanning) drive performance gains with motor learning<sup>61-65</sup>. Improvement in multi-element motor preplanning appears to result from faster preparatory action sequencing and an increased number of elements that can be preplanned<sup>61,62</sup>. This suggests a critical role for pre-movement neural activity in behavioral improvement. If multi-element preplanning involves the binding of preparatory activity patterns of multiple elements, it may require unique neural processes that do not project cleanly onto the classical model of control for individual movements. Which brain regions might support multi-element preplanning, and do their roles change with learning? How is functional connectivity involved? How might disruptions to these processes impact fine motor control?

Importantly, in individuals with Parkinson's Disease, for whom the impaired performance of both novel and habitual fine motor skills is often a primary issue, might pathological changes to learning-related neural activity in the lead-up to motor initiation relate to the observed deficit in complex movements?

## *Motor control in Parkinson's Disease*

The core motor features of PD relate to the progressive loss of dopaminergic neurons in the substantia nigra pars compacta of the midbrain. In humans, the substantia nigra pars compacta projects to somatomotor cortex and secondary motor cortex and has direct reciprocal connections with the striatum<sup>66</sup>. The loss of dopaminergic innervation from substantia nigra pars compacta in these regions is thought to lead to disruptions in both local activity and network dynamics, ultimately resulting in deficits in learning, motor planning and initiation, dexterity, speed, tremor, rigidity, coordination, sensory processing and even action sequencing<sup>3-8,67-77</sup>. This suggests pathological function at all levels of the proposed model of hierarchical motor sequence control. If all levels of sequence encoding might be impaired, a reasonable starting point to investigate dysfunction is the neural activity preceding motor onset, which, in the healthy state, sets the stage for effective movement.

The effect of PD on pre-movement neural activity is poorly understood, particularly as it relates to different motor symptoms over the course of motor sequence learning. Perturbation of pre-movement neural activity could relate to bradykinesia, a general motor deficit, or to impaired multi-element preplanning, a deficit specific to motor sequence preparation. Both bradykinesia and motor preparation deficit could impair motor initiation and execution. Thus, this section will discuss PD-related neural dysfunction for non-sequential movements, highlighting bradykinesia, before moving on to sequential movements and motor learning.

A classical circuit model of the basal ganglia proposes that high inhibitory output from the basal ganglia leads to PD symptoms such as bradykinesia (**Figure 1.2**). The theory postulates that, at rest in the healthy state, the basal ganglia output nuclei inhibit the thalamus, preventing it from exciting the motor cortex. To produce movement, the motor cortex excites the primary input nucleus of the basal ganglia, which leads to downstream inhibition of the basal ganglia output nuclei and, thus, disinhibition of the thalamus and excitation of the motor cortex. In PD, loss of dopaminergic input to the basal ganglia leads to excitation of the inhibitory output nuclei and excessive inhibition of the thalamus, suppressing movement.

Electrophysiological investigations in PD and nonhuman primate models of PD have found hypersynchronization of neural activity across the cortico-basal ganglia network at beta frequency ( $\beta$ , 12–30Hz)<sup>78</sup>. An emerging view is that, when movement is intended, basal ganglia  $\beta$  fails to desynchronize and therefore inadequately releases suppression of thalamus, resulting in inadequate excitation of motor cortex<sup>67,79–81</sup>. However, the evidence for this theory is mostly correlative. Dysregulation in preparatory  $\beta$  activity has been associated with ongoing bradykinesia and longer reaction times in humans<sup>82–84</sup>, yet causal studies in nonhuman primates reveal that bradykinesia and delayed motor onsets can develop before highly synchronous network  $\beta$ <sup>85</sup>. Some human studies employing deep brain stimulation (DBS) in the basal ganglia to treat motor symptoms have attempted to causally manipulate  $\beta$  by automatically increasing stimulation during periods of high basal ganglia  $\beta$  activity (a form of closed-loop DBS).  $\beta$ -triggered stimulation can produce therapeutic benefit, but efficacy is typically calculated for a range of motor symptoms or the most troublesome symptom per

subject, such as ongoing bradykinesia or tremor, rather than ease of motor preparation and initiation per sé<sup>86,87</sup>. This distinction is important, as impairments in motor initiation can occur independently of motor slowing<sup>88</sup>. To date, the effect of  $\beta$ -triggered stimulation on deficits in motor preparation has not been isolated. Furthermore, new evidence suggests that stimulation triggered by power fluctuations in other frequency bands may be more efficacious than  $\beta$ -triggered stimulation<sup>89</sup>. Taken together, evidence for a role for pathologically synchronous  $\beta$  in either bradykinesia or impaired motor preparation remains unclear.

Even less is known about PD neurophysiology in fine motor sequence tasks. It is unclear how changes in motor sequence preparation may impact motor sequence learning and performance. As in studies of healthy subjects, many studies of motor learning in individuals with PD have been limited by low spatiotemporal recording resolution. Furthermore, most motor learning research in PD has evaluated non-sequential movements or composite movements, the latter of which involve both the hand and arm, such as reaching to grasp an object. Non-sequential movements and composite movements likely rely on different encoding strategies than those employed for fine motor sequence learning<sup>90</sup>. Some work suggests that PD impacts fine motor sequence planning<sup>56,68,91</sup>. However, only one study has attempted to disambiguate motor planning- and motor execution-related neural activity without relying solely on imagined movements, and this study relied on low spatiotemporal resolution recordings of neural and behavioral activity<sup>56</sup>. The scope of this review will thus be broadened to include neuroimaging studies of fine motor sequence control during motor execution.



Both local and network PD-related dysfunction have been detected in the production and refinement of fine motor sequences. During sequence acquisition, possibly compensatory hyperactivity has been noted in the cerebellum and in the secondary motor and parietal cortices<sup>92</sup>. This hyperactivity decreases with disease progression<sup>7</sup>. Practice of a motor sequence may not adequately recruit cortical and corticostriatal activity and plasticity, resulting in atypical network functional connectivity and impairing stabilization of motor memories<sup>6,56,93–97</sup>. However, even setting aside limited spatiotemporal resolution, these studies, too, have been plagued by challenges to interpretation.

Rigorous interpretation of learning-related neurophysiology requires an understanding of the change in behavior, yet investigations of fine motor sequence learning in PD have detected a learning deficit in sequence acquisition, retention, both or neither<sup>5,7,69,98</sup>. This variability has likely been due to differences in disease stage, medication regimen (medication class and dose schedule) and task methodology (cue type, task demands feedback type, etc.)<sup>5,7,69</sup>. Furthermore, most studies have not evaluated retention across days in subjects with PD; those that have evaluated retention perform, at most, a retest after a single day of practice<sup>99</sup>. Thus, a full behavioral and neurophysiological characterization of fine motor sequence learning in PD is needed.

For the same reason, our understanding of the effect of currently available treatments on fine motor sequence learning is limited, with results suggesting therapeutic effects are mixed at best. While both dopamine replacement therapy and conventional DBS effectively treat many hallmark motor symptoms, they can have adverse effects on

cognitive processing<sup>7,100,101</sup>. In the case of dopamine replacement therapy, there may be a negative impact on high-level action sequencing, a central part of motor planning. Perhaps as a consequence—since the optimization of multi-element preplanning can drive performance gains—dopamine replacement therapy has also demonstrated mixed effects on fine motor learning<sup>5,7</sup>. In the case of conventional (open-loop) DBS of the basal ganglia, initial work suggested improvement of motor sequence acquisition<sup>7,102</sup>, but this effect may have stemmed from relief of hallmark motor symptoms rather than direct impact on sequence acquisition<sup>103</sup>. Furthermore, the effect of neither dopamine replacement therapy nor DBS on motor sequence preparation has been directly studied.

The confusion surrounding the formal characterization of fine motor sequence learning in PD notwithstanding, real-world tasks reveal impairment in fine motor sequence control not attributable to hallmark symptoms, with needs unmet by current treatments. For instance, impairments in daily activities such as shirt buttoning and preparing food have been associated with deficits in precise coordination of multiple fingers, ordering of sequence elements and movement of correct joints with appropriate motion parameters<sup>104–107</sup>. These deficits cannot be fully explained by cardinal motor symptoms or cognitive decline, and dopamine replacement therapy and conventional DBS produce inconsistent outcomes<sup>71–73,75,106,107</sup>. The underlying causes for inconsistent conventional treatment outcomes may vary<sup>5,7</sup>. Dopamine replacement therapy titrated to improve hallmark motor symptoms may “overdose” some brain regions and networks, failing to remediate some symptoms or even producing new side effects. Similarly, DBS protocols fine-tuned to hallmark symptoms may be poorly optimized for other symptoms. Furthermore, neural activity is highly dynamic, within individual neurons and across

networks. Conventional DBS and dopamine replacement therapy cannot mimic healthy neural dynamics in the cortico-basal ganglia system, which may contribute to their therapeutic limitations. Instead, event-related modulation of neural activity using closed-loop deep brain stimulation provides the most promise for restoration of fine motor control in PD, warranting characterization of learning-related neural activity in the lead-up to fine motor initiation at the spatiotemporal resolution captured by sense-capable DBS leads.

Thus, the central aim of this thesis is to describe a functional network model of pre-movement neural population activity for fine motor sequences in PD. *Chapter 2* presents research into this topic while addressing multiple historical limitations. While individuals with PD practiced fine motor sequences, invasive field potential recordings and a custom behavioral apparatus captured both neural activity and movement at spatiotemporal resolutions sufficient for distinguishing pre-movement neural activity from neural activity during ongoing movement. Further, neural recordings captured both cortical and basal ganglia activity, enabling a network-wide view of local activity and functional connectivity during motor learning. To extend knowledge of motor learning electrophysiology in PD beyond single-day retention tests, subjects were tested over multiple days of practice. Finally, to help assess and control for performance variability due to fluctuations in hallmark motor symptoms and medication state, subjects performed the motor task at consistent times within their medication schedules across days, with daily post-task quantification of hallmark motor symptoms. This approach revealed evidence of a hierarchical functional network architecture supporting multi-element preparatory activity and identified a possible oscillatory mechanism of

learning impairment. Building on these findings, *Chapter 3* outlines avenues for further research.

## Figures

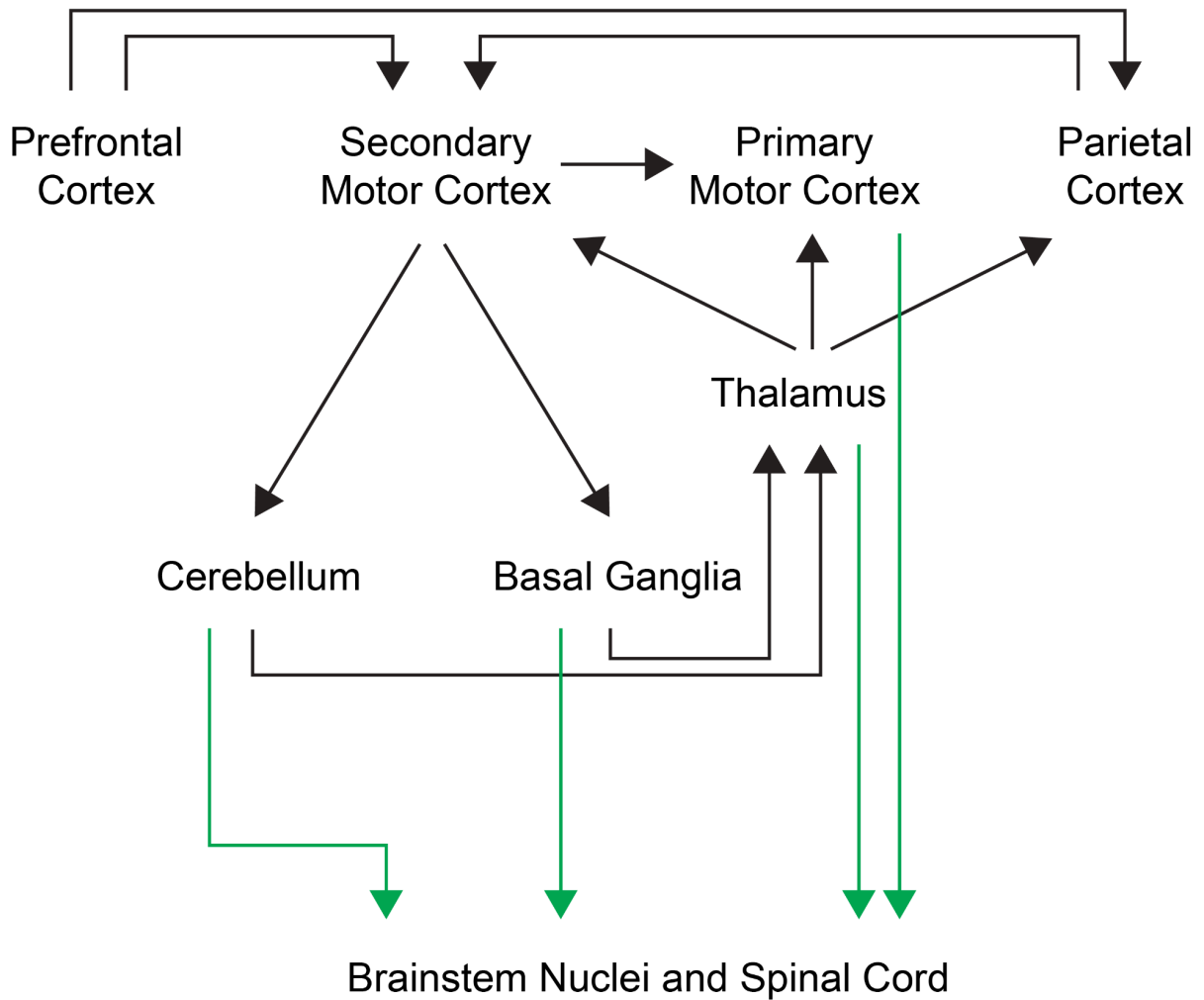
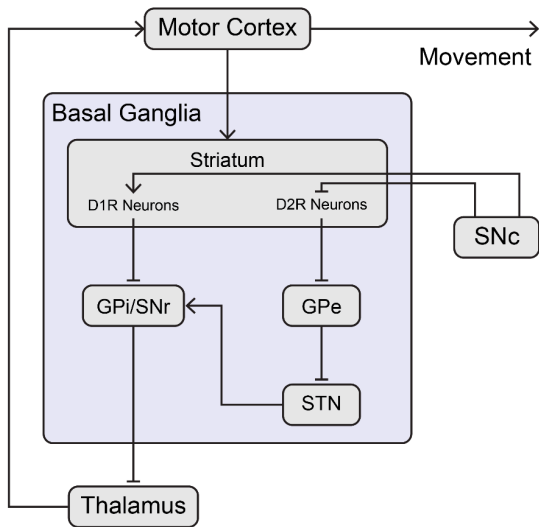


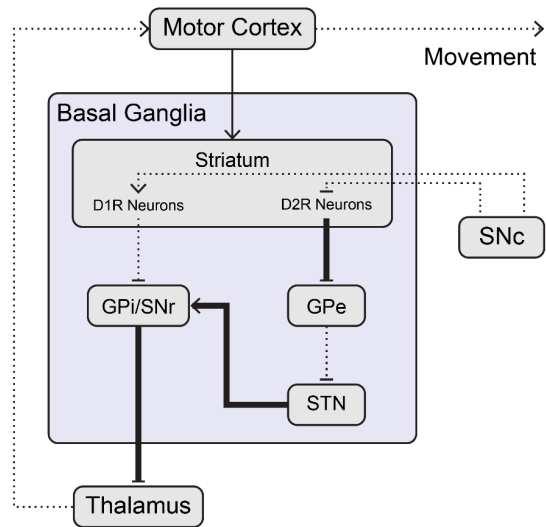
**Figure 1.1. A simple model of the motor control circuit.**

Circuit diagram indicates information flow in classically proposed models of motor control. Some anatomical connections are omitted for simplicity. Green lines correspond to motor output to the brainstem and spinal cord.

## Healthy State



## Parkinson's Disease



← Excitatory    — Inhibitory

**Figure 1.2. The classical circuit model of Parkinson's Disease.**

Circuit diagrams illustrating the impact of Parkinson's Disease on the basal ganglia in motor control. (Left) In the healthy state, dopaminergic input from the substantia nigra pars compacta excites and inhibits two different types of striatal neurons as a result of their divergent dopamine receptor expression. A specific balance is maintained to promote effective processing of motor information. (Right) In Parkinson's Disease, the loss of this dopaminergic input leads to an imbalance in striatal output to other areas of the basal ganglia, resulting in generally inhibitory basal ganglia output and also atypical processing of motor cortical input when an individual intends to move. The outcome is hallmark motor symptoms and difficulty initiating movement. D1R, D<sub>1</sub> Receptor; D2R, D<sub>2</sub> Receptor; GPe, Globus Pallidus externus; GPi, Globus Pallidus internus; STN, subthalamic nucleus; SNc, Substantia Nigra pars compacta; SNr, Substantia Nigra reticulata.

## **Chapter 2: Low-Frequency Cortico-Basal Ganglia Network Synchrony Organizes Motor Learning-Driven Patterns of Preparatory High-Frequency Activity in Parkinson's Disease**

### **Abstract**

Learning dexterous motor sequences is crucial to autonomy and quality of life but can be altered in Parkinson's Disease (PD). Learning involves optimizing pre-movement planning (preplanning) of multiple sequence elements to reduce computational overhead during active movement. However, it is unclear which brain regions mediate preplanning or how this process evolves with learning. Using cortico-basal ganglia field potential recordings during a multi-day typing task in four individuals with PD, we found evidence for network-wide multi-element preplanning that improved with learning, facilitated by functional connectivity. In both cortex and basal ganglia, pre-movement gamma ( $\gamma$ ) activity, a type of high-frequency activity linked to population spiking, distinguished between future action sequences and became increasingly predictive with learning. For motor cortex  $\gamma$ , this increase was tied to learning-related cross-frequency coupling led by cortically-driven network delta ( $\delta$ ) synchrony. Coordinated network  $\delta$  activity also supported a range of other learning-driven cross-frequency couplings within and between cortex and basal ganglia, reflecting the specialized roles of these brain regions in motor preparation. In contrast, impaired learning was characterized by practice-driven decreases in  $\gamma$ 's predictive value, a lack of cross-frequency coupling and a lack of cortically-led network  $\delta$  synchrony. Network dynamics may have been altered

by pathological basal ganglia  $\delta$  oscillations. These results suggest a model in which cortically-led  $\delta$  phase coordination optimizes cortico-basal ganglia multi-element preplanning through enhanced recruitment of high-frequency neural activity. This highlights how motor learning leverages a hierarchical functional network architecture to optimize information transfer and temporally structure neural activity.

## **Introduction**

Fine motor control is a fundamental aspect of human motor function. Skilled hand movements often require learning a sequence of finger movements, and proficiency is vital to maintaining autonomy. In Parkinson's Disease (PD), progressive decline in fine motor sequence learning and control, not solely attributable to hallmark motor symptoms, detrimentally impacts quality of life, with needs unmet by conventional deep brain stimulation (DBS) and dopamine replacement therapy<sup>5–9,71–73,75,100,101,103–107</sup>. This decline may be linked to dysfunction in motor preparation, so closed-loop DBS targeting pathological variations in preparatory neural activity could remediate symptoms<sup>60–62,108</sup>. However, the learning-dependent neural dynamics of fine motor sequence initiation are poorly understood.

Before the onset of rapid fine motor sequences like typing, humans can plan multiple sequence elements, and learning involves the optimization of this sequence-specific process<sup>61–65</sup>. Neurophysiology studies in rodents and nonhuman primates suggest that this multi-element preplanning is facilitated by the sequence-specific serial activation of



neurons in motor cortical and basal ganglia (BG) ensembles, with motor improvement partly driven by increased consistency of ensemble spiking patterns<sup>109–117</sup>. However, in humans, it is unknown which brain regions have sequence-specific pre-movement neural dynamics or how sequence-specific activity changes with learning.

The neural processes that promote consistent ensemble firing patterns with learning also remain unclear, but recent investigation highlights the potential role of pre-movement oscillatory network dynamics. Human studies suggest that network-wide beta ( $\beta$ ) desynchronization enables an increase in motor cortical excitability—reflected by a shift to the excitatory phase of motor cortical delta ( $\delta$ )—which facilitates the activation of motor cortical ensembles to initiate movement<sup>67,79,109,114,118–134</sup>. Work in animal models suggests that learning-driven corticostriatal  $\delta$  synchrony enhances  $\delta$ -ensemble spike coupling in striatum and motor cortex, resulting in the consistent ensemble firing patterns that support motor improvement<sup>90,109,114</sup>. However, these proposed network interactions have not been tested with cortico-basal ganglia electrophysiology and directed connectivity analysis in humans or animal models.

We postulated that motor cortex and basal ganglia regions all support multi-element preplanning in PD, which network activity optimizes with successful learning. To test this, we evaluated the learning-dependent motor control network dynamics of motor initiation in four individuals with PD. We recorded cortico-basal ganglia field potentials while subjects performed a multi-day, multi-sequence typing task (**Figure 2.1A**). We hypothesized that  $\beta \rightarrow \delta \rightarrow$ spike interactions influence motor cortex regardless of learning stage but that, with practice, coordinated network  $\delta$  activity increases the consistency of

sequence-specific cortical and basal ganglia spiking patterns through  $\delta \rightarrow$  spike coupling. Field potential gamma ( $\gamma$ ) activity correlates with neural population firing<sup>135</sup>. Thus,  $\gamma$  activity could reflect temporal patterns and variability in ensemble activity. This anticipates  $\beta \rightarrow \delta \rightarrow \gamma$  interactions, as well as sequence-specific motor cortex and basal ganglia  $\gamma$  activity that is increasingly predictive of future action sequences with learning (**Figure 2.1B**). We tested these predictions using single-trial classification of neural activity and directed connectivity analysis.

## Methods

### *Study criteria*

Four individuals enrolled in parent clinical trials (NCT03582891 and NCT04675398) for adaptive deep brain stimulation (DBS) for Parkinson's Disease (PD) participated in this study (**Table 2.1, Figure 2.2**). Subjects had sufficiently severe movement disorder symptoms, inadequately treated by oral medication, and requested surgical intervention. No subjects exhibited significant untreated depression, significant cognitive impairment, previous cranial surgery, drug or alcohol abuse, or evidence of a psychogenic movement disorder. For an exhaustive list of overarching clinical trial inclusion and exclusion criteria, see NCT03582891 and NCT04675398. Additional prescreening was performed for the typing task. Inclusion criterion: enthusiastic desire to participate in the task. Exclusion criteria: hand or wrist pain when typing, dyslexia, uncorrected visual impairment, sleep apnea, travel to other time zones in the past three months. Subjects

were also instructed not to consume nicotine or alcohol for the duration of the experiment. Subjects gave informed consent, and the University of California San Francisco Institutional Review Board pre-approved experimental design.

### *Task design*

On each day of a multi-day explicit motor learning experiment, subjects practiced typing two 5-element sequences in interleaved blocks using their dominant (right) hand while neural activity was recorded from the contralateral hemisphere (**Figure 2.3A**). The task design within each day was a variation of the common discrete sequence production task<sup>136</sup>. At the start of each session, subjects memorized that day's sequences during an initial Verification Period. In this Verification Period, they were briefly shown one sequence to memorize before repeatedly typing it from memory until achieving three consecutive fully correct repetitions. This was repeated with the second sequence. Subjects were then instructed to, in the subsequent training blocks, react as quickly as possible and type as quickly and accurately as possible. In each training block, they practiced only one sequence. They typed one sequence repetition from memory in response to each cue. Each practice block started with its own Verification Period for the sequence for that block. The sequence was not shown again in that block. Green go cues appeared after an exponentially jittered delay from the 5th keypress of the previous trial (range: 0.85s–3.75s,  $\mu = 1.75$ ,  $p = 0.4$  for Lilliefors test for  $h_0 = \text{exponential}$ ). A 10-second break followed each block. Subjects' hands and the keypad were completely visually occluded, and the sequences were never displayed during

typing. At the end of the task each day, subjects were assessed on the upper limb component of the Movement Disorder Society Unified Parkinson's Disease Rating Scale (MDS-UPDRS). The day before the experiment, subjects were familiarized with the task and keypad with a practice run-through (Familiarization).

They received two novel sequences on Day 1 and again on Day 4 (**Figure 2.3B**, **Table 2.2**). No sequences contained repeated adjacent elements, rising or falling triplets, or the thumb. All sequences paired for comparison within and between days started with the same first and last elements.

All subjects performed the experiment within one month after DBS surgery, before turning on DBS. No DBS was delivered during or between experimental sessions. To limit the effect of medication-related motor fluctuations, all experimental sessions were conducted at a consistent time across days within each subject's medication ON period.

### *Data collection*

In each brain hemisphere, a four-contact DBS lead spanned basal ganglia (BG) nuclei, and a four-contact electrocorticography (ECoG) paddle spanned sensorimotor cortex (**Figure 2.2**). Bipolar recording of subcortical local field potentials (LFPs) and sensorimotor electrocorticography (ECoG) signal granted coverage of the following approximate regions in the left (contralateral) brain hemisphere. Subjects GP1 and GP2: globus pallidus (GP), putamen (Put), M1 or primary sensorimotor cortex (M1/S1),

premotor cortex. Subjects STN1 and STN2: ventral subthalamic nucleus (vSTN), dorsal subthalamic nucleus (dSTN), M1, parietal cortex (spanning S1 and superior parietal lobule).

Leads from each brain hemisphere (Medtronic 3387 for globus pallidus, 3389 for subthalamic nucleus and 0913025 for cortex) were connected to a bidirectional neural interface in the ipsilateral chest (Medtronic Summit RC+S B35300R). LFP and ECoG signals were recorded at 500 Hz throughout the task. Channels were referenced to the metal casing of the implanted pulse generator. On-device hardware low and high pass filtered the data at 450 Hz and 0.85 Hz, amplified it, then performed another low pass filter at 1700 Hz.

Task events and keystroke data were captured in 4-kHz sweeps using a portable custom-made device run by a Teensy 4.1 microcontroller (**Figure 2.3C**), which acted as the master clock and motherboard for a custom keypad, visual stimulus detector and electrical impulse detector. To ensure accurate detection of finger movement onset/offset, even when finger position started above but not touching the key, a combination of custom capacitive proximity sensors (carved from copper sheet metal, 3DDeluxe), force-sensitive resistors (FSRs, Alpha MF01A-N-221-A04) and linear mechanical key switches (CHERRY MX1A-LxxA/B) were used for each digit. An FSR was fixed atop each custom keycap (3DDeluxe).

A small resin disk with a centered bulge less than a millimeter tall was fixed atop each FSR. This ensured even that off-center finger contact with the key face would result in force distribution to the FSR's center active zone sufficient to drive detectable FSR

activity. The resin disks also insulated the FSRs from the proximity sensors, which were cut from copper sheet metal and fixed atop each resin disk. To maximize proximity sensor read rate, each proximity sensor was sampled by its own Teensy 3.2 microcontroller, which each transmitted readings to the Teensy 4.1. Proximity sensors were covered with insulating tape and calibrated to detect proximity changes of fingers hovering up to ~2 cm above the keys. The capacitance sensors also detected changes in surface area of finger contact with the key. This enabled detection of changes in finger contact slight enough that the associated change in force was subthreshold for the force sensors. A photodiode (Everlight Electronics Co Ltd, PD333-3C/H0/L2) fixed to the task computer screen captured the timing of visual stimuli and progression of experimental epochs. For neural-behavioral data stream alignment, a unique temporal pattern of fifteen single DBS pulses was delivered at the start and end of each experimental session and detected along the metal casing of the pulse generator by an external electrical signal detector (MikroElektronika EEG Click MIKROE-3359). All sensors were calibrated and checked for electrical interference and cross-talk at the start of each experimental session.

### *Behavioral analysis*

To eliminate outlier trials, we excluded incorrect trials and any trials with a reaction time (RT, cue onset to movement onset) or trial duration (movement onset to offset) exceeding three standard deviations of the block average for correct trials.

To evaluate overall learning, we computed a block performance index for each subject. Each block performance index is the sum of block average error rate (1 – block accuracy), reaction time (cue presentation to movement initiation) and trial duration (movement onset to offset). For each subject, the block average trial durations and reaction times were each first min-max scaled to [0, 1], using data from all days to derive the minimum and maximum values. Lower performance index values indicate better performance.

### *Neural analysis*

All significance testing for neural analysis utilized permutation testing that simulates error within the null distribution, and secondary tests were performed only to assess the direction of primary detected effects. Multiple comparison correction was therefore not performed.

*Trial selection.* In addition to the behavioral cutoffs applied for behavioral analysis, the following trial exclusion criteria and trial subsampling methods were performed for neural analysis. Trials with less than 25 ms between final/first movements associated with adjacent trials were excluded. Subsequently, subsampling was performed within a given day to match trial counts between sequences within each group of four blocks to avoid a possible imbalance over time, e.g., 75% of remaining Sequence 1 (S1) trials coming from the first half of the session and 75% of remaining Sequence 2 (S2) trials coming from the second half of the session. Within each group of four blocks, sequence

subsampling followed epoch-specific selection rules. Only trials with  $RT \geq 100$  ms were considered. Trials from the higher count sequence were subsampled to match trials from the lower count sequence based on RT durations. Finally, random subsampling matched trial counts across days within each subject for each epoch type.

*Signal preprocessing.* Neural signal preprocessing used the following pipeline. Data from each channel was linearly detrended, demeaned and high-pass filtered at 0.25 Hz using a two-pass FIR filter. Electrical noise was excluded in the frequency domain. Two-pass Kaiser FIR filters with normalized transition widths of  $\leq 0.1$  were used for all subsequent bandpass filtering.

Data intended for single-trial classification, amplitude analysis and undirected phase analysis was filtered with the following passbands:  $\delta$  (0.5–4 Hz), theta (4–8 Hz), alpha (8–12 Hz) and  $\beta$  (12–30 Hz for amplitude analysis and cross-frequency coupling, 12–20 Hz and 20–30 Hz for single trial classification). For  $\gamma$ , filters were logarithmically spaced from 30 to 250 Hz. High  $\gamma$  (70–250 Hz) center frequencies were used for all analyses involving  $\gamma$ , while slow (30–50 Hz) and mid (50–70 Hz)  $\gamma$  center frequencies were used only for single-trial classification. These filters were all non-overlapping in the frequency domain to reduce collinearity between adjacent frequency bands when performing single-trial classification. The Hilbert transform was performed for instantaneous frequency estimation. For undirected cross-frequency coupling (CFC) analysis using pairwise phase consistency (PPC), the resulting amplitude envelope of each  $\beta$  and  $\gamma$  center frequency was filtered with the same bandpass filter previously used to extract  $\delta$ , followed by a second application of the Hilbert transform.



For analysis of directed phase coherence (including directed CFC) using phase slope index (PSI),  $\delta$  was instead extracted using linearly spaced passbands (0.5, 3.25; 0.75, 3.5; 1, 3.75; 1.25, 4). For directed  $\delta$ - $\beta$  and  $\delta$ - $\gamma$  coupling analysis, these linearly spaced  $\delta$  passbands were applied to the  $\beta$  amplitude envelope and to the amplitude envelope of each center frequency of high  $\gamma$  (70–250 Hz), followed by a second application of the Hilbert transform.

For artifact screening, filter-Hilbert was used to estimate 70–250 Hz broadband amplitude, which was then z-scored over the entire session. Any trial in which z ever surpassed 8 standard deviations was omitted from neural analysis.

*Single-trial classification.* Single-trial classification of neural activity was used to test for sequence-specific pre-movement neural dynamics. A different classifier was trained on data from each recording channel on each day, and mean decoding accuracy was used to estimate the discriminability of sequence-specific neural activity. S1- or S2-labeled trial data was extracted from the RT period in the  $t_n$  ms immediately prior to sequential movement onset, where  $t_n$  was the average RT on Day 3 for Subject  $n$ . Data then underwent feature selection and logistic classification with  $L_1$  regularization. For each subject, trials per sequence were balanced across classes, channels and days.

Time-frequency regions with maximal differences between sequences were selected as features. To assess, e.g., differences in narrowband amplitude dynamics in PM for S1 vs. S2 on Day 3 for GP1, we calculated the two-sided  $t$ -statistic for amplitude at each time-frequency point. For each of 10,000 permutations, trial labels were shuffled, and the  $t$ -statistic was recalculated. Thus, each time-frequency point had an associated null

distribution of 10,000  $t$ -statistic values. Time-frequency points at which the test value fell below the 80<sup>th</sup> percentile compared to its respective null distribution were masked. In each of the remaining islands of features for each center frequency, the time point with the highest percentile score relative to its null was selected as a feature to use in the model. For all resulting features, corresponding amplitude values were taken from S1 and S2 trial data. For phase data, the same process was implemented, save for two differences. Phase opposition sum<sup>137</sup> was used instead of the  $t$ -statistic, and since phase is a circular process, each selected phase value was converted into two features:  $\sin(\text{phase})$  and  $\cos(\text{phase})$ . Each amplitude and phase feature was median-centered and scaled according to its interquartile range to have unit variance.

Hyperparameter optimization, model training and model testing were performed with nested cross validation. The inverse  $L_1$  regularization constant ( $\lambda^{-1}$ ) was optimized per classifier in 10-fold, 10-repeat stratified cross validation performed on a stratified 90% subset of the data. The following  $\lambda^{-1}$  values were tested: 5E-2, 1E-1, 5E-1, 1, 5, 1E1, 5E1, 1E2, 5E2, 1E3, 5E3, 1E4, 5E4, 1E5, 5E5. Greater shrinkage produced performance at or below chance level. The selected value for  $\lambda^{-1}$  was then used for final model training and testing on the full dataset with 10-fold, 100-repeat stratified cross validation.

Right-sided permutation testing assessed significance of model mean decoding accuracy relative to chance. The outer 10-fold, 100-repeat stratified cross validation was repeated 1,000 times with permuted trial labels, and the resulting 1,000 null values were compared to test sample mean decoding accuracy.

Two-sided permutation testing assessed the change in mean decoding accuracy across days for a given channel. Mean decoding accuracies for each of the 100 repeats per day were permuted across days, and the between-day difference in overall mean decoding accuracy was recalculated for each permutation as the null value.

*Feature importance testing.* The absolute importance of various frequency bands and signal properties to the performance of trained models was evaluated. We permuted, in the test set, the trial labels for all phase or amplitude features associated with a given canonical frequency band, as the majority of across-frequency or across-phase/amplitude feature correlations were not high ( $\rho < 0.5$ ). For each fold in each repeat of the 10-fold 100-repeat outer cross-validation used for prior model training and testing, the test data trial labels for the respective trained model were permuted once for a given feature group, and the resulting change in test accuracy from test performance was computed. Change in decoding accuracy was then averaged across all 10 folds in each of the 100 repeats. Feature groups with negligible negative accuracy decreases were set to zero in data plots for visual clarity. No groups showed a negative accuracy decrease greater than 1% in any model.

We then repeated group permutation testing, except with all phase and amplitude features for  $\delta$  through  $\beta$  grouped together and likewise for low  $\gamma$  through high  $\gamma$ . Change in decoding accuracy was averaged across folds per repeat before between-day permutation testing.

*Coherence analysis.* Functional connectivity analysis evaluated pre-movement network interactions. Single-trial plots indicated that  $\delta$  phase aligned to cue in various regions,

so data was aligned to cue and evaluated in a window length of the mean RT of Day 3 per subject. Nonparametric cluster-based permutation across time, with a cluster size correction, was used for all phase analyses. To simplify data visualization, significant across-day effects associated with low and insignificant levels of within-day local or interregional coherence were not typically depicted with shaded time regions in the figures, but the  $p$ -values are still reported in the data tables.

For all phase analyses, we first computed each metric within sequence before averaging the resulting time series across sequences prior to statistical testing. This was intended to address two main issues. First, we expected possible sequence-specificity in spatiotemporal patterns of neural activity that could be reflected in mesoscale spectral activity—an idea for which both single-trial classification and single-trial  $\delta$  phase plots then provided confirmatory evidence. This implies that different sequences could be associated with different characteristic  $\gamma$  amplitude envelope morphologies, which may display different phase-specific coupling patterns with  $\delta$ . Second, in cases for which two sequences were not performance-matched on a given day (e.g., Sequences 3 and 4), one may observe differences in activity between sequences due to performance level (rather than learning stage). In either case, a reasonable approach would be to respect the sequence-specific relationships, so we first computed metrics within each sequence. However, we also expected the general oscillatory network dynamics associated with learning to be the same regardless of sequence, so we then averaged the resulting metric time series across sequences before statistical testing.

Inter-trial  $\delta$  phase locking value (PLV) assessed cue-aligned consistency of local  $\delta$  phase<sup>138</sup>. For a given recording channel, the resulting time series (one for each sequence) were smoothed with a 150 ms-long Gaussian window and averaged across sequences. To test for significant PLV on a given day, we randomly sampled phase data from the duration of the session for each permutation. PLV was computed for each sequence null group using the appropriate number of trials for each sequence. The magnitudes of the resulting two null PLV time series were then smoothed and averaged across trial groups to attain a single null time series for that permutation. This was repeated for each permutation. To test for a significant difference in PLV time series between days, we calculated the test time series by subtracting the PLV time series from one day from that of the other day. For each permutation, trials were shuffled across days but within sequence.

Inter-trial  $\delta$  pairwise phase consistency assessed cue-aligned interregional  $\delta$  phase coherence<sup>139</sup>. For each channel pair, the resulting time series (one for each sequence) were smoothed with a 150 ms-long Gaussian window and averaged across sequences. For baseline PPC testing, methods were identical to those used in baseline PLV testing, except the null was constructed by sampling channel data as pairs, i.e., the baseline distribution corresponded to an actual estimate of baseline session-wide coherence for that channel pair, not to the level of coherence that would be expected if the two channels were coupled only randomly. For between-day PPC permutation testing, test time series were calculated by subtracting the PPC time series between days, and for each permutation, phase data for both channels in a given channel pair were shuffled together across days but within sequence.

To assess the direction of pairwise  $\delta$  phase relationships observed with PPC, phase slope index between two channels was computed per time point for each sequence<sup>140</sup>. PSI values were not smoothed before being averaged across sequences. To assess whether significant  $\delta$  phase lead/lag occurred with respect to chance, i.e., neither channel led the other, rather than with respect to session baseline, data for each permutation was randomly sampled from the session duration separately for each channel in the pair, for each sequence.

Pairwise phase consistency and phase slope index were also used to estimate undirected and directed coherence, respectively, for cross-frequency couplings.  $\delta$  phase was paired with the  $\delta$  phase of the  $\beta$  or  $\gamma$  amplitude envelope. Computations analogous to those used for  $\delta$  synchrony analysis were performed, except for two modifications. For  $\delta$ -high  $\gamma$  coupling, PPC or PSI was calculated separately for each narrowband within 70–250 Hz for each sequence. The result was averaged across  $\gamma$  center frequencies before averaging across sequences. Second, for baseline permutation testing, the phase data was held constant while the amplitude data was sampled from the session. Shuffling amplitude while holding phase constant was intended to test for significant coherence *given* a specific phase distribution.

## Results

### *Behavioral stratification based on sequence learning*

Subjects were behaviorally stratified for sequence learning based on changes in a composite measure of block performance—a block performance index—for which lower value corresponds to better performance (**Figure 2.4A**). Day 1 to Day 3 comparisons of pooled block performance indices for each of S1 and S2 evaluated within-sequence practice-driven performance changes. Significant decrease in performance index would suggest sequence learning, but improvement on S1 and S2 could also have been driven by more general task learning, e.g., optimization of task-related cognitive processes and motor familiarization with the experimental apparatus<sup>50,61,141–145</sup>. Even so, superior performance of S1 and S2 on Day 3 compared to that upon subsequent presentation of novel sequences on Day 4 would suggest some sequence learning had in fact occurred for S1 and S2. Thus, subjects were labeled improvers (ID ending in 1) only if their performance both improved from Day 1 to Day 3 and worsened when presented with novel sequences on Day 4. A Day 1 to Day 4 comparison to assess general task learning is confounded by behavioral interference between the familiar sequences and those presented on Day 4, so we did not attempt to behaviorally stratify based on task learning.

GP1 and STN1 showed indications of sequence learning, whereas GP2 and STN2 did not (**Figure 2.4B, Figures 2.5–2.6, Tables 2.4–2.5**). In GP1 and STN1, performance index improved for both sequences from Day 1 to Day 3, then worsened when practicing novel sequences on Day 4. Neither GP2 nor STN2 showed significant

improvements in Sequence 1 (S1) and Sequence 2 (S2) performance index, and only GP2's performance index significantly differed between Days 3 and 4. These results suggest behavioral stratification as follows: improvers (GP1 and STN1) and nonimprovers (GP2 and STN2).

Sleep durations and end-of-session upper limb scores on the Movement Disorders Society Unified Parkinson's Disease Rating Scale (MDS-UPDRS) were similar between groups<sup>146</sup> (**Table 2.3**). This suggests relative differences in performance improvement may not have been due to large differences in sleep or motor symptom presentation in the typing arm.

*Pre-movement cortical and basal ganglia  $\gamma$  activity is sequence-specific and increasingly predictive of sequence content with performance improvement*

Next, we used single-trial classification of pre-movement neural activity to test which brain regions have sequence-specific preparatory neural dynamics and how this changes across days of learning. For each experiment day and each recording channel per subject, we performed feature selection on neural data preceding sequential movement onset and trained a model to predict the identity of the sequence that the subject was about to type (**Figure 2.7A–B**, **Figure 2.8**). To isolate practice-driven changes in sequence-specific neural activity from changes that occur as a byproduct of the changing behavior, we only directly compared neural activity between sequences for which overall behavioral performance was similar. In most subjects, performance levels



significantly differed between Sequences 3 and 4 (**Figure 2.9**), so Day 4 data was excluded from single-trial classification analysis. To reduce the influence of neural activity related to the first sequence element, we designated the same digit as the first element in all sequences for each subject. See *Methods: Trial Selection* and *Methods: Single-Trial Classification* for additional measures taken to reduce the influence of confounds.

We compared each model's performance to chance and tested within-channel change in decoding accuracy across Days 1 and 3, with the caveat that Day 1 to Day 3 changes in decoding accuracy may reflect changes in neural activity related to both sequence practice- and task exposure-related changes in neural activity. Notably, all models significantly outperformed chance (**Figure 2.7C**). Decoding accuracy for improvers' models broadly increased across days (GP, Put, M1/S1, PM, vSTN, dSTN, M1), whereas decoding accuracy for nonimprovers' models decreased in GP, STN and M1. These results suggest that pre-movement sequence-specific ensemble activity, reflected in mesoscale activity throughout the recorded channels, became more reliable across sessions in improvers but less reliable in some brain regions in nonimprovers.

To assess which electrophysiological signal properties were associated with sequence-specific predictive value, we performed feature analysis. We first visually assessed the importance of all canonical frequency bands and signal property types (amplitude and phase). After verifying the majority of features from different groups were not highly correlated ( $\rho > 0.5$ ), we performed initial grouped feature permutation testing (**Figure 2.7D**, **Figures 2.10–2.11**). Collectively, low  $\gamma$  (30–50 Hz), mid  $\gamma$  (50–70

Hz) and high  $\gamma$  (70–250 Hz) appeared to be the most important frequency bands for all models, though the importance of  $\gamma$  phase relative to  $\gamma$  amplitude was inconsistent. Thus, for formal statistical analysis, we repeated grouped feature permutation testing, except with features grouped into only two groups: 1)  $\delta$  through  $\beta$  and 2) low  $\gamma$  through high  $\gamma$  (**Figure 2.7E**, **Figure 2.12**). Grouped  $\gamma$  features were the most important to all models. In most brain regions, the direction of across-day change in model performance (**Figure 2.7C**) matched the direction of corresponding across-day change in accuracy drop associated with grouped  $\gamma$  features. Across-day changes in accuracy drop associated with  $\delta$  through  $\beta$  features were often insignificant, and their direction did not consistently match that of changes in model performance. These findings suggest that  $\gamma$  activity was sequence-specific throughout the recorded network and that  $\gamma$  was the primary driver of across-day changes in classification accuracy for most models.

*Improvement is associated with cortically-led  $\delta$  phase synchrony in response to cue*

We next evaluated how oscillatory network dynamics may have facilitated the observed learning-related changes in sequence-specific activity. While there may be sequence specificity in spatiotemporal patterns of neural activity, the overall architecture of functional connectivity is likely sequence-general and learning stage-dependent. We therefore calculated functional connectivity for each sequence and averaged the result across sequences per day before statistical testing, reducing the confounding influence of performance differences between learning stage-matched sequences on a given day. Thus, for functional connectivity, we could use neural data from all experimental

sessions, and between-day comparisons of neural activity fully mirrored the stratification employed for behavioral analysis. Sequence practice-related effects were those that occurred in overlapping time regions between *both* Days 1 and 3 and Days 3 and 4; though we did not behaviorally stratify task learning, we did examine neural correlates of task exposure by comparing activity between Days 1 and 4.

The supposition that  $\delta$  phase facilitates recruitment of sequence-specific ensemble activity implies  $\delta$  phase-spike coding, which ultimately predicts that  $\delta$  phase consistently aligns to motor events. Cortical  $\delta$  phase locks to movement-related visual cues in healthy subjects, so we computed  $\delta$  phase locking value (PLV) to cue in our subjects after confirming all recording channels had  $\delta$  amplitude sufficient for phase estimation<sup>121,124,138,147</sup> (**Figures 2.13–2.14, Figure 2.15A**). In GP subjects, while both GP1 and GP2 demonstrated significant PLV on all days throughout motor cortex and task exposure-related increase in M1 (or M1/S1), only GP1 demonstrated task exposure-related increase in PM. Furthermore, in GP1 but not GP2, PLV was significant on all days in GP and Put, with task exposure-related increase in GP. In STN subjects, PLV was also significant on all days in M1. In other channels (brain regions not surgically targeted in GP subjects), PLV developed differently for STN1 than STN2. In STN1, PLV increased with task exposure in vSTN and Par and with both sequence practice and task exposure in dSTN. In STN2, phase alignment to cue was mostly absent in STN and diminished with task exposure in Par. These results suggest that sequence learning in improvers might have been related to the presence of cue-related  $\delta$  phase alignment in motor cortex and striatum across days and the development of cue-related  $\delta$  phase alignment in dSTN with practice; a task exposure-driven

enhancement of motor network-wide  $\delta$  phase alignment to cue occurred in improvers only.

Such anatomically widespread  $\delta$  phase alignment to cue in improvers suggests cross-area coordinated  $\delta$  activity sufficient to facilitate coordinated recruitment of motor cortical and striatal ensembles with learning<sup>114</sup>. To assess this, we analyzed interregional  $\delta$  phase coupling. Using pairwise phase consistency (PPC), we tested for an *increase*, relative to session-wide baseline, in undirected phase coherence aligned to cue and compared PPC between days<sup>139</sup>. When undirected coherence was significant, we compared the phase slope index (PSI; directed coherence) to chance (no channel leads)<sup>140</sup>. Two brain regions with a common input could show significant and stable undirected coherence even if a phase lead developed with learning. Undirected coherence exceeded baseline too infrequently to justify systematic between-day PSI testing, so we also noted as sequence practice- or task exposure-related any directed coherence that occurred only on specific days (Day 3 for sequence practice; Days 3 and 4 or Day 4 for task exposure).

Only improvers demonstrated cortically-led network  $\delta$  synchrony, accompanied by M1 lead of dSTN with sequence learning and, with task exposure, possible GP→PM feedback and Par lead of dSTN and M1 (**Figure 2.15B**, **Figure 2.15D–E**). In GP subjects, only the improver showed widespread cue-related increase in  $\delta$  coherence above session-wide baseline. On all three days in GP1, PM led M1/S1 and Put, and Put led GP. M1/S1-striatal coherence was relatively low but significant, with phase leads observed for M1/S1→GP and Put→M1/S1. With task exposure, GP led PM. In GP2,

none of these effects occurred. Instead, M1 led PM for familiar sequences. In STN subjects, again only the improver showed cue-related cortically-led  $\delta$  coherence. In STN1, M1 led dSTN for familiar sequences, and Par led dSTN and M1 with task exposure. Significant cue-related vSTN-dSTN PPC for familiar sequences indicates STN was recruited to network  $\delta$  synchrony, partly by M1 and perhaps by an unrecorded region. In STN2, no directed phase leads occurred. While vSTN-dSTN PPC was significant for novel sequences, the lack of consistent local  $\delta$  phase (**Figure 2.15A**) indicates that inter-STN coherence was suboptimal for coordinated phase coding. Notably, in both nonimprovers, inter-BG  $\delta$  synchrony was initially high and decreased with task exposure—an effect mirrored in session-wide inter-BG  $\delta$  coherence, opposite that observed in improvers (**Figure 2.15C**). High inter-basal ganglia  $\delta$  synchrony in nonimprovers was linked to limited cue-related BG  $\delta$  activity, an absence of cortico-basal ganglia  $\delta$  synchrony and reversal of motor corticocortical  $\delta$  information transfer.

*Sequence learning is associated with  $\delta$ - $\gamma$  coupling within and between cortex and basal ganglia*

Having identified coordinated  $\delta$  activity theoretically capable of supporting  $\delta \rightarrow$  spike coupling to facilitate the sequence-specific activity reflected in classification analysis, we next directly evaluated  $\delta$ - $\gamma$  coupling. We assessed both local and cross-area  $\delta$  phase-high  $\gamma$  coupling. Using pairwise phase consistency and phase slope index, we calculated undirected and directed coherence between  $\delta$  phase and the  $\delta$  phase of the

$\gamma$  amplitude envelope ( $\gamma_h^\delta$ ). For interregional cross-frequency coupling (CFC), we report all results for which at least one subject demonstrates an effect of either sequence practice or task exposure.

Contrary to expectation, local  $\delta \rightarrow \gamma_h^\delta$  coupling was rare, suggesting that local  $\delta \rightarrow$ spike coupling may not have been a primary mechanism facilitating sequence-specific activity (**Figure 2.16**). Strikingly, practice-dependent  $\gamma_h^\delta \rightarrow \delta$  coupling was more common, though also inconsistent across subjects. Nonetheless, M1 high  $\gamma$  amplitude still significantly increased in the RT period on all days in all subjects (**Figure 2.17**), as expected for successful movement. This indicates that activity reflected in local  $\delta \rightarrow \gamma_h^\delta$  coupling was not a necessary step in general motor initiation for these subjects<sup>79,148</sup>.

Sequence learning was more associated with a range of interregional  $\delta$ - $\gamma_h^\delta$  effects (**Figure 2.18A–B**). These effects differed depending on the involved brain regions, which is consistent with the specialized roles of different regions in the cortico-basal ganglia network. In GP1 but not GP2, sequence practice was associated with premotor lead of M1/S1, as well as M1/S1 and PM lead of putamen. In STN1 but not STN2, sequence practice was associated with dSTN lead of M1 and vSTN, as well as M1 lead of Par. In STN2, Par instead led M1 on Days 1 and 3, but this effect diminished with task exposure. Otherwise, there were no task exposure-related effects in any subjects. Notably,  $\delta$  led  $\gamma_h^\delta$  only for M1  $\gamma_h^\delta$  with sequence learning in improvers, potentially reflecting underlying  $\delta \rightarrow$ spike coupling that led to the improvement-related increase in M1  $\gamma$ 's predictive value (**Figure 2.7**).

### *Network $\beta$ does not gate motor cortical $\delta$*

Using the same approach, we finally tested whether network  $\beta$  gates motor cortical excitability by assessing  $\delta$ - $\beta$  coupling. We calculated coupling between  $\delta$  phase and the  $\delta$  phase of the  $\beta$  amplitude envelope ( $\beta^\delta$ ). Cortical excitability reflected as a deflection in cortical  $\delta$ , could be led by cortical  $\beta$ , subcortical  $\beta$  or a combination of both. Thus, we assessed both intraregional and interregional  $\delta$ - $\beta^\delta$  coupling.

There was substantial overlap of regions with consistent movement-related  $\beta$  desynchronization and regions with cue-related  $\delta$  phase alignment (all motor regions in improvers; motor cortex and putamen in nonimprovers) (**Figure 2.15A**, **Figure 2.19**), suggesting widespread local  $\delta$ - $\beta$  coupling. However, significant local  $\delta$ - $\beta^\delta$  directed coupling was rare, never occurred across all days and demonstrated inconsistent direction of phase lead in M1 across subjects (**Figure 2.20**). Local  $\beta$  gating of low-frequency shifts in M1 excitability was not likely a general mechanism in motor initiation.

This was also true for interregional  $\beta$  gating of M1 excitability; however, striatocortical  $\delta \rightarrow \beta^\delta$  coupling developed with sequence learning in GP1 (**Figure 2.21A–B**). This contrasts with sequence practice-related corticostriatal  $\delta$ - $\beta^\delta$  coupling in GP2. With task exposure, primary motor cortex led PM in both GP subjects, but only in GP1 was GP led by all recorded brain regions (Put, M1/S1, PM) (**Figure 2.21C–D**). In STN subjects, no sequence practice-related effects were observed. However, with task exposure in STN1, Par led M1 and dSTN, effects absent in STN2. These results associate

sequence learning and task exposure with unique, anatomically-specific patterns of  $\delta$ - $\beta$  coupling in improvers.

## Discussion

This study investigated learning-dependent neural dynamics of motor sequence initiation in PD. We hypothesized that  $\beta \rightarrow \delta \rightarrow$ spike interactions influence motor cortex regardless of learning stage but that, with practice, coordinated network  $\delta$  activity increases the consistency of sequence-specific cortical and basal ganglia spiking patterns through  $\delta \rightarrow$ spike coupling (**Figure 2.1B**). Though all subjects demonstrated M1  $\beta$  desynchronization,  $\delta$  phase alignment to cue and  $\gamma$  synchronization, in no subjects was a continuous cascade of  $\beta \rightarrow \delta \rightarrow \gamma$  consistently present—possibly reflecting PD-related neuropathophysiology (**Figures 2.22–2.23**). Rather,  $\delta$ - $\beta$  and  $\delta$ - $\gamma$  coupling were highly learning-dependent, related to optimization of preparatory activity. However, we did observe cortically-led network  $\delta$  synchrony alongside increasingly predictive sequence-specific cortical and basal ganglia  $\gamma$  activity in improvers. Furthermore, M1  $\gamma$ 's increasing predictive value was linked to coupling with synchronized network  $\delta$ . This ties cue-aligned coordinated network  $\delta$  to enhanced recruitment of sequence-specific neural activity. In contrast, in nonimprovers, a lack of coordinated network  $\delta$  activity corresponded with a lack of CFC and decreasingly predictive  $\gamma$  in some brain regions. Highly coherent inter-basal ganglia  $\delta$  did not synchronize with cortex or align to visual cues, suggesting that pathologically synchronized BG  $\delta$  could interfere with BG  $\delta$  phase coding by reducing BG sensitivity to cortical input during motor initiation, ultimately



disrupting motor learning. These results are consistent with the possibility that motor cortex and basal ganglia regions support multi-element preplanning in PD, which network activity optimizes with successful learning.

More broadly, sequence learning and task exposure brought distinct patterns of functional connectivity, linked by a common framework of cortically-led  $\delta$  synchrony in improvers. The joint absence of sequence practice- and task exposure-related functional connectivity involving BG  $\delta$  in nonimprovers suggests their possible interdependence. These findings support a model for sequence initiation in PD wherein preparatory cortically-led network  $\delta$  reflects an organizing network process common to sequence and task learning, with the two learning types distinguished by a unique interplay of  $\delta$  synchrony and CFC.

#### *The $\beta \rightarrow \delta \rightarrow \gamma$ framework for motor initiation: an assessment in Parkinson's Disease*

A cascade of basal ganglia or cortical  $\beta \rightarrow$  cortical  $\delta \rightarrow$  cortical  $\gamma$  to produce general motor initiation, suggested by previous work, was absent in our subjects<sup>67,79,84,114,133,134,148–154</sup>. Nevertheless, our subjects still successfully initiated movement, indicating that the gating framework might only describe contributing, rather than prerequisite, factors to motor initiation in some individuals with PD.

In contrast to this cascade, we observed a notable prevalence of local and interregional  $\gamma \rightarrow \delta$  coupling with cortical  $\delta$ . This direction is opposite of that which we predicted, but

most studies assessing  $\delta$  coupling with  $\gamma$  or with spiking activity have assessed only undirected coupling<sup>34,155–157</sup>. The local motor cortical  $\delta$ - $\gamma$  coupling in our subjects could have been compensatory or pathological, related to the increase in cortical  $\delta$  sometimes seen with PD progression<sup>158–160</sup>. This would be analogous to the coincidence of elevated cortical  $\delta$  and disrupted  $\delta$ -spike coupling after stroke, which recovers alongside motor improvements<sup>114</sup>.

### *Practice-driven pre-movement sequence-specific activity*

Though pre-movement sequence-specific activity has been observed in nonhuman primate motor cortex, there has been limited electrophysiological investigation of pre-movement sequence-specific activity in the human brain<sup>116,117</sup>. Decoding analysis of pre-movement neural activity revealed sequence specificity throughout the recorded network in all subjects on all days, suggesting that activity in all recorded brain regions reflected a sequence-specific initiation signal irrespective of learning stage. Among canonical frequency bands,  $\gamma$  had the widest bandwidth, resulting in the highest number of constituent narrowband features after spectral transformation. This inherently increased the representation of  $\gamma$  features in the total feature set, potentially biasing their importance relative to features of other bands. However, the application of lasso regularization and within-time-frequency percentile-based feature selection mitigated this risk by prioritizing features based on sparsity and discriminative value. Sequence-specific  $\gamma$  activity may have arisen because distinct ensembles can consist of

unique constituent neurons, with specific firing patterns and spatial proximities to the recording contacts resulting in distinct field potential dynamics<sup>135,161</sup>.

Changes in classification accuracy of sequence-specific activity could likewise indirectly relate to changes in variability of local sequence-specific ensemble activity. This predicts increasing classification accuracy in improvers, associated with  $\delta$  synchrony and enhanced  $\delta \rightarrow \gamma$  coupling<sup>109–112,114</sup>—which we observed. However, while classification accuracy increased in most brain regions in improvers, sequence learning-related  $\delta \rightarrow \gamma$  coupling only occurred for M1  $\gamma$ . Unrecorded regions may have contributed to the increase in  $\gamma$ 's predictive value in regions outside of M1. Alternatively,  $\delta$  may have influenced sequence-specific activity indirectly through its lead of  $\beta$ , which has also been proposed to bind together action plan-specific neural ensembles across the motor network<sup>114</sup>. In nonimprovers, the lack of performance decline despite decreased classification accuracy in some brain regions suggests that increased variability in ensemble activity was insufficient to worsen improvement or offset by compensatory mechanisms.

Importantly, these suppositions are ultimately conjecture. Given our small sample size and recordings at the level of populations rather than individual neurons, this predictive analysis may best serve as a recommendation system to inspire future experimental work.

*Sequence learning and task exposure produced distinct patterns of cortico-basal ganglia coupling*

Sequence learning and task exposure were associated with distinct changes in cross-frequency activity in improvers. Most notably, basal ganglia→cortex CFC occurred only in improvers, only with sequence learning and only involving dSTN and putamen  $\delta$ . This is broadly consistent with models of the cortico-basal ganglia system implicating these regions in motor learning and action selection and with the possibility that pre-movement  $\delta$ → $\beta$  and  $\delta$ → $\gamma$  are involved in enhanced neural pattern organization<sup>5,7,17,162–166</sup>. This centers basal ganglia feedback during motor initiation as a possible factor in motor improvement<sup>134</sup>.

Changes in  $\delta$  synchrony also differed for sequence learning and task exposure. Our finding of sequence learning-related corticostriatal synchrony is consistent with findings from human neuroimaging<sup>54,167,168</sup>. We further established a cortex→striatum direction of lead and found sequence learning-related M1→dSTN connectivity. In contrast, task exposure involved the development of parietal  $\delta$  lead of M1. This aligns with S1→M1 activation previously detected in a human ECoG finger movement study that suggested a predictive efference copy<sup>169</sup>. Another notable effect of task exposure was the development of GP→PM  $\delta$  synchrony, which completed a possible loop of cortico-basal ganglia  $\delta$  phase coordination, through PM→Put→GP→PM. Motor cortical  $\beta$  lead of both GP  $\delta$  and PM  $\delta$  with task exposure may have facilitated the  $\delta$  loop. This task exposure-related coordinated activity could reflect an electrophysiological substrate for

the general motor familiarization or optimization of attentional processes, which could aid future sequence learning<sup>155,170–172</sup>.

Perhaps the most apparent inconsistencies between ours and previous work relate to a rodent study of the reach-to-grasp (RTG) task<sup>90</sup>. Lemke et al. found that low-frequency (3–6 Hz) corticostriatal LFP activity was essential to motor learning but not present during skill acquisition and not important to the dexterous component of movement. This contrasts with our finding that corticostriatal low frequency (0.5–4 Hz) synchrony was present during skill acquisition for dexterous movement. This discrepancy could result from differences in learning stage or type. The rodents learned a novel grasping task without extensive prior motor familiarization, whereas our subjects had typing experience and a full task run-through before the experiment. Our task also required learning the serial order of individuated digit movements, which is thought to rely on striatum in primates—a key component absent in rodent RTG<sup>173</sup>. Taken together, our studies suggest that corticostriatal low-frequency synchrony may be related to both the initiation of externally cued dexterous movements and the execution of coarse movements.

*Few effects of sequence practice and task exposure in nonimprovers: possible impact of pathologically synchronized basal ganglia  $\delta$*

In nonimprovers, all effects of sequence practice seen in improvers were absent, and there were strikingly few neural correlates of task exposure. All observed sequence

practice- or task exposure-related effects occurred in GP2 and involved M1 leading PM and GP. This is consistent with GP2's trending but insignificant performance improvement and suggests that some sequence learning occurred through M1 compensatory processes, insufficient to drive detectable changes in behavior, or that some observed M1 activity was maladaptive—possibly both<sup>93,174,175</sup>. In STN2, the relatively short reaction time window may have quantitatively limited the likelihood of detecting across-day connectivity increases. However, the detection of across-day decrease in STN2's inter-BG  $\delta$  synchrony and corticocortical  $\delta$ - $\gamma$  coupling shows that changes in functional connectivity were detectable. That both sequence practice- and task exposure-related effects involving subcortical  $\delta$  in improvers were absent in nonimprovers highlights a possible role of cortico-basal ganglia  $\delta$  communication in both processes and, likewise, suggests a possible interdependence of these processes that warrants future study.

The shared absence of sequence practice- and task exposure-related effects involving BG  $\delta$  may have been related to high session-wide inter-basal ganglia  $\delta$  synchrony. Human and animal studies have detected  $\delta$ -range spiking activity in GP and STN in low dopamine states, which could represent either a low tremor frequency or a unique biomarker of motor symptoms<sup>176–178</sup>. Either case proposes that ineffective therapeutic restoration of BG dopaminergic transmission permits pathological  $\delta$  activity. Consistent with this, subjects exhibiting elevated BG  $\delta$  synchrony were those for whom general motor function remained the most compromised while on dopamine medication (**Table 2.1**). However, their daily post-task UPDRS upper limb scores were comparable to those of other subjects and demonstrated no apparent across-day drop alongside the

across-day decrease in BG  $\delta$  synchrony (**Table 2.3**). It is possible that task exposure drove the across-day BG  $\delta$  synchrony decrease, promoting the possibility of future learning, and that the MDS-UPDRS upper limb component was too insensitive to detect associated changes in hallmark upper limb motor symptoms<sup>179</sup>. Alternatively, a temporary functional lesion from subcortical lead insertion may have temporarily increased  $\delta$ , similar to the effect of cortical stroke<sup>114</sup>. Given the small sample size and inherent inter-individual variability, it is possible that, by chance, BG  $\delta$  had recovered in improvers before the start of the experiment, while nonimprovers had longer BG  $\delta$  recovery timelines, in part leading to the learning differences between these groups. In any case, the concurrent lack of improvement and lack of sequence practice- or task exposure-related effects involving BG  $\delta$  suggests that event-related coordination of basal ganglia  $\delta$  may have been crucial to motor learning in these subjects.

*Coordinated network  $\delta$  as a facilitatory network state for learning-dependent cross-frequency coupling during sequence initiation*

From the theoretical standpoint,  $\delta$  is an ideal substrate for information multiplexing, local gain modulation and information transfer between distant phase-aligned brain regions<sup>118,120,170–172</sup>. Experimental evidence supports this, showing a role for  $\delta$  in information sequencing through phase-specific ensemble patterning; sensory integration and attentional control through gain modulation achieved by changes in neural excitability; and functional network organization, information transfer and

distributed representation through cross-area coordinated activity that coactivates distributed ensembles<sup>34,90,109,118,120,121,123,180,181</sup>.

Consistent with these roles, in our study, cross-area coordination of  $\delta$  phase may have formed the infrastructure for a cue-responsive network state, within which learning-related  $\delta$ - $\beta$  and  $\delta$ - $\gamma$  coupling developed. Almost every instance of significant  $\delta$  phase alignment to cue was synchronized with network  $\delta$ , and many of these cases involved directed phase lead. While  $\delta$  synchrony and phase alignment to cue occurred on Day 1 and increased across days, directed  $\delta$ - $\beta$  and  $\delta$ - $\gamma$  couplings were initially mostly absent. Only brain regions that demonstrated  $\delta$  phase alignment to cue contributed  $\delta$  to interregional  $\delta \rightarrow \beta$  or  $\delta \rightarrow \gamma$  coupling. Coupling in which  $\beta$  or  $\gamma$  led  $\delta$  was often associated with the receiving  $\delta$  demonstrating enhanced cue alignment or enhanced lead of other brain regions, suggesting a possible learning-dependent role for  $\beta$  and  $\gamma$  in the organization of network  $\delta$ . These results highlight a potential role for cross-area  $\delta$  synchrony in driving consistent event-related  $\delta$  phase dynamics in local activity, which can, in turn, support phase coding in the patterning of high frequency activity.

This link between motor performance-related  $\delta$  activity and CFC is consistent with lesion experiments in animal models and observational studies of the human cortical grasp network<sup>34,90,109</sup>. Other work has found reaction time-correlated cue-responsive  $\delta$  phase reset in human hippocampus; reaction time-correlated  $\delta$  phase in rat motor thalamus coupled to local spiking; motor learning-related M1-cerebellar  $\delta$  synchrony in rats with enhanced cross-area spiking activity and even evidence for prefrontal



guidance of motor plans via  $\delta$ - $\beta$  coupling in humans<sup>182–185</sup>. Coordinated  $\delta$  may ultimately reflect a motor system-wide neural process facilitating local and distributed activity patterns over the course of learning.

An important question is what neurophysiological activity is actually reflected in spectral estimates of  $\delta$  recorded with mesoscale electrophysiology, and the answer may be a combination of multiple possibilities. While  $\delta$  has been associated with excitability and with single-unit spiking at  $\delta$  frequency, it has also, similar to  $\gamma$ , been linked to the dynamics of population spiking activity<sup>157,186</sup>, and it could reflect synaptic input<sup>187–190</sup>. It is thus important to clarify that  $\delta$  activity may not directly drive other neural activity, per sé, but rather reflect the dynamics of some component of the underlying process that is directly responsible for driving the observed network effects.

### *Clinical implications*

To the best of our knowledge, this study is the first invasive electrophysiological investigation of human cortico-basal ganglia dynamics in motor sequence learning and possibly the first formal evaluation of isolated fine motor sequence learning in PD across multiple days of practice. This work helps clarify the intricate and dynamic functional architecture of the human motor control network in the initiation of fine motor sequences in Parkinson's Disease. Our findings posit pre-movement  $\delta$  phase-specific striatal or subthalamic neurostimulation as a therapeutic neuromodulatory strategy for skilled fine motor control.

### *Central limitations*

While our study demonstrates meaningful advances, it is limited by a small sample size. Recordings in GP and STN subjects were largely anatomically nonoverlapping, enabling observation of the unique roles of various brain regions but leaving unverifiable the consistency of effects across improvers or across nonimprovers. That half of subjects did not improve enabled stratification of subjects by improvement status, but the resulting  $n = 1$  per learner type per brain region necessitated reliance on within-subjects comparisons. Consequently, conclusions based on comparison of improvers and nonimprovers are inherently weak and may not generalize, as is often the nature of work in invasive human electrophysiology.

One surprising behavioral observation was that nonimprovers moved at least as quickly as improvers, indicating that lack of improvement in nonimprovers was not likely due to greater difficulty in manipulating the keyboard. Nonimprovers may have found the task too easy at baseline to show measurable speed increases across days, despite actually learning the sequences. However, while improvers' single-trial trial durations frequently demonstrated performance decrement when switching between sequences within day, suggesting a sequence-switching effect indicative of sequence learning, this effect was less apparent in nonimprovers. It is possible that improvers more effectively learned the sequences used during task familiarization prior to the experiment. This could have resulted in slower initial typing speeds on Day 1 in improvers due to greater interference from the familiarization sequences. Alternatively, the observed inter-individual variation in Day 1 typing speeds may reflect typical inter-individual variability prior to learning.

Finally, the complex nature of the system and the methods of recording and analyses employed introduce considerable room for bias. This is particularly true for the interpretation of data from bipolar montages spanning multiple brain regions and for the interpretation of cross-frequency and directed coherence. Large task exposure-related effects may have obscured smaller overlapping effects of sequence practice, and learning-related functional connectivity likely also occurs in frequency bands beyond those addressed herein.

Future studies should aim to replicate these findings in a larger cohort and to explore the impact of Parkinson's Disease stage and treatment modalities.

### *Conclusion*

In individuals experiencing Parkinson's Disease, we outline a hierarchical, learning-dependent functional architecture of oscillatory cortico-basal ganglia activity for the initiation of fine motor sequences. The findings illuminate how disparities in information content and flow may relate to disparities in motor learning outcomes. Extending this work in larger cohorts of individuals with PD could help elucidate the relationship between clinical characteristics and practice-related neural dynamics and further clarify the potential for phase-specific basal ganglia stimulation to modulate pathological neural dynamics in the production of fine motor skills.

# Figures

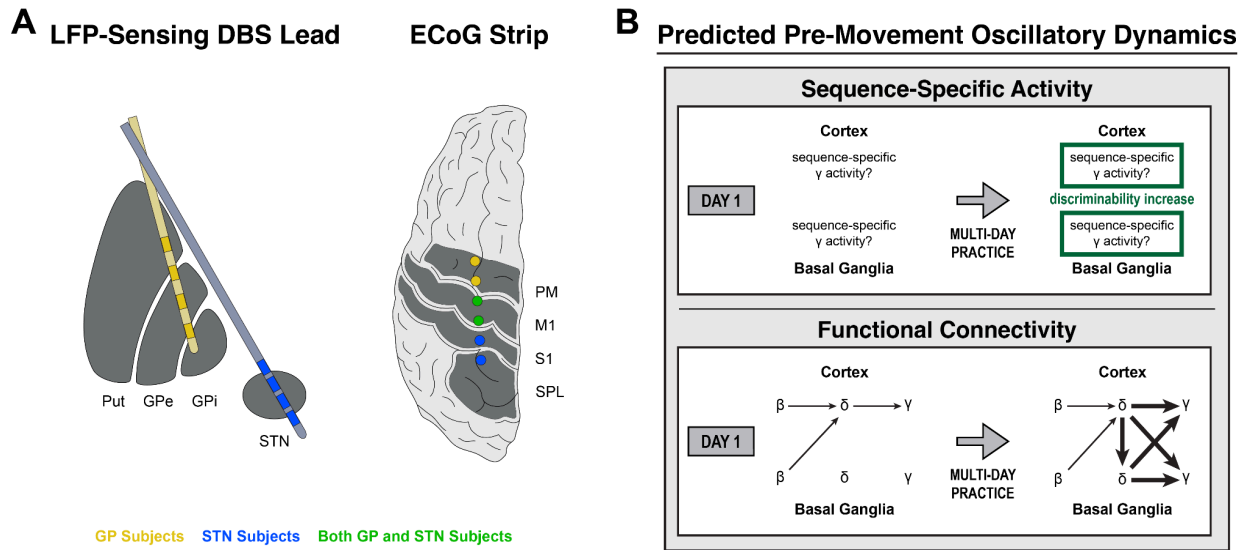


**Figure 2.1. Predicted learning-related cortico-basal ganglia activity during motor sequence initiation.**

(A) Illustration of lead targeting for subject groups (LFP, local field potential; DBS, deep brain stimulation; ECoG, electrocorticography; Put, putamen; GPe, globus pallidus externus; GPi, globus pallidus internus; STN, subthalamic nucleus; PM, premotor cortex; M1, primary motor cortex; S1, primary somatosensory cortex; SPL, superior parietal lobule). (B) Diagram of predicted learning-related changes in sequence-specific activity and functional connectivity prior to the onset of motor sequences over multiple days of practice. (Top) For rapid, sequential finger movements, learning involves the optimization of preplanning for multiple sequence elements, potentially implemented by increased reliability of sequence-specific ensemble firing patterns in cortex and basal ganglia. As  $\gamma$  activity correlates with population spiking, this could be reflected by sequence-specific  $\gamma$  activity that becomes increasingly predictive of future action sequences with practice. (Bottom) Oscillatory network dynamics are thought to drive general motor initiation and may display learning-dependent changes that lead to increased reliability of ensemble activity patterns. One possibility is that network  $\beta$  desynchronization enables increased motor cortical excitability, reflected as a shift to the excitatory phase of cortical  $\delta$ . In turn, excitability facilitates activation of motor cortical ensembles to produce movement, reflected by increasing  $\gamma$  amplitude. With motor learning, increased cortico-basal ganglia  $\delta$  synchrony facilitates enhanced ensemble recruitment, reflected by  $\delta$ - $\gamma$  coupling.

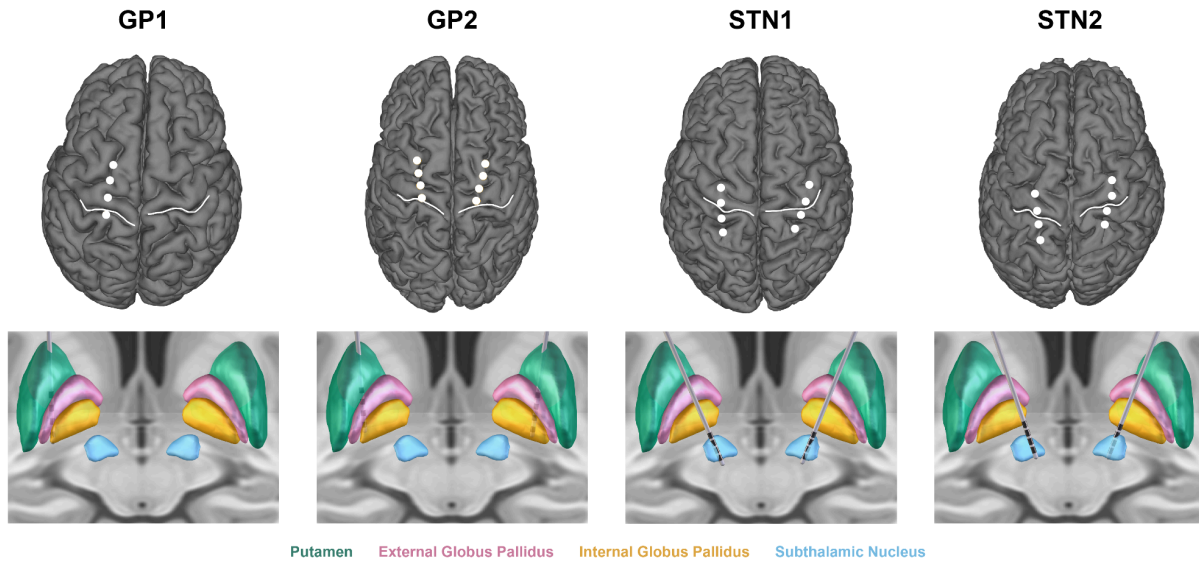


**Figure 2.2. Cortical and subcortical lead reconstructions.**

(Top) Sensorimotor quadripolar electrocorticography strips, central sulcus (white), and (Bottom) quadripolar deep brain stimulation leads localized within the basal ganglia.

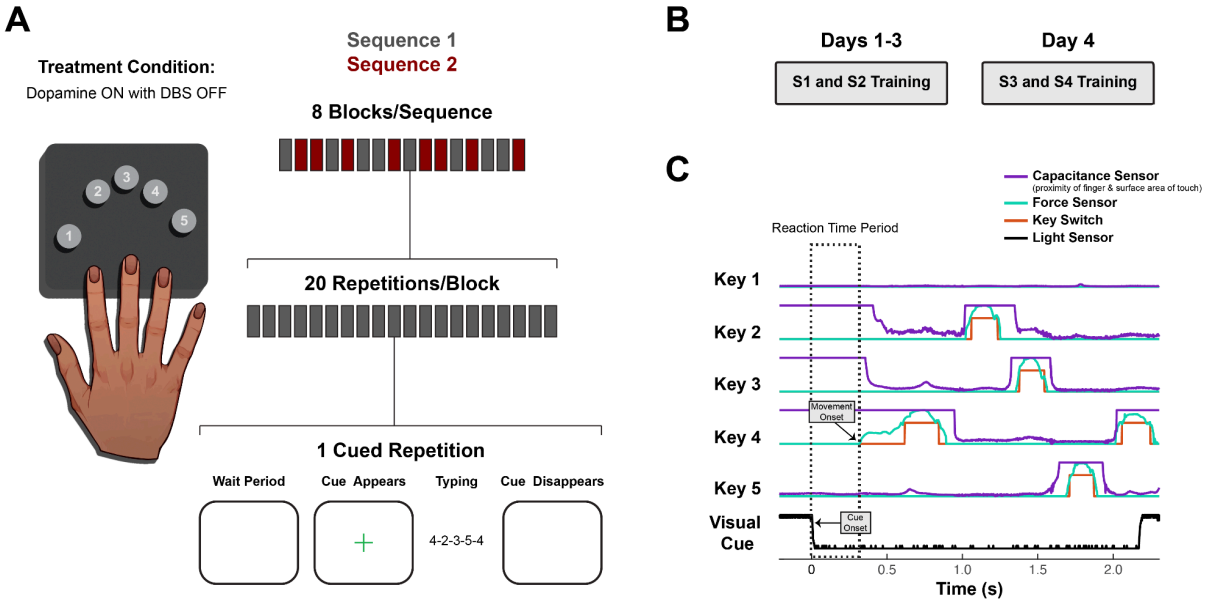


**Figure 2.3. Experimental design and behavioral data collection.**

(A) On each day, subjects practiced typing two sequences. Interleaved practice blocks each contained 20 repetitions of visually cued sequence production for a single sequence. Subjects performed the task while on dopamine medication, and no DBS was delivered during the task or between days. (B) Days 1–3 employed novel Sequences 1 and 2 (S1 and S2), and Day 4 employed novel Sequences 3 and 4 (S3 and S4). (C) The reaction time period (dashed box) used for neural analysis is demonstrated in an example trial showing raw data from a custom behavioral setup used to capture finger movement (using capacitive proximity/touch sensors, force-sensitive resistors and mechanical key switches) and the visual cue (using a photodiode placed on the task computer screen). Capacitance sensors were calibrated to detect proximity changes of fingers hovering 0 to 2 cm above the keys (capacitance variation around low values). They could also detect changes in surface area of finger contact with the key associated with changes in force subthreshold for the force sensors (capacitance variation between low/mid-range and ceiling values). Thus, capacitance sensor readings were used for motor onset detection, except when motor onset began with a finger already in full contact with the key, in which case force sensor readings were used (as in the first keypress of this example trial).

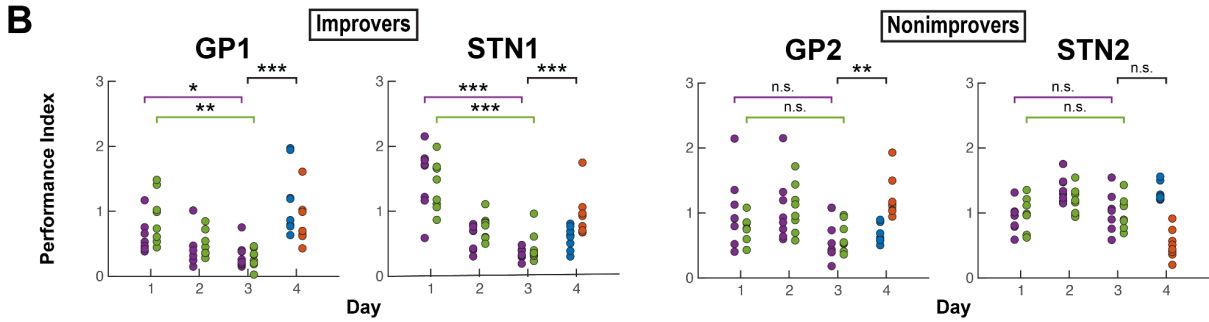
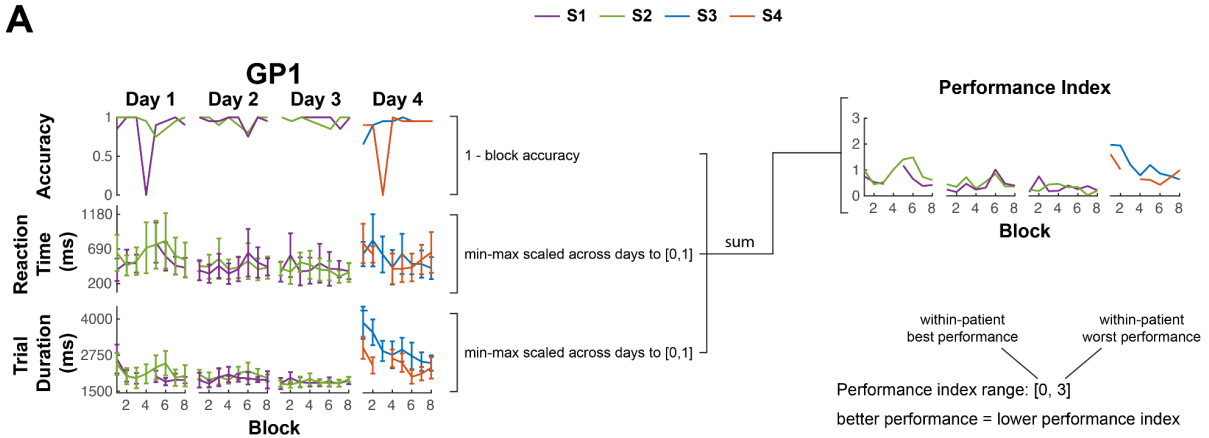


**Figure 2.4. Behaviorally distinguishing improvers and nonimprovers.**

(A) Example calculation of block performance index (PI) from block average data. Each block performance index is the sum of block average error rate [1 – accuracy], reaction time [cue onset to movement onset] and trial duration [movement onset to offset]. For each subject, the block average trial durations and reaction times were each first min-max scaled to [0, 1], using data from all days to derive the minimum and maximum values. Error bars indicate  $\pm s$ . (B) Block performance index for each subject. Comparison across Days 1 and 3 for each of S1 and S2 assessed within-sequence practice-driven performance changes. To help evaluate whether performance changes from Day 1 to Day 3 were at least in part related to sequence learning and not solely attributable to changing familiarity with the task and keypad, performance was also compared between pooled Day 3 sequences and pooled Day 4 sequences. Subjects were labeled improvers (ID ending in 1) only if their performance both improved from Day 1 to Day 3 and worsened when presented with novel sequences on Day 4 (For all comparisons:  $\alpha=0.05$ , two-sided, two-sample *t*-test with unequal variance. See Tables 2.4–2.5 for *p*-values.). \* $p<0.05$ , \*\* $p<0.01$ , \*\*\* $p<0.001$ .

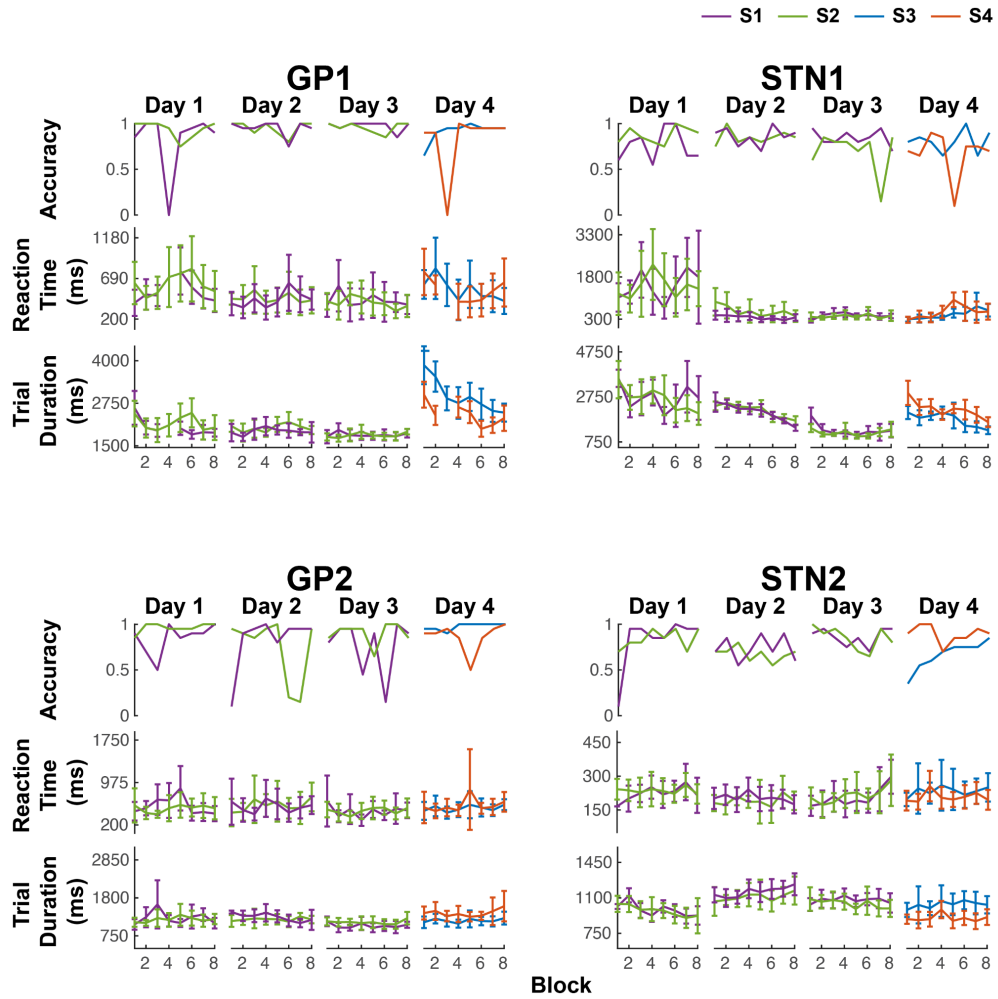


**Figure 2.5. Block average performance data.**

Per subject: (Top) block average accuracy, (Middle) block average reaction time [cue onset to movement onset], (Bottom) block average trial duration [movement onset to offset]. Error bars indicate  $\pm$ s.



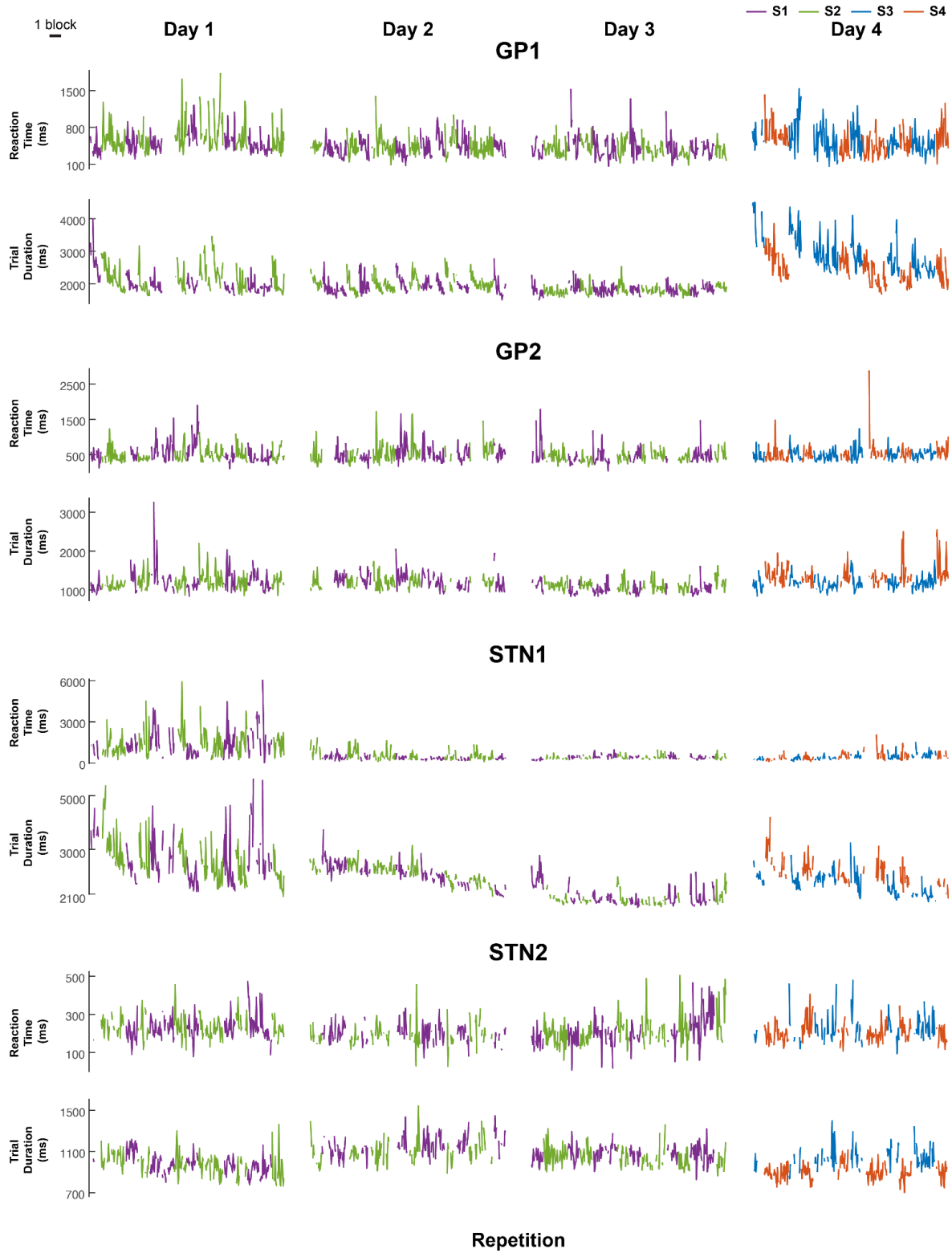


**Figure 2.6. Single-trial performance data.**  
Single-trial reaction time and trial duration for all fully correct trials.

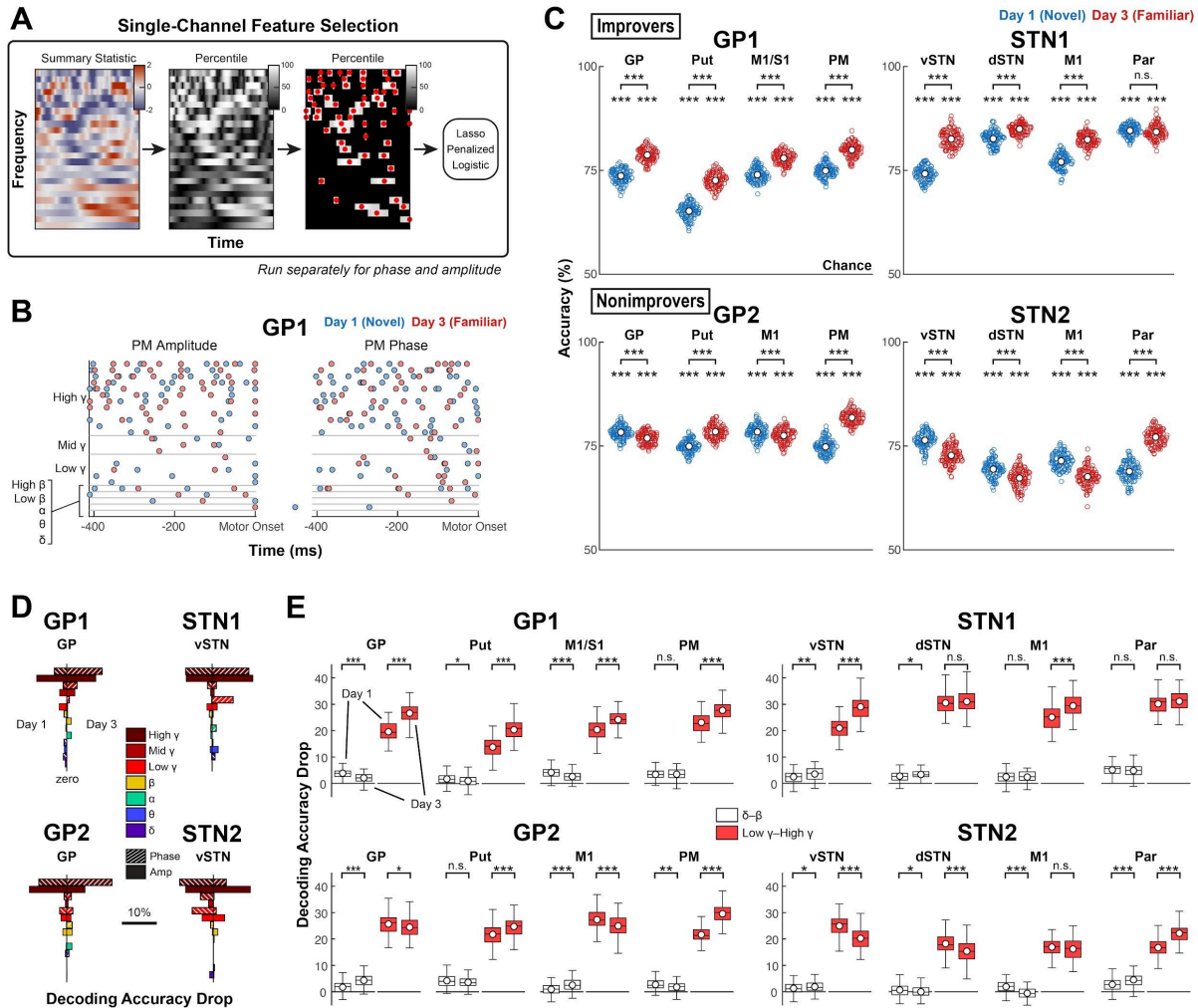


**Figure 2.7. Pre-movement sequence-specific  $\gamma$  activity, present in all brain regions, demonstrates practice-driven increases and decreases in discriminability in improvers and nonimprovers, respectively.**

(A) Visualization of feature selection pipeline. Features were selected separately for each channel on each day in each subject. (Left) For selection of amplitude features, the S1 vs. S2 two-sided  $t$ -statistic was computed at each time-frequency point. (Middle) The  $t$ -statistic at each time-frequency point was recomputed for 10,000 permutations of trial labels to determine the percentile ranking of the test value at each time-frequency point relative to its null distribution. (Right) Time-frequency points falling below their respective 80th-percentile cutoffs were masked, and in each of the remaining time-frequency regions, the time point achieving the highest percentile was selected as an amplitude feature. This process was repeated for phase data, using phase opposition sum as the summary statistic. Each resulting phase feature was split into two features comprised of the cartesian phase coordinates. Classification utilized 10-fold 100-repeat lasso-penalized logistic classification. (B) Example selected features for Days 1 and 3 in GP1's PM. (C) Mean decoding accuracy per model after feature selection (Comparison to chance:  $\alpha=0.05$ , one-sided, permutation testing with 1,000 resamples. See Table 2.7 for  $p$ -values. Comparison across days:  $\alpha=0.05$ , two-sided, permutation test with 10,000 resamples. See Table 2.8 for  $p$ -values.). Empty circle reflects mean decoding accuracy across folds for one repeat; white circle reflects mean decoding accuracy across repeats. (D) Absolute decoding accuracy decreases for features grouped by canonical frequency band and signal property (amplitude or phase)—a subset of representative plots. (E) Absolute decoding accuracy decreases for features grouped by frequency into two groups:  $\delta$  through  $\beta$  (0.5–30 Hz, phase and amplitude) and low  $\gamma$  through high  $\gamma$  (30–250 Hz, phase and amplitude) (Comparison across days:  $\alpha=0.05$ , two-sided, permutation testing with 10,000 resamples. See Tables 2.9–2.10 for  $p$ -values.). White circle reflects mean; black horizontal line reflects median. Box edges correspond to 25th and 75th percentiles. Whiskers span the entire data range excluding outliers. Outliers were computed as  $1.5 \cdot IQR$  away from the upper or lower quartile and are not shown. \* $p < 0.05$ , \*\* $p < 0.01$ , \*\*\* $p < 0.001$ .

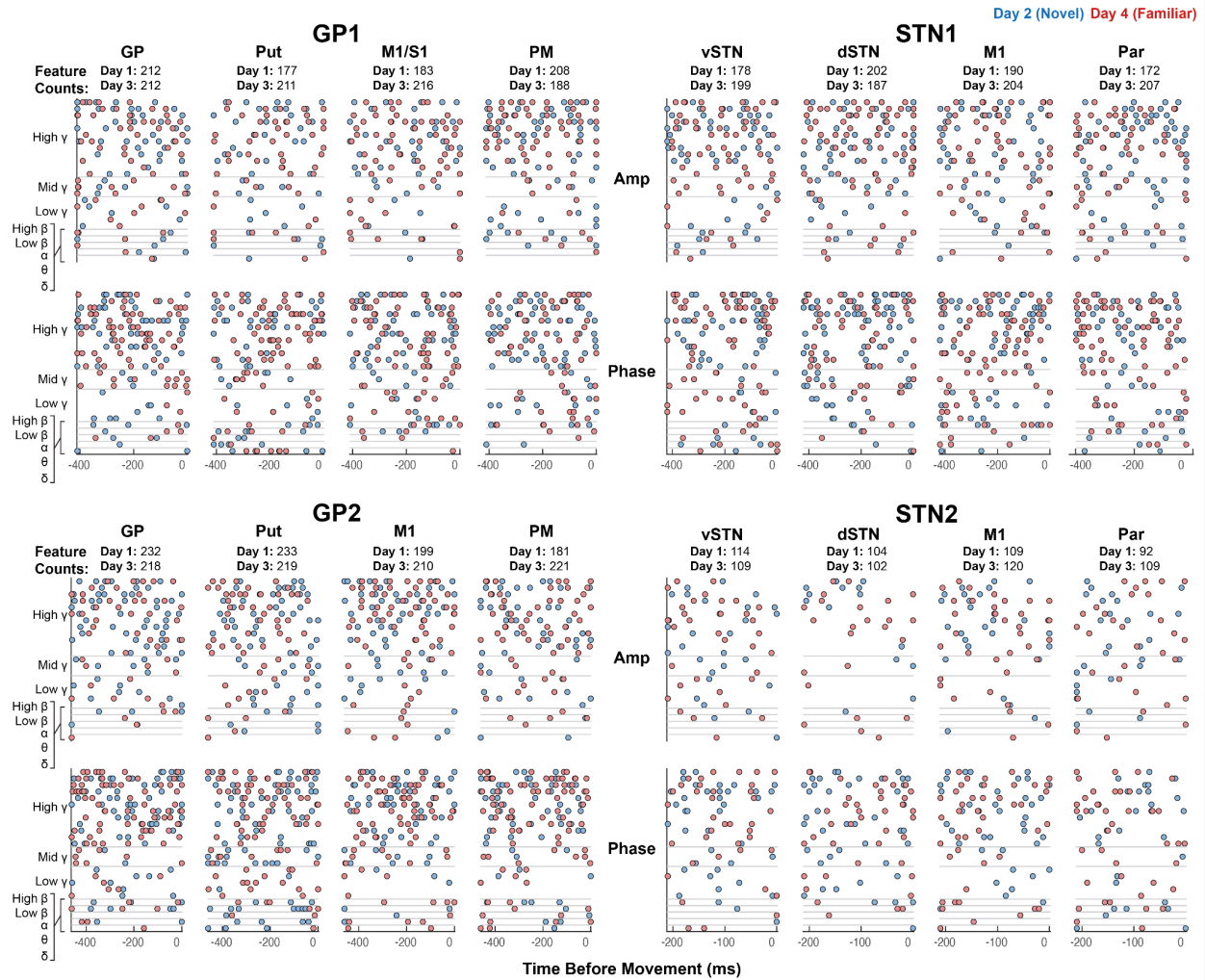


**Figure 2.8. Features selected prior to lasso regularization.**

Features were selected separately for each model. Total feature count per model (i.e., per subject per channel per day) prior to lasso regularization is shown above each channel's amplitude and phase feature plots. **Feature counts are based on each design matrix and thus include a feature for both the  $\sin(\text{phase})$  and the  $\cos(\text{phase})$  of each selected phase time-frequency point.** As a larger number of phase than amplitude time-frequency points tended to reach the 80th percentile cutoff for feature selection, the indicated total feature counts are at least 50% higher than the number of initially selected time-frequency points.

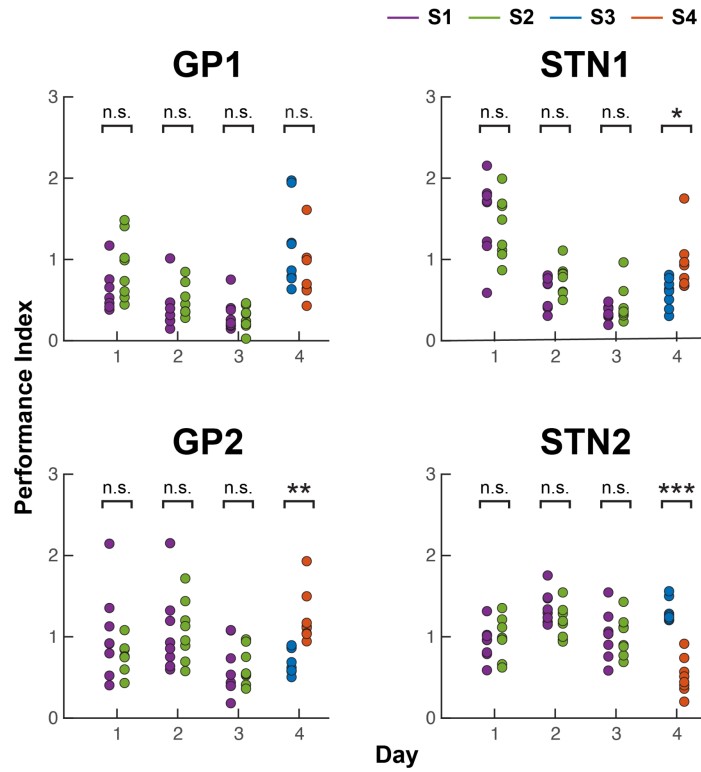


**Figure 2.9. On Days 1–3, overall sequence performance was comparable between S1 and S2.** Across-sequence comparison of performance within each day assessed differences in overall performance level ( $\alpha=0.05$ , two-sided, two-sample t-test with unequal variance. See **Table 2.6** for  $p$ -values.). \* $p<0.05$ , \*\* $p<0.01$ , \*\*\* $p<0.001$ .

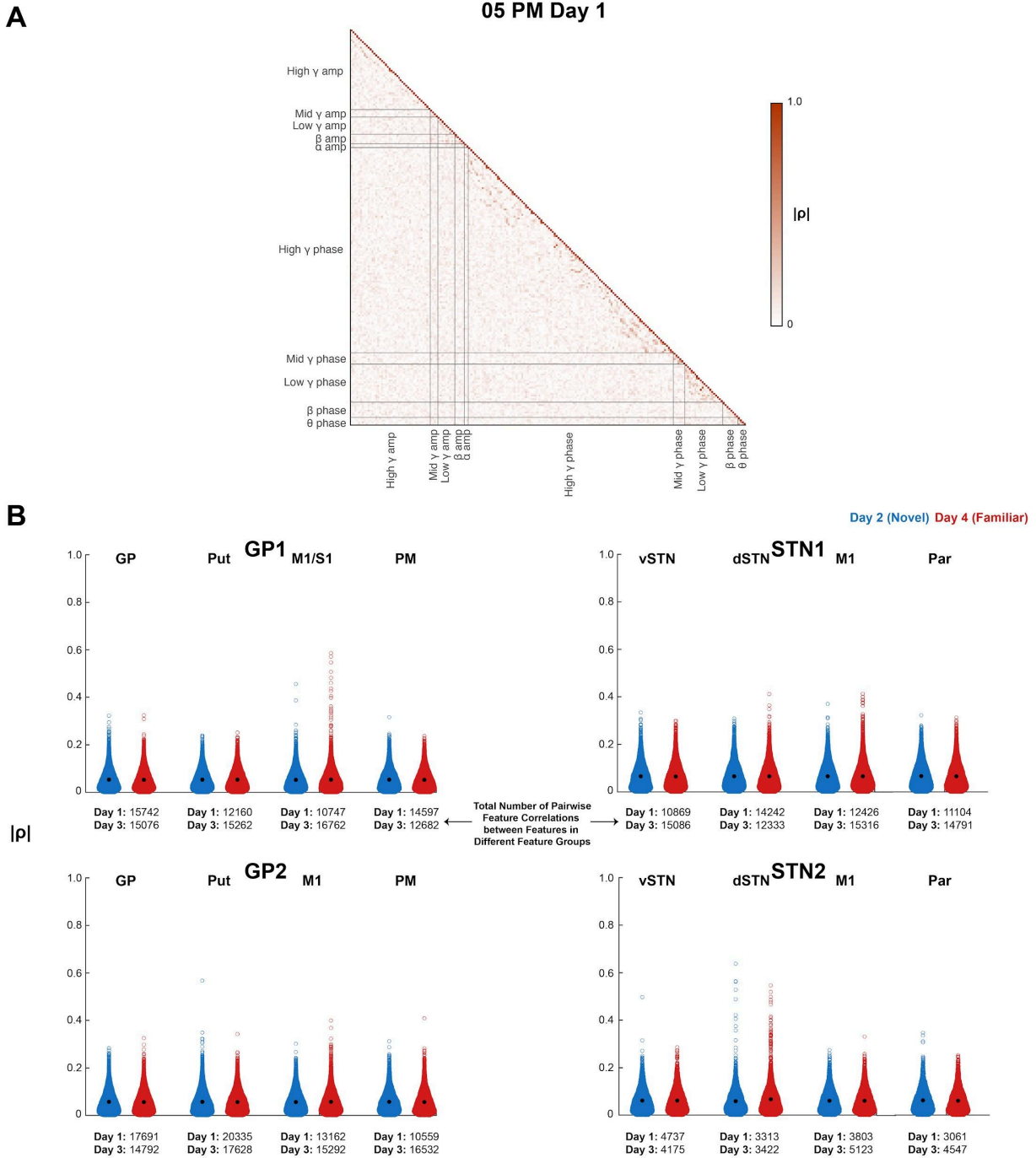


**Figure 2.10. Correlations between features after grouping by canonical frequency band and signal property.**

(A) Example feature correlation matrix for a single model, where light gray lines separate feature groups. (B) For each model, a swarm plot of all possible feature correlations between features in different groups. Features were grouped by canonical frequency band and also by signal property, i.e.,  $\delta$  phase features were grouped separately from  $\delta$  amplitude features, as well as from all other canonical frequency bands. Total number of feature correlations between features in different feature groups for a given model is shown below corresponding swarm plots.

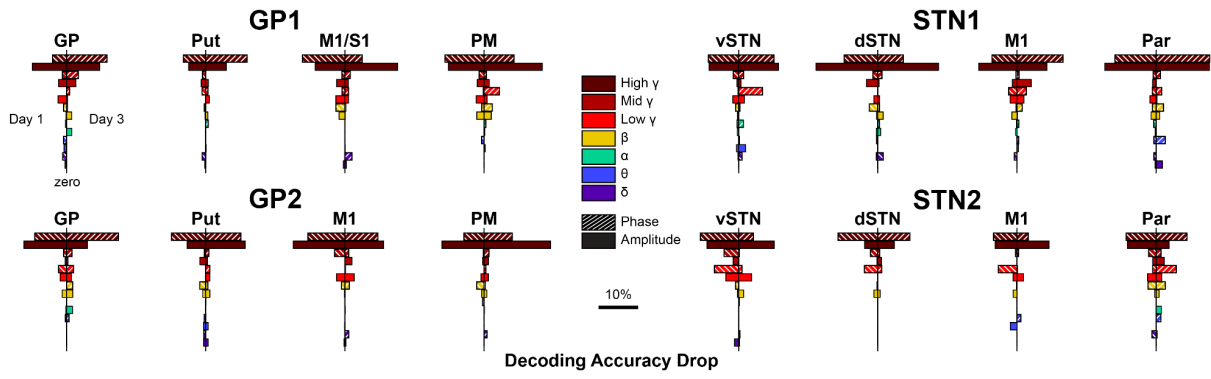
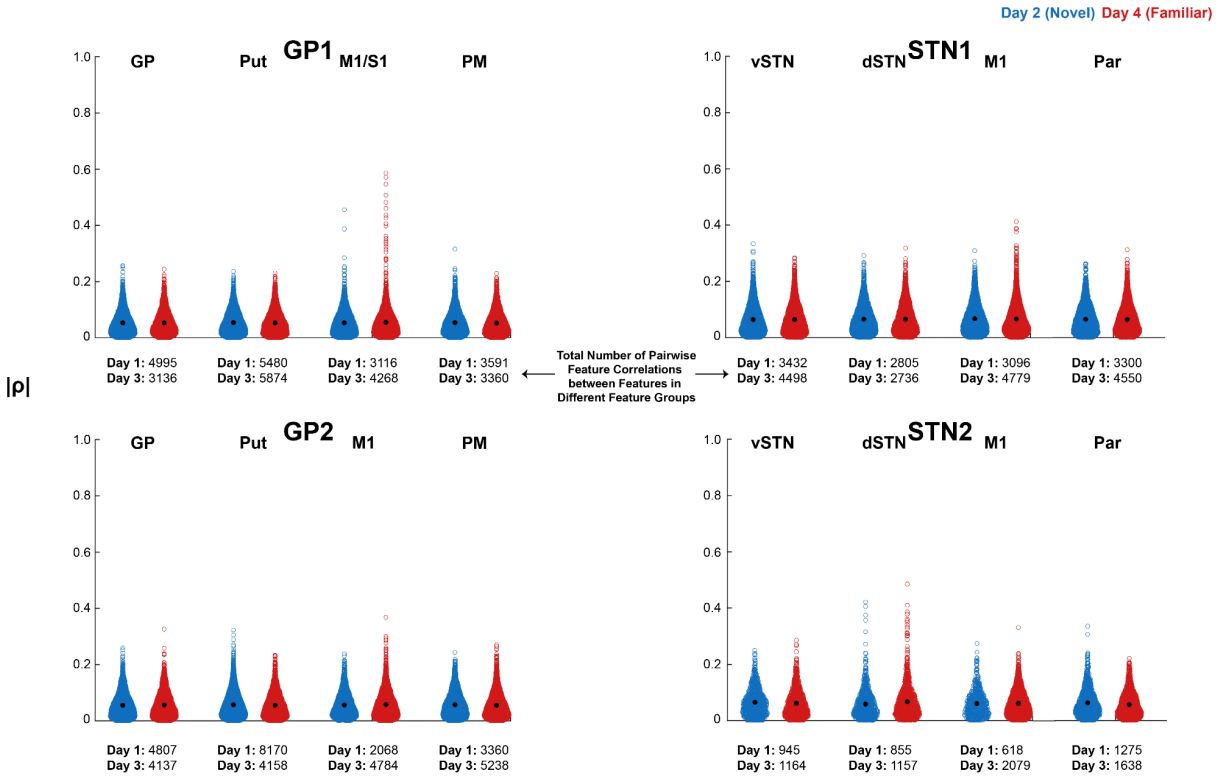


Figure 2.11. Absolute decoding accuracy decreases for features grouped by canonical frequency band and signal property.



**Figure 2.12. Correlations between features after grouping into 1)  $\delta$  through  $\beta$  and 2) low  $\gamma$  through high  $\gamma$ .**

For each model, a swarm plot of all possible feature correlations between features in different groups. Features were grouped into  $\delta$  through  $\beta$  (0.5–30 Hz) and low  $\gamma$  through high  $\gamma$  (30–250 Hz), with amplitude and phase features grouped together. Total number of feature correlations between features in different groups for a given model is shown below corresponding swarm plots.



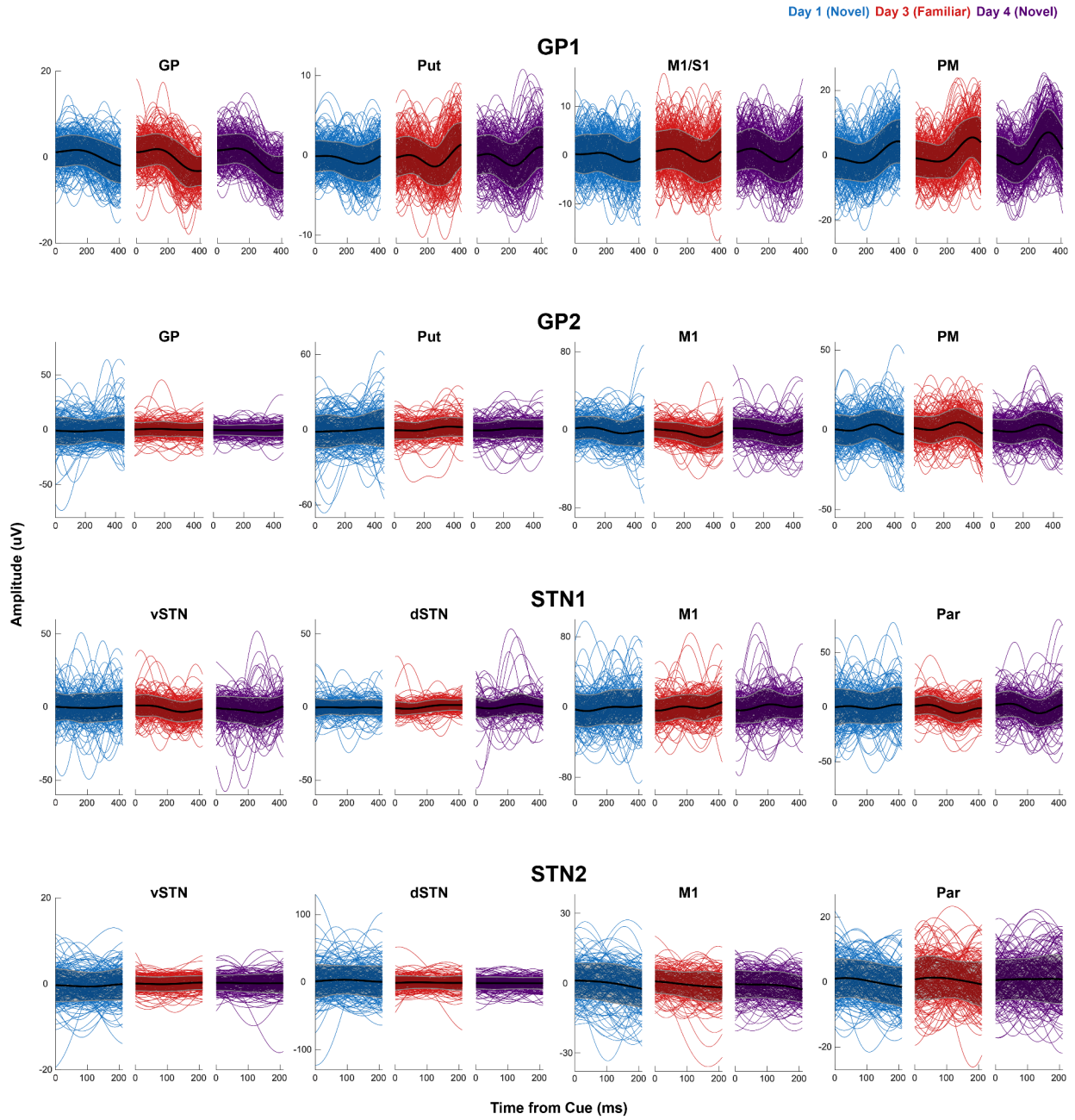


**Figure 2.13. Single-trial  $\delta$  time domain data.**  
 Data is aligned to cue onset and plotted as  $\bar{x} \pm s$ .



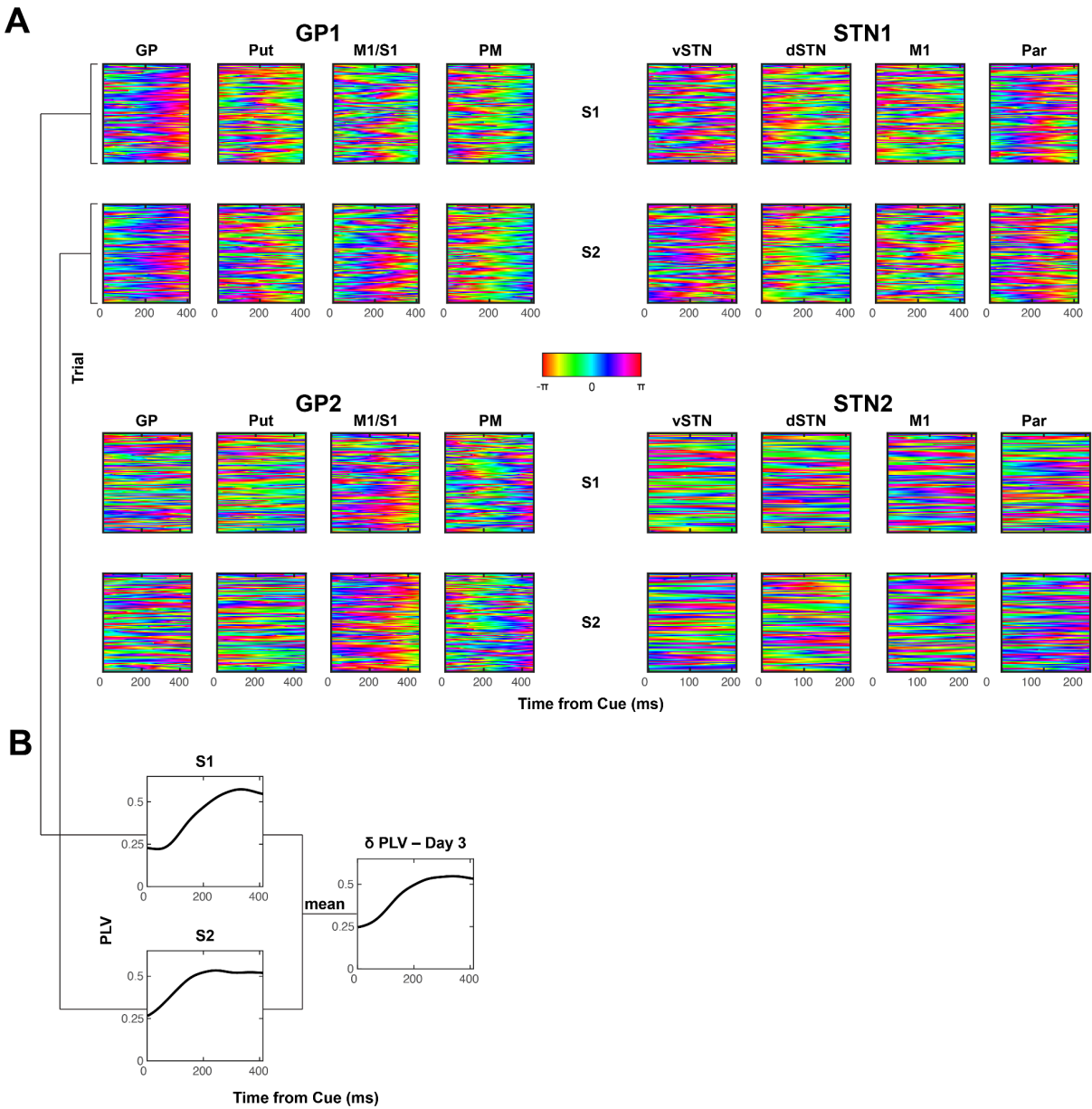


**Figure 2.14. Day 3 single-trial  $\delta$  phase.**

(A)  $\delta$  phase data aligned to cue onset. (B) Example of phase locking value calculation. Phase locking value was first calculated within sequence and smoothed with a 150 ms-long Gaussian window. Resulting time series were averaged across the two sequences to compute the overall phase locking value for this brain region on this day.

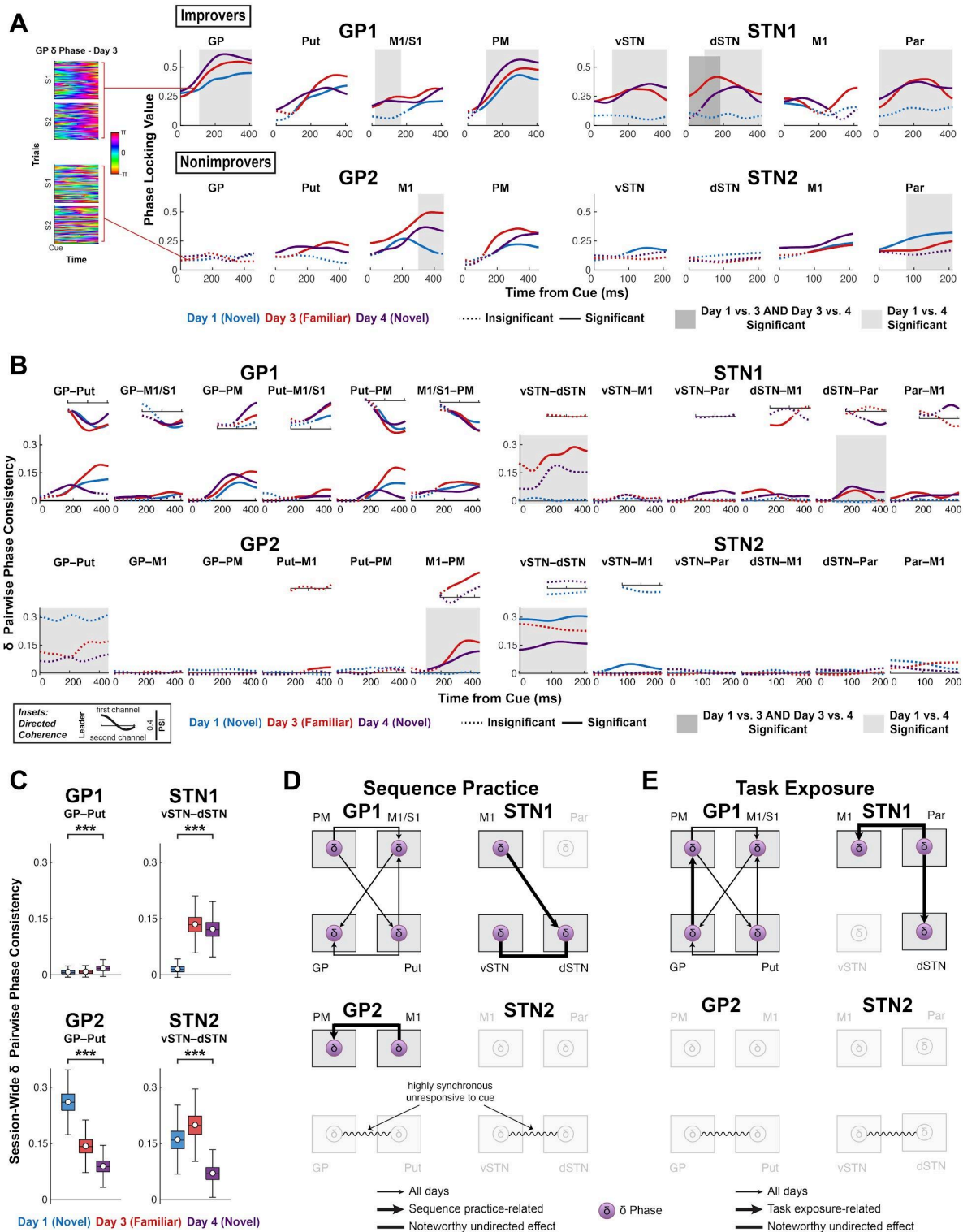


**Figure 2.15. Improvement is associated with cortically-led network  $\delta$  phase synchrony, to which sequence learning and task exposure add distinct effects, while lack of improvement is associated with highly synchronous BG  $\delta$ .** (A) (Left) All Day 3 single-trial  $\delta$  phase time series after cue onset in the pallidum of GP1 and GP2. (Right) Phase locking value (PLV) after cue onset on Days 1, 3 and 4. (Figure caption continued on the next page.)

(Figure caption continued from the previous page). Solid line indicates PLV significantly higher than chance ( $\alpha=0.05$ , one-sided, cluster-based permutation test with 10,000 resamples. See **Table 2.11** for  $p$ -values.). Shaded box indicates significant difference in PLV between days ( $\alpha=0.05$ , two-sided, cluster-based permutation with 10,000 resamples. See **Table 2.12** for  $p$ -values.). **(B)** Effects in  $\delta$  synchrony. (Large plots)  $\delta$  pairwise phase consistency (PPC, undirected measure) time series for all channel pairs. Solid line indicates PPC significantly higher than session-wide baseline, i.e.,  $h_0$ =coherence aligned cue is the same as general coherence levels not aligned to cue (rather than  $h_0$ =no coherence) ( $\alpha=0.05$ , one-sided, cluster-based permutation with 10,000 resamples. See **Table 2.13** for  $p$ -values.). Shaded box indicates significant difference in PPC between days ( $\alpha=0.05$ , two-sided, cluster-based permutation with 10,000 resamples. See **Table 2.14** for  $p$ -values.). (Insets) Phase slope index (PSI, directed measure) for significant PPC time series. Solid line indicates significant PSI ( $h_0$ =no channel leads,  $\alpha=0.05$ , two-sided, cluster-based permutation with 10,000 resamples. See **Table 2.15** for  $p$ -values.). **(C)** Session-wide baseline basal ganglia  $\delta$  pairwise phase consistency averaged across time. Calculated by taking the null distribution of time series resampled from each session in **(B)** and averaging each null PPC sample across time. Change in session baseline across Days 1 and 4 was tested ( $\alpha=0.05$ , two-sided, permutation testing with 10,000 resamples. See **Table 2.16**:  $p$ -values.). White circle reflects mean; black horizontal line reflects median. Box edges correspond to 25th and 75th percentiles. Whiskers span entire data range excluding outliers. Outliers were computed as  $1.5 \cdot IQR$  away from the upper or lower quartile and are not shown. \*\*\* $p < 0.001$ . **(D)** Network diagrams illustrating sequence practice-related  $\delta$  coherence effects. **(E)** Network diagrams illustrating task exposure-related  $\delta$  coherence effects.

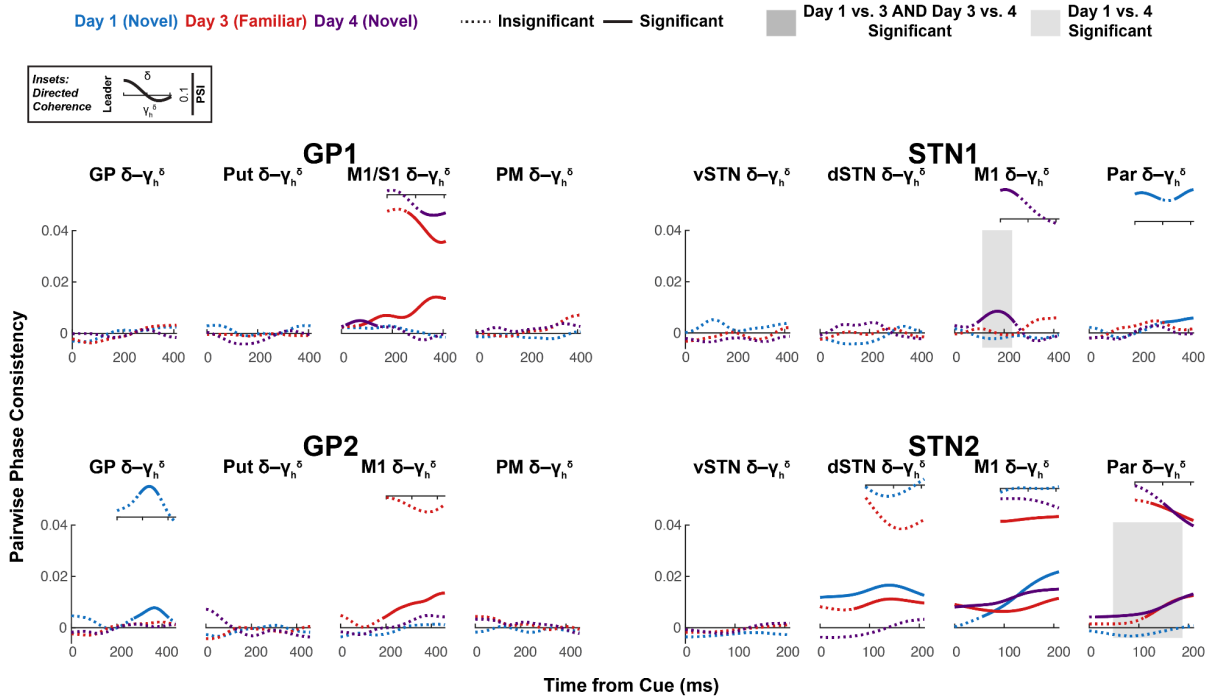


**Figure 2.16. Intraregional  $\delta$ - $\gamma$  coupling.**

(Large plots) Pairwise phase consistency (PPC, undirected measure) was calculated between  $\delta$  phase and the  $\delta$  phase of the high  $\gamma$  amplitude envelope. Solid line indicates significant PPC ( $h_0$ =coherence is not higher than expected given the phase distribution,  $\alpha=0.05$ , one-sided, cluster-based permutation with 10,000 resamples. See **Table 2.17** for  $p$ -values.). Shaded box indicates significant difference in PPC between days ( $\alpha=0.05$ , two-sided, cluster-based permutation with 10,000 resamples. See **Table 2.18** for  $p$ -values.). (Insets) Phase slope index (PSI, directed measure) for significant PPC time series. Solid line indicates significant PSI ( $h_0$ =no channel leads,  $\alpha=0.05$ , two-sided, cluster-based permutation with 10,000 resamples. See **Table 2.19** for  $p$ -values.).

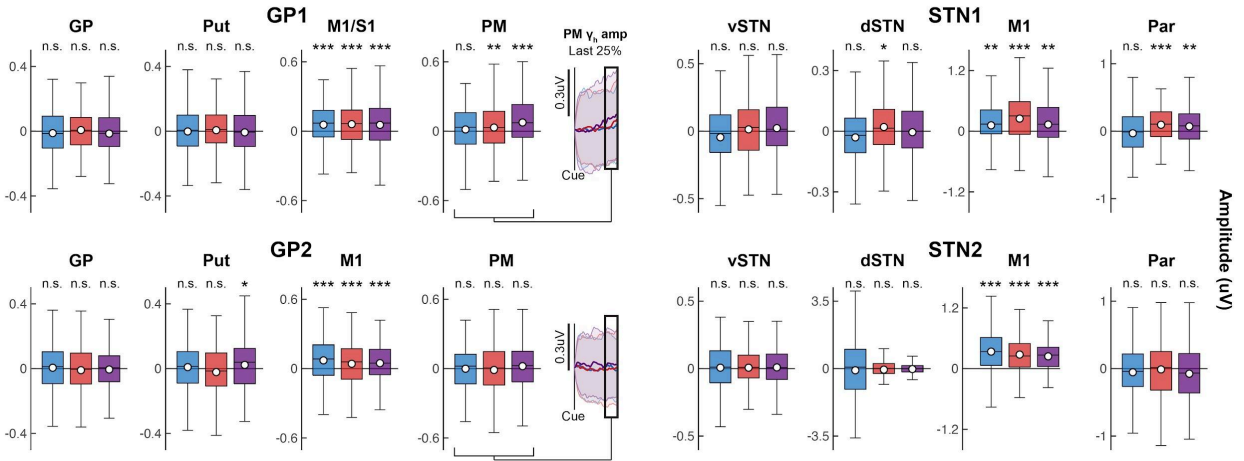


**Figure 2.17. High  $\gamma$  amplitude distributions.**

(Box plots) Change in high  $\gamma$  amplitude from cue onset to the last 25% of the reaction time period, after linear interpolation of all RT period trials to the same length and smoothing of  $\gamma$  amplitude across time ( $\alpha=0.05$ , one-sided, bootstrap estimation of  $\bar{x}$  with 10,000 resamples. See **Table 2.20** for  $p$ -values.). White circle reflects mean; black horizontal line reflects median. Box edges correspond to 25th and 75th percentiles. Whiskers span entire data range excluding outliers. Outliers were computed as  $1.5 \cdot IQR$  away from the upper or lower quartile and are not shown. (Insets) GP1 and GP2 trial average  $\gamma$  amplitude time series in premotor cortex, with black rectangle indicating the window over which  $\gamma$  amplitude is averaged for individual trials. Error bars indicate  $\pm s$ . \* $p < 0.05$ , \*\* $p < 0.01$ , \*\*\* $p < 0.001$ .

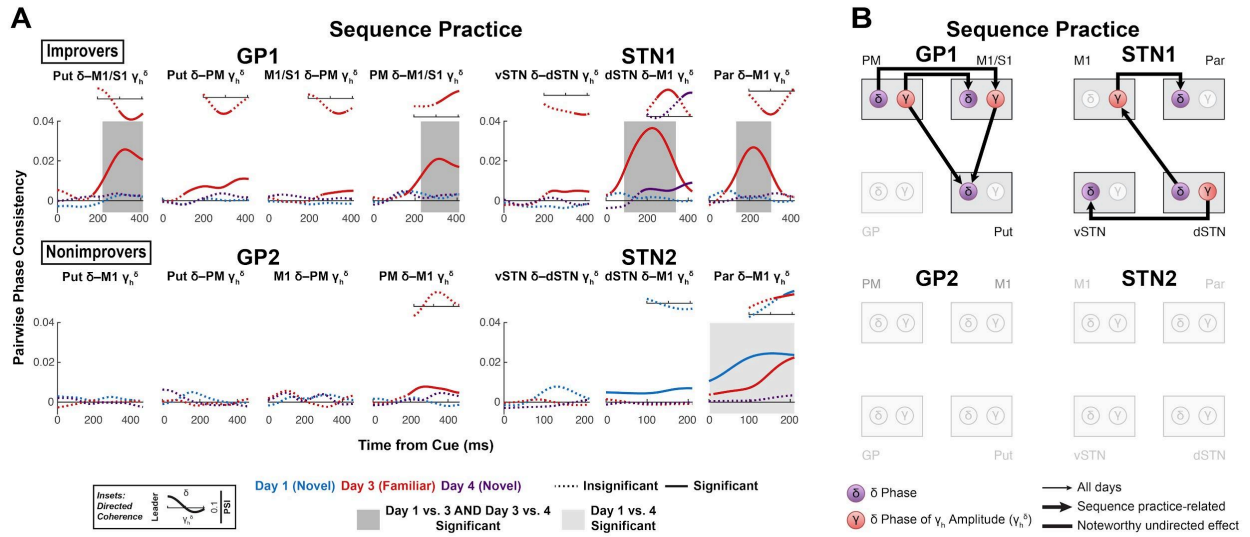


**Figure 2.18. Sequence learning is associated with specific corticocortical, cortico-basal ganglia and inter-basal ganglia  $\delta$ - $\gamma$  couplings.**

(A) Sequence practice-related effects in interregional  $\delta$ - $\gamma_h^\delta$  coherence. (Large plots) Pairwise phase consistency (PPC, undirected measure) was calculated between  $\delta$  phase and the  $\delta$  phase of the high  $\gamma$  amplitude envelope. Solid line indicates significant PPC ( $h_0$ =coherence is not higher than expected given the phase distribution,  $\alpha=0.05$ , one-sided, cluster-based permutation with 10,000 resamples. See **Table 2.21** for  $p$ -values.). Shaded box indicates significant difference in PPC between days ( $\alpha=0.05$ , two-sided, cluster-based permutation with 10,000 resamples. See **Table 2.22** for  $p$ -values.). (Insets) Phase slope index (PSI, directed measure) for significant PPC time series. Solid line indicates significant PSI ( $h_0$ =no channel leads,  $\alpha=0.05$ , two-sided, cluster-based permutation with 10,000 resamples. See **Table 2.23** for  $p$ -values.). (B) Network diagrams illustrating sequence practice-related  $\delta$ - $\gamma_h^\delta$  effects.

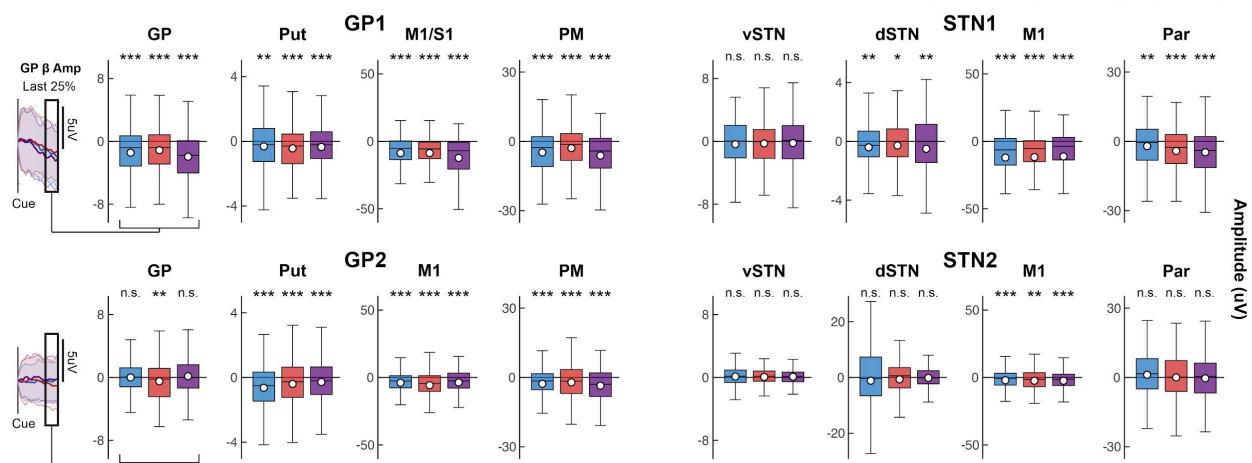


**Figure 2.19.  $\beta$  amplitude distributions.**

(Box plots) Change in  $\beta$  amplitude from cue onset to the last 25% of the reaction time period, after linear interpolation of all RT period trials to the same length and smoothing of  $\beta$  amplitude across time ( $\alpha=0.05$ , one-sided, bootstrap estimation of  $\bar{x}$  with 10,000 resamples. See **Table 2.24** for  $p$ -values.). White circle reflects mean; black horizontal line reflects median. Box edges correspond to 25th and 75th percentiles. Whiskers span entire data range excluding outliers. Outliers were computed as  $1.5 \cdot IQR$  away from the upper or lower quartile and are not shown. (Insets) GP1 and GP2 trial average  $\beta$  amplitude time series in pallidum, with black rectangle indicating the window over which  $\beta$  amplitude is averaged for individual trials. Error bars indicate  $\pm s$ . \* $p < 0.05$ , \*\* $p < 0.01$ , \*\*\* $p < 0.001$ .

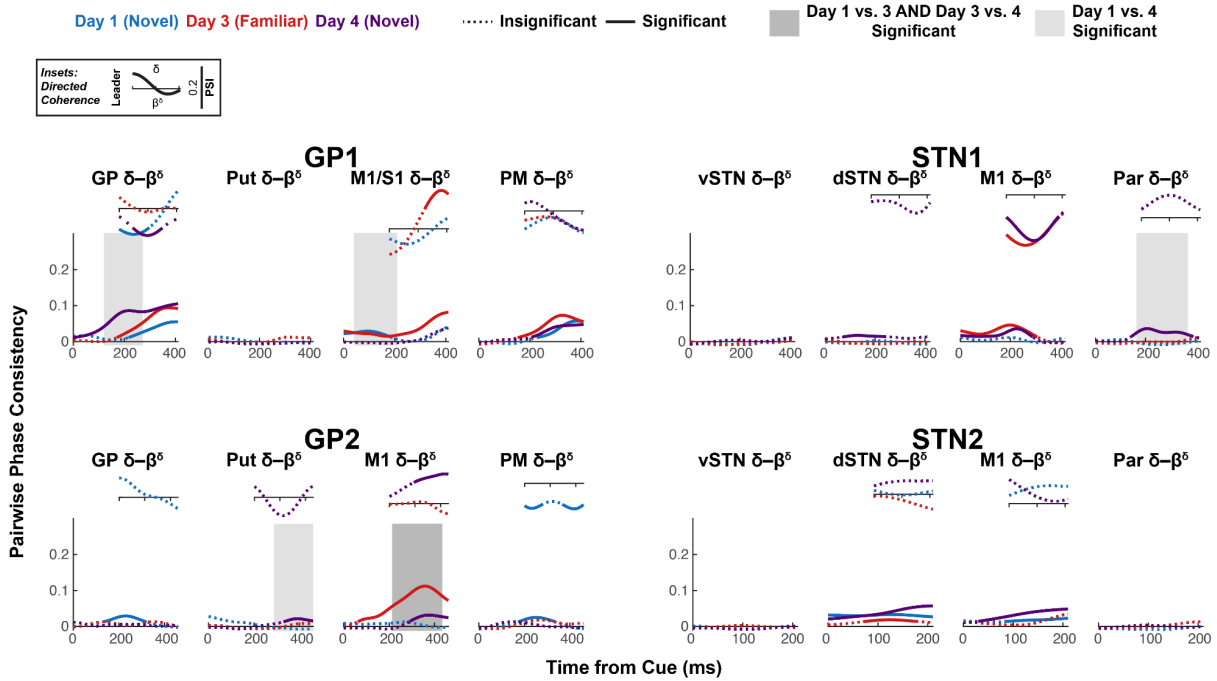


**Figure 2.20. Intraregional  $\delta$ - $\beta$  coupling.**

(Large plots) Pairwise phase consistency (PPC, undirected measure) was calculated between  $\delta$  phase and the  $\delta$  phase of the  $\beta$  amplitude envelope. Solid line indicates significant PPC ( $h_0$ =coherence is not higher than that expected given the phase distribution,  $\alpha=0.05$ , one-sided, cluster-based permutation with 10,000 resamples. See **Table 2.25** for  $p$ -values.). Shaded box indicates significant difference in PPC between days ( $\alpha=0.05$ , two-sided, cluster-based permutation with 10,000 resamples. See **Table 2.26** for  $p$ -values.). (Insets) Phase slope index (PSI, directed measure) for significant PPC time series. Solid line indicates significant PSI ( $h_0$ =no channel leads,  $\alpha=0.05$ , two-sided, cluster-based permutation with 10,000 resamples. See **Table 2.27** for  $p$ -values.).



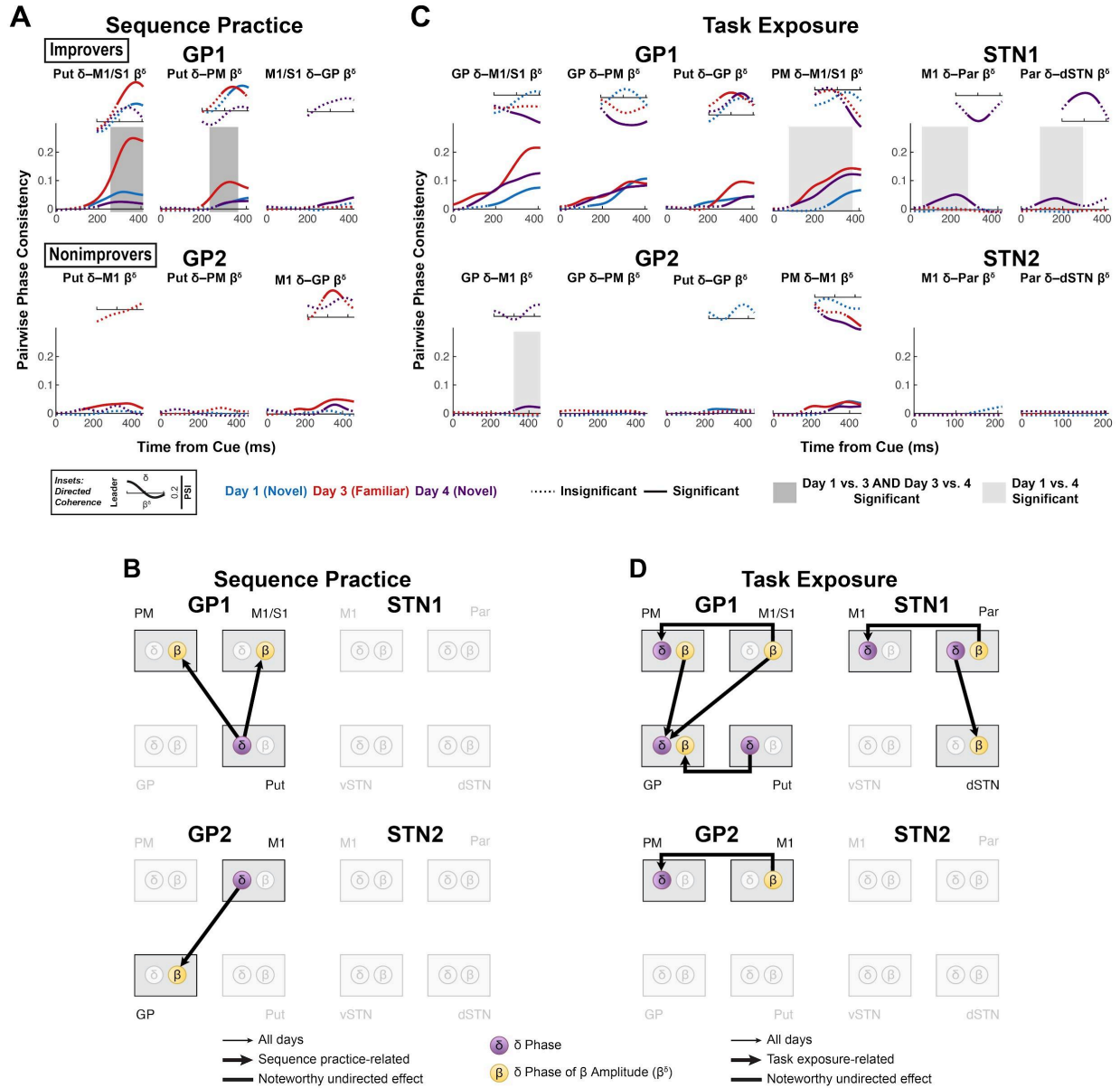


**Figure 2.21. Striatocortical  $\delta$ - $\beta$  coupling increases with sequence learning, while task exposure brings a range of  $\delta$ - $\beta$  couplings in improvers mostly absent in nonimprovers.**

(A) Sequence practice-related effects in interregional  $\delta$ - $\beta^{\delta}$  coherence. (Large plots) Pairwise phase consistency (PPC, undirected measure) was calculated between  $\delta$  phase and the  $\delta$  phase of the  $\beta$  amplitude envelope. Solid line indicates significant PPC ( $h_0$ =coherence is not higher than expected given the phase distribution,  $\alpha=0.05$ , one-sided, cluster-based permutation with 10,000 resamples. See **Table 2.28** for  $p$ -values.). Shaded box indicates significant difference in PPC between days ( $\alpha=0.05$ , two-sided, cluster-based permutation with 10,000 resamples. See **Table 2.29** for  $p$ -values.). (Insets) Phase slope index (PSI, directed measure) for significant PPC time series. Solid line indicates significant PSI ( $h_0$ =no channel leads,  $\alpha=0.05$ , two-sided, cluster-based permutation with 10,000 resamples. See **Table 2.30** for  $p$ -values.). (B) Network diagrams illustrating sequence practice-related  $\delta$ - $\beta^{\delta}$  effects. (C) Task exposure-related effects in interregional  $\delta$ - $\beta^{\delta}$  coherence. Visualization and statistics identical to (A) (See **Tables 2.31–2.33** for  $p$ -values.). (D) Network diagrams illustrating task exposure-related  $\delta$ - $\beta^{\delta}$  effects.

## Observed Pre-Movement Oscillatory Dynamics

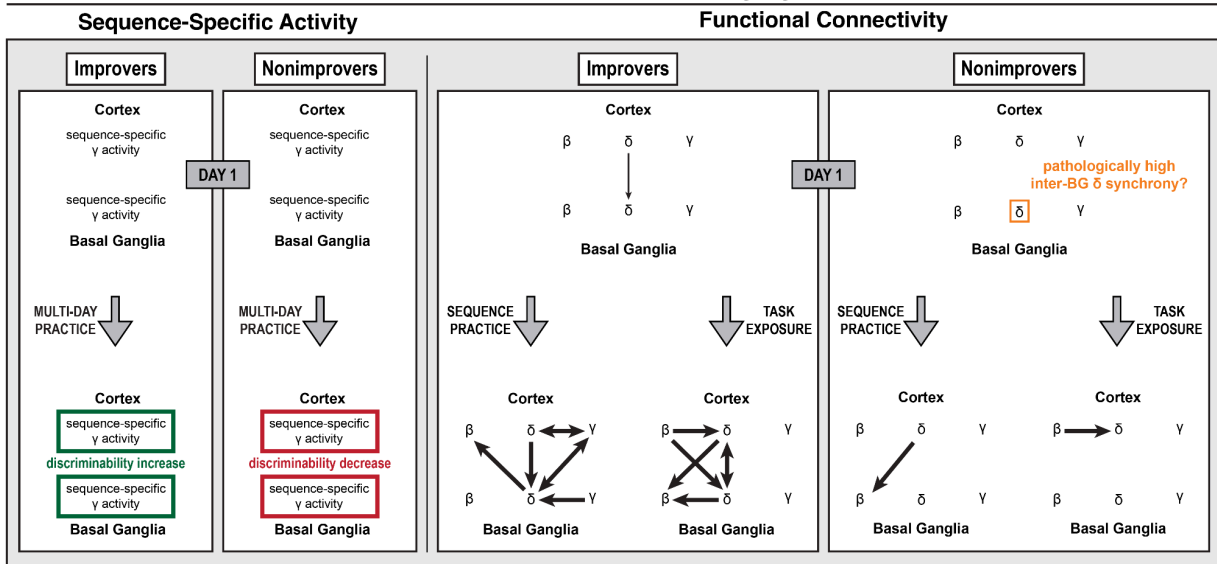


**Figure 2.22. Observed learning-related cortico-basal ganglia activity during motor sequence initiation.**

Diagram of observed learning-related changes in sequence-specific activity and functional connectivity prior to the onset of motor sequences over multiple days of practice. (Left) Sequence-specific  $\gamma$  activity was present in all brain regions for all subjects. With practice,  $\gamma$ 's predictive value increased in subjects who demonstrated performance improvement (improvers) but decreased in subjects who did not (nonimprovers). (Right) As motor sequence learning overlaps with increasing familiarity with the experimental process, we dissociated the effects related to sequence practice from those related to task exposure. Improvers exhibited cortico-basal ganglia  $\delta$  synchrony that, with sequence learning and task exposure, coincided with distinct patterns of functional connectivity. In nonimprovers, inter-basal ganglia  $\delta$  was highly coherent and did not consistently respond to task events or coordinate with cortex. Very little learning-related functional connectivity was observed. Notably, no subjects demonstrated a consistent  $\beta \rightarrow \delta \rightarrow \gamma$  cascade—possibly a reflection of PD-related neuropathophysiology.

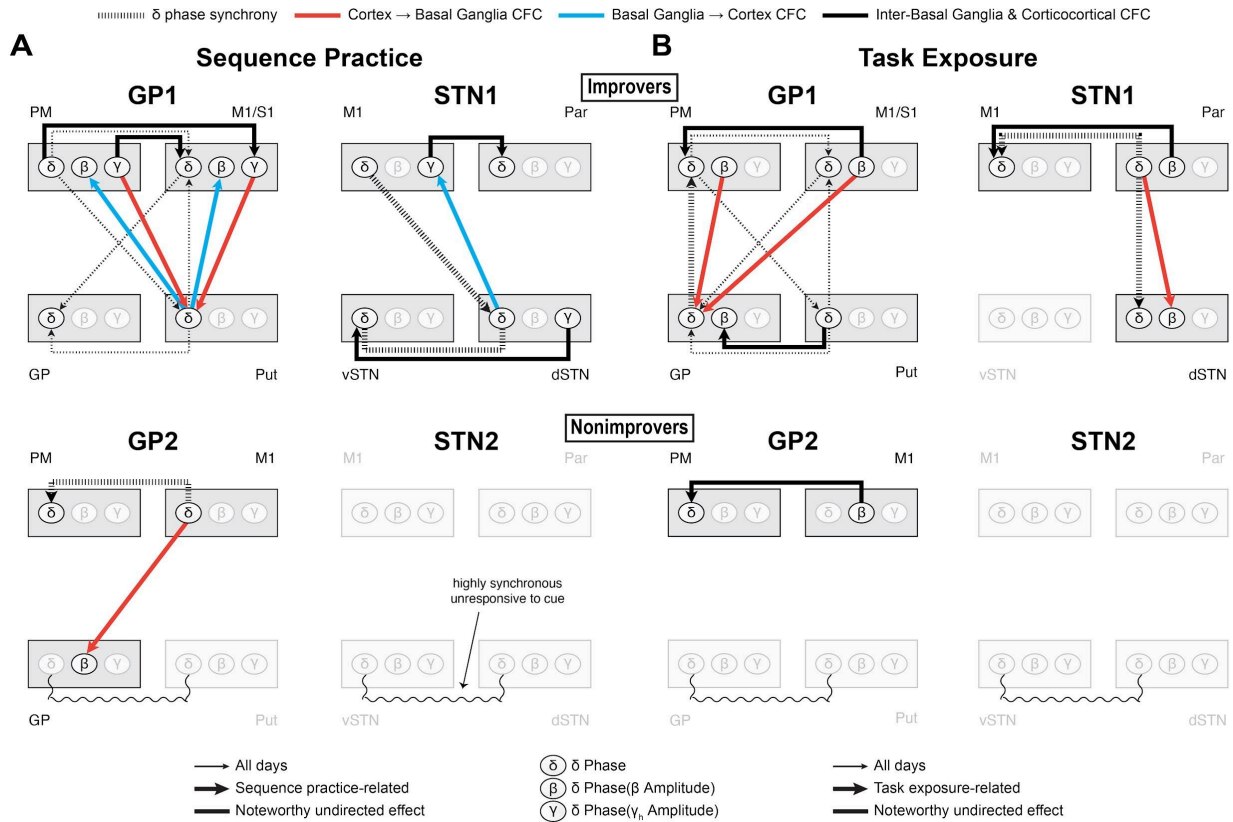


**Figure 2.23. Coordinated  $\delta$  activity supports a hierarchical functional network that reflects the specialized roles of cortico-basal ganglia regions in motor learning.**

Composite diagrams of interregional effects associated with (A) sequence practice and (B) task exposure. Notably, no directed  $\delta$ - $\beta^\delta$  or  $\delta$ - $\gamma_h^\delta$  interregional couplings were associated with general sequence initiation across days, and cross-frequency coupling (CFC) instead developed with sequence practice or task exposure. Furthermore, only brain regions that demonstrated  $\delta$  phase alignment to cue and synchronized with motor cortical  $\delta$  contributed  $\delta$  to any learning-related interregional  $\delta$ - $\beta^\delta$  or  $\delta$ - $\gamma_h^\delta$  coupling. In improvers, sequence learning and task exposure brought different CFC patterns and changes to network  $\delta$  dynamics, though sequence learning and task exposure were linked by a common framework of cortically-led network  $\delta$  synchrony. Almost all observed communication between cortex and basal ganglia in improvers involved basal ganglia  $\delta$ . Nevertheless, for each type of communication, the presence and direction of coupling depended on the involved brain regions, indicative of their specialized roles. In nonimprovers, highly synchronized basal ganglia  $\delta$  coincided with minimal functional connectivity in the assessed frequency bands.

## Tables

**Table 2.1. Subject demographic and clinical information.**

MoCA, Montreal Cognitive Assessment; UPDRS, Unified Parkinson's Disease Rating Scale. *Given the small sample size, age and sex have been omitted to retain participant privacy.*

	Dominant Hand	Pre-Op MoCA	Pre-Op UPDRS ON Med	Pre-Op UPDRS OFF Med	% Change ON Med	Primary Symptoms
GP1	R	28	9	18	-50%	Hand tremor, bradykinesia, gait
GP2	R	27	17	31	-45%	Hand tremor, bradykinesia, gait
STN1	R	26	5	32	-84%	Hand tremor, bradykinesia
STN2	R	28	10	31	-68%	Hand tremor, bradykinesia

**Table 2.2. Sequences.**

No sequences contained repeated adjacent elements, rising or falling triplets, or the thumb. All sequences paired for comparison within and across days started with the same first and last elements. Block order of S1 and S2 was switched on Day 2.

	Familiarization	Day 1	Day 2	Day 3	Day 4
<b>GP1</b>	2-4-5-3-2 2-3-5-4-2	4-2-3-5-4 4-5-3-2-4	4-5-3-2-4 4-2-3-5-4	4-2-3-5-4 4-5-3-2-4	4-2-5-3-4 4-3-5-2-4
<b>GP2</b>	2-5-3-4-2 2-4-3-5-2	3-4-2-5-3 3-5-2-4-3	3-5-2-4-3 3-4-2-5-3	3-4-2-5-3 3-5-2-4-3	3-2-4-5-3 3-5-4-2-3
<b>STN1</b>	2-4-3-5-2 2-5-3-4-2	3-4-2-5-3 3-5-2-4-3	3-5-2-4-3 3-4-2-5-3	3-4-2-5-3 3-5-2-4-3	3-2-4-5-3 3-5-4-2-3
<b>STN2</b>	2-4-5-3-2 2-3-5-4-2	4-2-3-5-4 4-5-3-2-4	4-5-3-2-4 4-2-3-5-4	4-2-3-5-4 4-5-3-2-4	4-2-5-3-4 4-3-5-2-4

**Table 2.3. Supplementary data collection.**

Scores for the upper limb component of the UPDRS performed immediately after the typing task each day and the prior night's sleep duration, collected with a sleep journal. F, Familiarization.

	Day	Postural Tremor	Kinetic Tremor	Finger Tapping	Hand Movements	Pronation/Supination	Total	Prior Night's Sleep (hr)	
GP1	F	1	1	2	2	1	7	7.75	
	1	1	0	3	2	3	9	4	
	2	1	1	3	2	2	9	8	
	3	2	1	3	2	1	9	7	
	4	1	1	2	2	2	8	7	
GP2	F	1	2	2	3	1	9	7.5	
	1	1	1	3	3	2	10	7	
	2	1	2	2	2	1	8	8.25	
	3	1	2	2	2	1	8	8	
	4	2	2	2	2	1	9	8	
STN1	F	1	0	2	1	2	6	7	
	1	2	1	0	0	1	4	7.25	
	2	1	0	0	1	0	2	8.5	
	3	0	0	1	1	1	3	5.25	
	4	1	0	0	0	1	2	8.75	
STN2	F	1	0	2	2	1	6	6	
	1	1	0	2	2	1	6	6.5	
	2	0	1	2	2	1	6	9.5	
	3	0	1	2	1	1	5	8	
	4	0	1	2	2	1	6	8.5	
		(R/task hand)	Range: [0, 4]		0 = none, 4 = severe				

Table 2.4. Behavioral comparison within sequences across days (Day 1 vs. Day 3): *p*-values.

	Sequence	<i>n</i>	<i>p</i> -value
GP1	S1	15	<b>0.031648</b>
	S2	16	<b>0.002312</b>
GP2	S1	16	0.089923
	S2	16	0.243550
STN1	S1	16	<b>0.000241</b>
	S2	16	<b>0.000087</b>
STN2	S1	16	0.496600
	S2	16	0.853360

Table 2.5. Behavioral comparison of pooled sequences across days (Day 3 vs. Day 4): *p*-values.

	<i>n</i>	<i>p</i> -value
GP1	31	<b>0.000033</b>
GP2	32	<b>0.005224</b>
STN1	32	<b>0.000666</b>
STN2	32	0.440650



Table 2.6. Within-day across-sequence comparison of performance index: *p*-values.

		<i>p</i> -value			
	<i>n</i>	Day 1	Day 2	Day 3	Day 4
GP1	15	0.133600	0.531500	0.676200	0.211800
GP2	16	0.231800	0.928800	0.858200	<b>0.002000</b>
STN1	16	0.545000	0.149700	0.317100	<b>0.030900</b>
STN2	16	0.651000	0.090300	0.927000	<b>0.000002</b>

Table 2.7. Baseline testing of model performance in single-trial classification: *p*-values.

		<i>p</i> -value		
	Region	<i>n</i>	Day 1	Day 3
<b>GP1</b>	GP	238	0.000999	0.000999
	Put	238	0.000999	0.000999
	M1/S1	238	0.000999	0.000999
	PM	238	0.000999	0.000999
<b>GP2</b>	GP	206	0.000999	0.000999
	Put	206	0.000999	0.000999
	M1	206	0.000999	0.000999
	PM	206	0.000999	0.000999
<b>STN1</b>	vSTN	158	0.000999	0.000999
	dSTN	158	0.000999	0.000999
	M1	158	0.000999	0.000999
	Par	158	0.000999	0.000999
<b>STN2</b>	vSTN	182	0.000999	0.000999
	dSTN	182	0.000999	0.000999
	M1	182	0.000999	0.000999
	Par	182	0.000999	0.000999

Table 2.8. Across-day testing of model performance in single-trial classification: *p*-values.

	Region	<i>n</i>	<i>p</i> -value
<b>GP1</b>	GP	476	<b>0.000100</b>
	Put	476	<b>0.000100</b>
	M1/S1	476	<b>0.000100</b>
	PM	476	<b>0.000100</b>
<b>GP2</b>	GP	412	<b>0.000100</b>
	Put	412	<b>0.000100</b>
	M1	412	<b>0.000200</b>
	PM	412	<b>0.000100</b>
<b>STN1</b>	vSTN	316	<b>0.000100</b>
	dSTN	316	<b>0.000100</b>
	M1	316	<b>0.000100</b>
	Par	316	0.140086
<b>STN2</b>	vSTN	364	<b>0.000100</b>
	dSTN	364	<b>0.000100</b>
	M1	364	<b>0.000100</b>
	Par	364	<b>0.000100</b>

Table 2.9. Across-day testing of feature importance (high frequencies):  $p$ -values.

	Region	$n$	$p$ -value
<b>GP1</b>	GP	476	<b>0.000100</b>
	Put	476	<b>0.000100</b>
	M1/S1	476	<b>0.000100</b>
	PM	476	<b>0.000100</b>
<b>GP2</b>	GP	412	<b>0.024698</b>
	Put	412	<b>0.000100</b>
	M1	412	<b>0.000200</b>
	PM	412	<b>0.000100</b>
<b>STN1</b>	vSTN	316	<b>0.000100</b>
	dSTN	316	0.395160
	M1	316	<b>0.000100</b>
	Par	316	0.059694
<b>STN2</b>	vSTN	364	<b>0.000100</b>
	dSTN	364	<b>0.000100</b>
	M1	364	0.226777
	Par	364	<b>0.000100</b>

Table 2.10. Across-day testing of feature importance (low frequencies):  $p$ -values.

	Region	$n$	$p$ -value
<b>GP1</b>	GP	476	<b>0.000100</b>
	Put	476	<b>0.013299</b>
	M1/S1	476	<b>0.000100</b>
	PM	476	0.831917
<b>GP2</b>	GP	412	<b>0.000100</b>
	Put	412	0.069293
	M1	412	<b>0.000100</b>
	PM	412	<b>0.001200</b>
<b>STN1</b>	vSTN	316	<b>0.003500</b>
	dSTN	316	<b>0.020398</b>
	M1	316	0.777222
	Par	316	0.378362
<b>STN2</b>	vSTN	364	<b>0.049995</b>
	dSTN	364	<b>0.024498</b>
	M1	364	<b>0.000100</b>
	Par	364	<b>0.000100</b>

**Table 2.11. Baseline testing of local cue-related  $\delta$  phase locking value: *p*-values.**

Blank cells indicate no time regions passed initial thresholding. Multiple values in a single cell correspond to multiple time regions that passed initial thresholding. Earlier time regions are listed first.

		<i>p</i> -value			
	Region	<i>n</i>	Day 1	Day 3	Day 4
<b>GP1</b>	GP	238	<b>0.000100</b>	<b>0.000100</b>	<b>0.000100</b>
	Put	238	<b>0.002300</b>	<b>0.002500</b>	<b>0.000100</b>
	M1/S1	238	<b>0.015898</b>	<b>0.000100</b>	<b>0.000100</b>
	PM	238	<b>0.000500</b>	<b>0.000500</b>	<b>0.000900</b>
<b>GP2</b>	GP	202		0.155084	
	Put	202		<b>0.009099</b>	<b>0.000100</b>
	M1	202	<b>0.001400</b>	<b>0.000100</b>	<b>0.000300</b>
	PM	202	<b>0.003100</b>	<b>0.001700</b>	<b>0.004000</b>
<b>STN1</b>	vSTN	192		<b>0.000100</b>	<b>0.000100</b>
	dSTN	192		<b>0.000100</b>	<b>0.001200</b>
	M1	192	<b>0.045195</b> 0.130987	<b>0.042196</b> <b>0.036096</b>	<b>0.008199</b>
	Par	192	0.120588 0.158384	<b>0.000100</b>	<b>0.000100</b>
<b>STN2</b>	vSTN	182	<b>0.034497</b>		0.098290
	dSTN	182			
	M1	182	<b>0.024198</b>	<b>0.021398</b>	<b>0.000100</b>
	Par	182	<b>0.000100</b>	<b>0.000100</b>	0.106189 0.078192

**Table 2.12. Across-day testing of local cue-related  $\delta$  phase locking value: *p*-values.**

Blank cells indicate no time regions passed initial thresholding. Multiple values in a single cell correspond to multiple time regions that passed initial thresholding. Earlier time regions are listed first.

		<i>p</i> -value			
	Region	<i>n</i>	Day 1 vs. 3	Day 3 vs. 4	Day 1 vs. 4
<b>GP1</b>	GP	238	<b>0.035096</b>		<b>0.002700</b>
	Put	238	0.195580 0.075092	0.082892	0.094291
	M1/S1	238	<b>0.0150985</b> 0.195780		<b>0.041896</b>
	PM	238			<b>0.002400</b>
<b>GP2</b>	GP	202			
	Put	202	<b>0.043596</b>		0.170983 0.170983
	M1	202	<b>0.020798</b>	0.074493	<b>0.044496</b>
	PM	202	<b>0.022298</b>	0.206479	
<b>STN1</b>	vSTN	192	<b>0.000100</b>		0.189781 <b>0.001500</b>
	dSTN	192	<b>0.000100</b>	<b>0.022098</b>	<b>0.001200</b>
	M1	192	0.108189	<b>0.032097</b>	
	Par	192	<b>0.000600</b>		<b>0.000100</b>
<b>STN2</b>	vSTN	182			
	dSTN	182			
	M1	182			
	Par	182			<b>0.017498</b>

**Table 2.13. Baseline testing of  $\delta$  PPC:  $p$ -values.**

Blank cells indicate no time regions passed initial thresholding. Multiple values in a single cell correspond to multiple time regions that passed initial thresholding. Earlier time regions are listed first.

		<i>p</i> -value			
	Region	<i>n</i>	Day 1	Day 3	Day 4
<b>GP1</b>	GP-Put	238	<b>0.001400</b>	<b>0.001300</b>	<b>0.003200</b>
	GP-M1/S1	238	<b>0.016798</b>	<b>0.001800</b>	<b>0.007499</b> 0.124588
	GP-PM	238	<b>0.004500</b>	<b>0.000400</b>	<b>0.000400</b>
	Put-M1/S1	238	0.094291 <b>0.042696</b>	<b>0.005799</b>	<b>0.012799</b>
	Put-PM	238	<b>0.004100</b>	<b>0.004900</b>	<b>0.002000</b>
	M1/S1-PM	238	<b>0.002900</b>	<b>0.004100</b>	<b>0.000500</b>
<b>GP2</b>	GP-Put	202			
	GP-M1	202			
	GP-PM	202			
	Put-M1	202		<b>0.037796</b>	
	Put-PM	202	0.164084 0.106589		0.060794
	M1-PM	202		<b>0.004500</b>	<b>0.000600</b>
<b>STN1</b>	vSTN-dSTN	192		0.174083 <b>0.005999</b>	0.126987
	vSTN-M1	192		0.076692	0.054195
	vSTN-Par	192			<b>0.001900</b>
	dSTN-M1	192	0.180782	<b>0.010099</b>	<b>0.002100</b>
	dSTN-Par	192		<b>0.003400</b>	<b>0.000600</b>
	Par-M1	192		<b>0.000300</b>	<b>0.002400</b>
<b>STN2</b>	vSTN-dSTN	182	<b>0.000100</b>		<b>0.000100</b>
	vSTN-M1	182	<b>0.005699</b>		
	vSTN-Par	182	0.130587		0.074693
	dSTN-M1	182			
	dSTN-Par	182	0.088791		0.111189 0.087591
	Par-M1	182			



**Table 2.14. Across-day testing of  $\delta$  PPC:  $p$ -values.**

Blank cells indicate no time regions passed initial thresholding. Multiple values in a single cell correspond to multiple time regions that passed initial thresholding. Earlier time regions are listed first.

		<i>p</i> -value			
	Region	<i>n</i>	Day 1 vs. 3	Day 3 vs. 4	Day 1 vs. 4
<b>GP1</b>	GP-Put	476	0.121488	<b>0.022398</b>	0.089191
	GP-M1/S1	476			
	GP-PM	476	0.182882		0.073093
	Put-M1/S1	476	0.140886		0.075392
	Put-PM	476	0.105789	<b>0.028097</b>	0.092891
	M1/S1-PM	476			
<b>GP2</b>	GP-Put	404	<b>0.000100</b>	0.118988	<b>0.000100</b>
	GP-M1	404			
	GP-PM	404	<b>0.006199</b>		<b>0.028197</b> <b>0.007699</b>
	Put-M1	404	<b>0.022098</b>	0.242376	0.208179
	Put-PM	404			0.067693
	M1-PM	404	<b>0.001700</b>		<b>0.000400</b>
<b>STN1</b>	vSTN-dSTN	384	<b>0.000100</b>	0.053395 0.095890	<b>0.000100</b>
	vSTN-M1	384		0.161384	
	vSTN-Par	384		<b>0.017998</b>	0.174183
	dSTN-M1	384	<b>0.020598</b>	0.130387	
	dSTN-Par	384	<b>0.005199</b>	0.197480 0.138986	<b>0.000600</b>
	Par-M1	384	0.185581		
<b>STN2</b>	vSTN-dSTN	364		0.086191	<b>0.000100</b>
	vSTN-M1	364	<b>0.006799</b>	0.115288	0.069793
	vSTN-Par	364			
	dSTN-M1	364			
	dSTN-Par	364			0.163184
	Par-M1	364		0.131287	

**Table 2.15. Baseline testing of  $\delta$  PSI:  $p$ -values.**

Blank cells indicate no time regions passed initial thresholding. Multiple values in a single cell correspond to multiple time regions that passed initial thresholding. Earlier time regions are listed first. NA, not applicable.

		<i>p</i> -value			
	Region	<i>n</i>	Day 1	Day 3	Day 4
<b>GP1</b>	GP-Put	238	0.081592 <b>0.000300</b>	<b>0.000100</b>	<b>0.000300</b>
	GP-M1/S1	238	<b>0.003400</b>	<b>0.001600</b>	<b>0.000800</b>
	GP-PM	238		<b>0.032897</b>	<b>0.005799</b>
	Put-M1/S1	238	<b>0.018798</b>	0.088191 <b>0.001300</b>	<b>0.001600</b>
	Put-PM	238	<b>0.001500</b>	<b>0.000800</b>	<b>0.000300</b>
	M1/S1-PM	238	<b>0.000400</b>	<b>0.000600</b>	<b>0.000600</b>
<b>GP2</b>	GP-Put	202	NA	NA	NA
	GP-M1	202	NA	NA	NA
	GP-PM	202	NA	NA	NA
	Put-M1	202	NA		NA
	Put-PM	202	NA	NA	NA
	M1-PM	202	NA	<b>0.000600</b>	0.089691
<b>STN1</b>	vSTN-dSTN	192	NA		NA
	vSTN-M1	192	NA	NA	NA
	vSTN-Par	192	NA	NA	
	dSTN-M1	192	NA	<b>0.004400</b>	0.059394
	dSTN-Par	192	NA		<b>0.012499</b>
	Par-M1	192	NA		<b>0.013399</b>
<b>STN2</b>	vSTN-dSTN	182		NA	
	vSTN-M1	182		NA	NA
	vSTN-Par	182	NA	NA	NA
	dSTN-M1	182	NA	NA	NA
	dSTN-Par	182	NA	NA	NA
	Par-M1	182	NA	NA	NA

Table 2.16. Across-day testing of session-wide null PPC:  $p$ -values.

	$p$ -value
GP1	0.000100
GP2	0.000100
STN1	0.000100
STN2	0.000100

**Table 2.17. Baseline testing of intraregional  $\delta\text{-}\gamma_n^{\delta}$  PPC: sequence learning-related  $p$ -values.**

Blank cells indicate no time regions passed initial thresholding. Multiple values in a single cell correspond to multiple time regions that passed initial thresholding.

		$p$ -value			
	Region	$n$	Day 1	Day 3	Day 4
<b>GP1</b>	GP	238			
	Put	238	0.284870		
	M1/S1	238		<b>0.000400</b>	<b>0.046695</b>
	PM	238		0.097890	0.203880
<b>GP2</b>	GP	202	0.19548 <b>0.034697</b>		
	Put	202			0.198180
	M1	202		0.297770 <b>0.001100</b>	0.058994
	PM	202		0.130990	
<b>STN1</b>	vSTN	192	0.184380		
	dSTN	192			0.304670
	M1	192		0.070593	<b>0.024998</b>
	Par	192	<b>0.041596</b>	0.166280	
<b>STN2</b>	vSTN	182			
	dSTN	182	<b>0.000100</b>	0.143390 <b>0.010499</b>	
	M1	182	<b>0.006999</b>	<b>0.000100</b>	<b>0.000100</b>
	Par	182		<b>0.040096</b>	<b>0.002900</b>

**Table 2.18. Across-day testing of intraregional  $\delta\text{-}\gamma_h^{\delta}$  PPC: sequence learning-related  $p$ -values.**

Blank cells indicate no time regions passed initial thresholding. Multiple values in a single cell correspond to multiple time regions that passed initial thresholding.

		<i>p</i> -value			
	Region	<i>n</i>	Day 1 vs. 3	Day 3 vs. 4	Day 1 vs. 4
<b>GP1</b>	GP	476		0.228380	
	Put	476			
	M1/S1	476	0.050295	<b>0.015898</b>	
	PM	476			0.250570
<b>GP2</b>	GP	404			0.186080
	Put	404		0.102790	0.115090
	M1	404	0.186280 <b>0.000300</b>	0.277470	
	PM	404			
<b>STN1</b>	vSTN	384			0.110190
	dSTN	384			<b>0.008599</b>
	M1	384	0.081292	0.133390 <b>0.028397</b>	<b>0.034097</b>
	Par	384			
<b>STN2</b>	vSTN	364			
	dSTN	364			
	M1	364			
	Par	364			<b>0.006899</b>

**Table 2.19. Baseline testing of intraregional  $\delta\gamma_n^{\delta}$  PSI: sequence learning-related  $p$ -values.**

Blank cells indicate no time regions passed initial thresholding. Multiple values in a single cell correspond to multiple time regions that passed initial thresholding. Earlier time regions are listed first. NA, not applicable.

		<i>p</i> -value			
	Region	<i>n</i>	Day 1	Day 3	Day 4
<b>GP1</b>	GP	238	NA	NA	NA
	Put	238	NA	NA	NA
	M1/S1	238	NA	<b>0.001200</b>	<b>0.016998</b>
	PM	238	NA	NA	NA
<b>GP2</b>	GP	202	<b>0.021698</b>	NA	NA
	Put	202	NA	NA	NA
	M1	202	NA		NA
	PM	202	NA	NA	NA
<b>STN1</b>	vSTN	192	NA	NA	NA
	dSTN	192	NA	NA	NA
	M1	192	NA	NA	<b>0.031397</b>
	Par	192	<b>0.008699</b> <b>0.026997</b>	NA	NA
<b>STN2</b>	vSTN	182	NA	NA	NA
	dSTN	182			NA
	M1	182		<b>0.000100</b>	
	Par	182	NA	<b>0.005599</b>	<b>0.017498</b>

**Table 2.20. Baseline testing of movement-related  $\gamma$  amplitude synchronization:  $p$ -values.**

Blank cells indicate no time regions passed initial thresholding. Multiple values in a single cell correspond to multiple time regions that passed initial thresholding. For each statistical test, 10,000 bootstrap samples of gamma amplitude were generated. The  $p$ -value was computed as percent of bootstrap sample means  $< 0$ .

		$p$ -value			
	Region	$n$	Day 1	Day 3	Day 4
<b>GP1</b>	GP	238	0.884712	0.192081	0.956804
	Put	238	0.558444	0.238276	0.788321
	M1/S1	238	<b>0.000100</b>	<b>0.000100</b>	<b>0.000100</b>
	PM	238	0.120588	<b>0.009799</b>	<b>0.000100</b>
<b>GP2</b>	GP	206	0.308669	0.762524	0.695830
	Put	206	0.232177	0.936106	<b>0.047995</b>
	M1	206	<b>0.000100</b>	<b>0.000900</b>	<b>0.000100</b>
	PM	206	0.522548	0.770323	0.067493
<b>STN1</b>	vSTN	154	0.984202	0.202380	0.185681
	dSTN	154	0.996300	<b>0.021198</b>	0.627437
	M1	154	<b>0.006599</b>	<b>0.000100</b>	<b>0.001100</b>
	Par	154	0.853415	<b>0.000100</b>	<b>0.001100</b>
<b>STN2</b>	vSTN	184	0.317568	0.297170	0.198980
	dSTN	184	0.686131	0.794721	0.779622
	M1	184	<b>0.000100</b>	<b>0.000100</b>	<b>0.000100</b>
	Par	184	0.967303	0.647535	0.988501

**Table 2.21. Baseline testing of interregional  $\delta\text{-}\gamma_n^{\delta}$  PPC: sequence learning-related  $p$ -values.**

Blank cells indicate no time regions passed initial thresholding. Multiple values in a single cell correspond to multiple time regions that passed initial thresholding.

		<i>p</i> -value			
	Region	<i>n</i>	Day 1	Day 3	Day 4
<b>GP1</b>	Put-M1/S1	238		0.194480 <b>0.002200</b>	0.178580
	Put-PM	238		<b>0.000500</b>	0.141290
	M1/S1-PM	238		<b>0.026197</b>	0.305570
	PM-M1/S1	238	0.051495 0.309370	<b>0.001500</b>	0.086391
<b>GP2</b>	Put-M1	202			
	Put-PM	202	0.137190		0.140690
	M1-PM	202	0.312570	0.072593	0.199380 0.299170
	PM-M1	202		<b>0.001500</b>	0.103290
<b>STN1</b>	vSTN-dSTN	192		<b>0.007399</b>	0.110590
	dSTN-M1	192	0.333870	<b>0.000100</b>	<b>0.002100</b>
	Par-M1	192	0.151680	<b>0.001700</b>	
<b>STN2</b>	vSTN-dSTN	182			
	dSTN-M1	182	<b>0.000100</b>		
	Par-M1	182	<b>0.000100</b>	<b>0.002700</b>	



**Table 2.22. Across-day testing of interregional  $\delta\text{-}\gamma_h^{\delta}$  PPC: sequence learning-related  $p$ -values.**

Blank cells indicate no time regions passed initial thresholding. Multiple values in a single cell correspond to multiple time regions that passed initial thresholding.

		<i>p</i> -value			
	Region	<i>n</i>	Day 1 vs. 3	Day 3 vs. 4	Day 1 vs. 4
<b>GP1</b>	Put-M1/S1	238	<b>0.047695</b> <b>0.002000</b>	0.223680 <b>0.005400</b>	0.192780
	Put-PM	238	0.060894 0.051795	0.051095 0.152480	
	M1/S1-PM	238	0.050395		
	PM-M1/S1	238	<b>0.008599</b>	<b>0.007899</b>	
<b>GP2</b>	Put-M1	202			
	Put-PM	202	0.267070		0.257170
	M1-PM	202			
	PM-M1	202	0.069393		
<b>STN1</b>	vSTN-dSTN	192	<b>0.003200</b>		
	dSTN-M1	192	<b>0.001100</b>	<b>0.000800</b>	0.076792 0.136990
	Par-M1	192	<b>0.004600</b>	<b>0.011999</b>	
<b>STN2</b>	vSTN-dSTN	182			
	dSTN-M1	182			
	Par-M1	182			<b>0.000100</b>

**Table 2.23. Baseline testing of interregional  $\delta\gamma_n^{\circ}$  PSI: sequence learning-related  $p$ -values.**

Blank cells indicate no time regions passed initial thresholding. Multiple values in a single cell correspond to multiple time regions that passed initial thresholding. Earlier time regions are listed first. NA, not applicable.

		<i>p</i> -value			
	Region	<i>n</i>	Day 1	Day 3	Day 4
<b>GP1</b>	Put-M1/S1	238	NA	<b>0.005399</b>	NA
	Put-PM	238	NA	<b>0.025097</b>	NA
	M1/S1-PM	238	NA	<b>0.031497</b>	NA
	PM-M1/S1	238	NA	<b>0.006699</b>	NA
<b>GP2</b>	Put-M1	202	NA	NA	NA
	Put-PM	202	NA	NA	NA
	M1-PM	202	NA	NA	NA
	PM-M1	202	NA		NA
<b>STN1</b>	vSTN-dSTN	192	NA	0.105989 <b>0.043797</b>	NA
	dSTN-M1	192	NA	<b>0.006399</b>	<b>0.047595</b>
	Par-M1	192	NA	<b>0.022698</b>	NA
<b>STN2</b>	vSTN-dSTN	182	NA	NA	NA
	dSTN-M1	182		NA	NA
	Par-M1	182	<b>0.048195</b>	<b>0.021898</b>	NA

**Table 2.24. Baseline testing of movement-related  $\beta$  amplitude desynchronization: *p*-values.**

Blank cells indicate no time regions passed initial thresholding. Multiple values in a single cell correspond to multiple time regions that passed initial thresholding.

		<i>p</i> -value			
	Region	<i>n</i>	Day 1	Day 3	Day 4
<b>GP1</b>	GP	238	<b>0.000100</b>	<b>0.000100</b>	<b>0.000100</b>
	Put	238	<b>0.000900</b>	<b>0.000100</b>	<b>0.000300</b>
	M1/S1	238	<b>0.000100</b>	<b>0.000100</b>	<b>0.000100</b>
	PM	238	<b>0.000100</b>	<b>0.000100</b>	<b>0.000100</b>
<b>GP2</b>	GP	206	0.518448	<b>0.002800</b>	0.839816
	Put	206	<b>0.000100</b>	<b>0.000300</b>	<b>0.001000</b>
	M1	206	<b>0.000100</b>	<b>0.000100</b>	<b>0.000100</b>
	PM	206	<b>0.000100</b>	<b>0.000500</b>	<b>0.000100</b>
<b>STN1</b>	vSTN	154	0.072893	0.128887	0.230977
	dSTN	154	<b>0.001900</b>	<b>0.017898</b>	<b>0.009299</b>
	M1	154	<b>0.000100</b>	<b>0.000100</b>	<b>0.000100</b>
	Par	154	<b>0.004400</b>	<b>0.000100</b>	<b>0.000100</b>
<b>STN2</b>	vSTN	184	0.878312	0.796820	0.958004
	dSTN	184	0.200280	0.142286	0.298270
	M1	184	<b>0.000600</b>	<b>0.003700</b>	<b>0.000100</b>
	Par	184	0.931507	0.510249	0.300370

**Table 2.25. Baseline testing of intraregional  $\delta$ - $\beta^{\delta}$  PPC: sequence learning-related  $p$ -values.**

Blank cells indicate no time regions passed initial thresholding. Multiple values in a single cell correspond to multiple time regions that passed initial thresholding

		<i>p</i> -value			
	Region	<i>n</i>	Day 1	Day 3	Day 4
<b>GP1</b>	GP	238	0.078792 <b>0.007699</b>	<b>0.002000</b>	<b>0.000100</b>
	Put	238	0.101590	0.137790	
	M1/S1	238	<b>0.008199</b> 0.122790	<b>0.000100</b>	0.082492
	PM	238	<b>0.011399</b>	<b>0.002400</b>	<b>0.006799</b>
<b>GP2</b>	GP	202	<b>0.013999</b>	0.227380 0.175280	
	Put	202	0.066593		<b>0.048995</b>
	M1	202		<b>0.000200</b>	<b>0.017298</b>
	PM	202	<b>0.019398</b>	0.060294	0.154080
<b>STN1</b>	vSTN	192			
	dSTN	192			<b>0.015498</b>
	M1	192		<b>0.000500</b>	<b>0.001600</b>
	Par	192			<b>0.002300</b>
<b>STN2</b>	vSTN	182			
	dSTN	182	<b>0.000100</b>	<b>0.027397</b>	<b>0.000100</b>
	M1	182	0.134290 <b>0.015798</b>	0.085591	<b>0.004100</b>
	Par	182			

**Table 2.26. Across-day testing of intraregional  $\delta$ - $\beta^5$  PPC: sequence learning-related  $p$ -values.**

Blank cells indicate no time regions passed initial thresholding. Multiple values in a single cell correspond to multiple time regions that passed initial thresholding.

		<i>p</i> -value			
	Region	<i>n</i>	Day 1 vs. 3	Day 3 vs. 4	Day 1 vs. 4
<b>GP1</b>	GP	476		<b>0.045295</b>	<b>0.025497</b>
	Put	476			
	M1/S1	476	0.153880	<b>0.033597</b>	<b>0.009299</b>
	PM	476	0.212180		
<b>GP2</b>	GP	404			
	Put	404			0.244980 <b>0.006199</b>
	M1	404	<b>0.003300</b>	<b>0.000400</b>	0.239280 0.158480
	PM	404		0.220780	
<b>STN1</b>	vSTN	384			
	dSTN	384		0.193880	
	M1	384			
	Par	384			<b>0.005699</b>
<b>STN2</b>	vSTN	364			
	dSTN	364			
	M1	364			
	Par	364			

**Table 2.27. Baseline testing of intraregional  $\delta\text{-}\beta^5$  PSI: sequence learning-related  $p$ -values.**

Blank cells indicate no time regions passed initial thresholding. Multiple values in a single cell correspond to multiple time regions that passed initial thresholding. Earlier time regions are listed first. NA, not applicable.

		<i>p</i> -value			
	Region	<i>n</i>	Day 1	Day 3	Day 4
<b>GP1</b>	GP	238	<b>0.005799</b>		<b>0.008199</b>
	Put	238	NA	NA	NA
	M1/S1	238		0.059694 <b>0.014699</b>	NA
	PM	238	0.080892		0.096390
<b>GP2</b>	GP	202		NA	NA
	Put	202	NA	NA	
	M1	202	NA		<b>0.001200</b>
	PM	202	<b>0.028397</b> <b>0.015998</b>	NA	NA
<b>STN1</b>	vSTN	192	NA	NA	NA
	dSTN	192	NA	NA	
	M1	192	NA	<b>0.000100</b>	<b>0.000300</b>
	Par	192	NA	NA	0.067693
<b>STN2</b>	vSTN	182	NA	NA	NA
	dSTN	182			
	M1	182		NA	0.060394
	Par	182	NA	NA	NA

**Table 2.28. Baseline testing of interregional  $\delta\text{-}\beta^{\delta}$  PPC: sequence learning-related  $p$ -values.**

Blank cells indicate no time regions passed initial thresholding. Multiple values in a single cell correspond to multiple time regions that passed initial thresholding.

		<i>p</i> -value			
	<b>Region</b>	<i>n</i>	<b>Day 1</b>	<b>Day 3</b>	<b>Day 4</b>
<b>GP1</b>	Put-M1/S1	238	<b>0.002300</b>	<b>0.001100</b>	<b>0.005799</b>
	Put-PM	238	<b>0.025697</b>	<b>0.003700</b>	<b>0.027197</b>
	M1/S1-GP	238	0.108990		<b>0.013499</b>
<b>GP2</b>	Put-M1	202		<b>0.000500</b>	0.137590 0.066093
	Put-PM	202		0.075092	0.148190
	M1-GP	202	0.238080	<b>0.000500</b>	<b>0.042296</b>

**Table 2.29. Across-day testing of interregional  $\delta$ - $\beta^5$  PPC: sequence learning-related  $p$ -values.**

Blank cells indicate no time regions passed initial thresholding. Multiple values in a single cell correspond to multiple time regions that passed initial thresholding.

		<i>p</i> -value			
	Region	<i>n</i>	Day 1 vs. 3	Day 3 vs. 4	Day 1 vs. 4
<b>GP1</b>	Put-M1/S1	238	<b>0.016398</b>	<b>0.005500</b>	
	Put-PM	238	<b>0.028997</b>	<b>0.006799</b>	
	M1/S1-GP	238			
<b>GP2</b>	Put-M1	202	0.175780		0.129790
	Put-PM	202		<b>0.033297</b>	
	M1-GP	202	0.118190		



**Table 2.30. Baseline testing of interregional  $\delta\text{-}\beta^{\text{S}}$  PSI: sequence learning-related  $p$ -values.**

Blank cells indicate no time regions passed initial thresholding. Multiple values in a single cell correspond to multiple time regions that passed initial thresholding. Earlier time regions are listed first. NA, not applicable.

		<i>p</i> -value			
	Region	<i>n</i>	Day 1	Day 3	Day 4
GP1	Put-M1/S1	238	<b>0.046895</b>	<b>0.002900</b>	
	Put-PM	238	<b>0.012599</b>	<b>0.006699</b>	
	M1/S1-GP	238	NA	NA	
GP2	Put-M1	202	NA		NA
	Put-PM	202	NA	NA	NA
	M1-GP	202	NA	<b>0.006599</b>	0.057394

**Table 2.31. Baseline testing of interregional  $\delta\text{-}\beta^{\delta}$  PPC: task exposure-related  $p$ -values.**

Blank cells indicate no time regions passed initial thresholding. Multiple values in a single cell correspond to multiple time regions that passed initial thresholding.

		<i>p</i> -value			
	Region	<i>n</i>	Day 1	Day 3	Day 4
<b>GP1</b>	GP-M1/S1	238	<b>0.002600</b>	<b>0.000100</b>	<b>0.000400</b>
	GP-PM	238	<b>0.001800</b>	<b>0.000100</b>	<b>0.000300</b>
	Put-GP	238	<b>0.001400</b>	<b>0.004600</b>	<b>0.024698</b>
	PM-M1/S1	238	<b>0.020798</b>	<b>0.000300</b>	<b>0.000200</b>
<b>GP2</b>	GP-M1	202			<b>0.043396</b>
	GP-PM	202			
	Put-GP	202	<b>0.031797</b> 0.236980 0.231280		
	PM-M1	202	<b>0.018498</b>	<b>0.001000</b>	<b>0.020098</b>
<b>STN1</b>	M1-Par	192			<b>0.002600</b>
	Par-dSTN	192			<b>0.006799</b> 0.100790
<b>STN2</b>	M1-Par	182	0.110690		
	Par-dSTN	182			

**Table 2.32. Across-day testing of interregional  $\delta\text{-}\beta^{\circ}$  PPC: task exposure-related  $p$ -values.**

Blank cells indicate no time regions passed initial thresholding. Multiple values in a single cell correspond to multiple time regions that passed initial thresholding.

		<i>p</i> -value			
	Region	<i>n</i>	Day 1 vs. 3	Day 3 vs. 4	Day 1 vs. 4
<b>GP1</b>	GP-M1/S1	238	<b>0.036996</b> <b>0.004900</b>	0.137690	0.110190
	GP-PM	238			
	Put-GP	238		0.131690	
	PM-M1/S1	238	<b>0.000200</b>		<b>0.000400</b>
<b>GP2</b>	GP-M1	202			<b>0.010399</b>
	GP-PM	202	0.240780		0.215780
	Put-GP	202			
	PM-M1	202	0.192780		
<b>STN1</b>	M1-Par	192		0.058994	<b>0.004100</b>
	Par-dSTN	192		0.130390 0.156380	<b>0.004600</b> 0.140990
<b>STN2</b>	M1-Par	182	0.157680		0.135390
	Par-dSTN	182			

**Table 2.33. Baseline testing of interregional  $\delta\text{-}\beta^{\delta}$  PSI: task exposure-related  $p$ -values.**

Blank cells indicate no time regions passed initial thresholding. Multiple values in a single cell correspond to multiple time regions that passed initial thresholding. Earlier time regions are listed first. NA, not applicable.

		<i>p</i> -value			
	Region	<i>n</i>	Day 1	Day 3	Day 4
<b>GP1</b>	GP-M1/S1	238	0.079892		<b>0.002200</b>
	GP-PM	238			<b>0.000400</b>
	Put-GP	238		<b>0.005699</b>	<b>0.018698</b>
	PM-M1/S1	238		0.057894	<b>0.028197</b>
<b>GP2</b>	GP-M1	202	NA	NA	
	GP-PM	202	NA	NA	NA
	Put-GP	202		NA	NA
	PM-M1	202		<b>0.028497</b>	<b>0.000300</b>
<b>STN1</b>	M1-Par	192	NA	NA	<b>0.006099</b>
	Par-dSTN	192	NA	NA	<b>0.001500</b>
<b>STN2</b>	M1-Par	182	NA	NA	NA
	Par-dSTN	182	NA	NA	NA

## **Chapter 3: Recommendations for Future Work and the Restoration of Fine Motor Control**

Over the past century, the focus of motor control research has shifted from simple reflex models to more complex network-based models that account for hierarchical organization, dynamic neural coding and cross-regional interactions. With this development has come the idea that movement is not simply a direct output of motor cortex activity but rather an emergent property of a distributed network, which integrates signals across various cortical and subcortical regions. Despite these advances, an understanding of motor-related local activity in the context of cross-area coordinated dynamics remains unclear, particularly in the deterioration of skilled dexterous control in Parkinson's Disease (PD). This dissertation sought to address this knowledge gap by evaluating the learning-dependent oscillatory local and network dynamics that prepare for the production of fine motor sequences in PD. However, further research across several domains is necessary to achieve a comprehensive understanding and to inform effective therapeutic restoration of fine motor learning and control in PD.

*Chapter 2* examined how initiation-related neural activity varies with overall performance across days but did not quantitatively differentiate the effects of bradykinesia and sequence preplanning on motor initiation or execution. Differentiating the relative impact of bradykinesia and efficacy of sequence preplanning is challenging, particularly given the possibility that bradykinesia and impaired sequence preplanning are interdependent or are covariates of the same underlying process. In *Chapter 2*, bradykinesia ratings were relatively stable across days, which may allow coarse qualitative differentiation

from variation in preplanning, but future work should quantitatively model these processes' effects on reaction time and trial duration and correlate them with neural activity. For example, changes in sequence preplanning could correlate with lasting changes in reaction time across days that follow an expected learning curve shape, with the degree of bradykinesia producing variation around that curve. Immediately prior to each sequence trial, bradykinesia could be estimated on a trial of non-sequential movement or repetitive movements lacking variation in serial order (e.g., repeated taps with the same finger). If bradykinesia and impaired sequence preplanning are even partially non-overlapping processes in explained variance (i.e., in the absence of a perfect correlation), such an approach may prove fruitful in disambiguating them and modeling their joint effect.

Even without quantitatively disambiguating impaired sequence preplanning from bradykinesia, *Chapter 2* identified potential pre-movement neural correlates of successful and impaired learning, warranting further characterization of the observed neural dynamics. The observation herein of a frequency-based framework for hierarchical cross-regional coordination of preparatory neural activity is consistent with the emerging view of motor control as a process supported by hierarchical neural architectures in both structure and function<sup>17,191,192</sup>. The identification of learning-related cross-area cross-frequency coupling as a potential optimization mechanism for the organization of motor preparation in a temporally structured manner was particularly important. It suggests that disrupted temporal coordination between cortical and basal ganglia structures during motor planning could result in less effective multi-element preplanning, leading to greater computational overhead during movement and worse

motor performance. Work in animal models of PD could probe whether these oscillatory signals are purely epiphenomenal and whether they can be manipulated to improve multi-element preplanning by improving neural ensemble activation. Further, characterizing and manipulating any plasticity associated with across-day changes in pre-movement neural dynamics may inform stimulation protocols to enhance motor learning-related circuit plasticity in humans with PD.

After sequence initiation, ongoing fine motor control is impaired in PD, and extending analysis into the active movement epoch would allow behavioral and neurophysiological characterization of this motor deficit. While it is known that dexterity and possibly online action sequencing are impaired, additional investigation is required to fully clarify the precise aspects of motor sequence execution that are compromised in PD<sup>7,71,72,74,75,104,193,194</sup>. The pursuit of this aim may combine behavioral characterization of online action sequencing with electrophysiological characterization of the encoding of fingers, sequence elements and motor chunks. Future work may ask, if cortico-basal ganglia temporal coordination is disrupted during motor execution, how does this impact online action sequencing and finger coordination? How does pre-movement functional connectivity influence the unfolding of neural dynamics during motor execution? Analyzing the motor execution epoch might further position the sequence encoding hierarchy within a hierarchy of local and network activity, which may grant insight into the optimal temporal windows for therapeutic modulation of fine motor control in PD.

Investigating the impact of degeneration in cognition and sensory processing—often overlooked in PD—on multi-element preplanning may provide a more comprehensive

view of fine motor control in PD. *Chapter 2* identified task exposure-related effects of network functional connectivity that were largely absent in subjects with impaired sequence learning. These included functional connectivity led by the premotor and parietal cortices, two regions connected to each other and immediately downstream of the prefrontal cortex. The premotor cortex has a known role in flexible action sequencing, and the parietal cortex helps integrate sensory feedback with spatial information to influence premotor commands<sup>12</sup>. Thus, sensory processing and its influence on flexible action sequencing may dynamically adjust based on task familiarity, while cognitive functions like attention could modulate these adjustments through input from the prefrontal cortex. This high-level process may be essential to adapting to new or complex motor tasks. If the ability to learn a specific motor sequence depends on adaptation to the overarching task, then improving a subject's ability to adapt to new motor tasks would broadly impact their ability to learn and perform motor sequences in different contexts. Enhancing high-level adaptability may thus prove therapeutically superior to targeting specific motor skills, underscoring the importance of this avenue of research for efficient identification of broadly effective treatment for impaired fine motor control.

Given the historically high variability in sequence learning outcomes in individuals with PD, the present findings' generalizability should be evaluated across other movement and treatment types, for larger cohorts and over longer learning windows. For example, does cortically-led network delta ( $\delta$ ) coherence precede composite or internally cued motor sequences? Does it precede non-sequential movements? Does it still appear to form a framework for the development of cross-frequency coupling? For larger cohorts,



in what fraction of subjects is excessive basal ganglia  $\delta$  synchrony associated with impaired motor learning? If any subjects demonstrate improved motor learning on open-loop deep brain stimulation (DBS), is it associated with suppression of highly synchronized and unresponsive basal ganglia  $\delta$ ? Furthermore, motor skill learning and memory stabilization have a long tail that can last months or years—a fact readily apparent in the careers of professional athletes. Longer observation windows would grant novel insight into long-term learning, consolidation and memory retrieval. This would help characterize the neural basis of the gradual deterioration in the ability to refine and recall mastered skills in PD. Such investigation would help clarify the usefulness of the identified oscillatory dynamics for predicting effective long-term and perhaps disease stage-specific therapeutic strategies in individuals with impaired fine motor control.

Finally, as this thesis identified a failure of dopamine replacement therapy to allow demonstration of learning in half of subjects, therapeutic methods employing movement-locked neuromodulation should be considered. For example, *Chapter 2* suggests that putamen  $\delta$  phase—likely both the absolute phase and the relative phase offset with respect to premotor cortex  $\delta$  phase—might be critically important to acquiring new motor sequences or initiating learned sequences. Artificially inducing premotor cortex-putamen  $\delta$  phase coherence may be a promising direction to restore corticostriatal temporal coordination. In subjects with sensing-capable DBS leads and electroencephalography or motor electrocorticography arrays, putamen phase and its offset from premotor phase could be correlated with single-trial performance. Alternatively, variably timed putamen stimulation could assess learning and

performance outcomes across the space of induced putamen phase dynamics. Detection of motor intention in the cortex could then trigger phase-specific stimulation of the putamen, aligning it with the optimal phase for motor onset. The practicality of this approach would depend in part on the generalizability across sequences of the optimal putamen phase. Extending these investigations will be key to assessing the practicality of phase-specific modulation for improving the performance of complex dexterous movements in PD.

### *Summary*

Motor symptoms remain one of the most debilitating aspects of PD, and understanding the neural bases of these symptoms is essential for developing more effective treatments that improve the quality of life of individuals with PD. By focusing on complex hand movements, this research has provided critical insights into an often-overlooked aspect of motor dysfunction in PD that directly impacts daily life activities and autonomy. The central aim presented at the start of this thesis was to describe a functional network model of learning-related pre-movement neural population activity for fine motor sequences in PD. *Chapter 2* describes evidence suggestive of distributed learning-dependent multi-element preparatory activity, links it to a hierarchical functional network architecture and identifies a subcortical oscillatory process that may contribute to learning impairments by disrupting optimization of preparatory neural population dynamics. This dissertation has begun to untangle the complex neural processes

underpinning motor sequence initiation and learning in PD, laying the groundwork for future breakthroughs in both the neuroscientific study of PD and clinical treatment.

## References

1. Dorsey ER, Sherer T, Okun MS, et al. The Emerging Evidence of the Parkinson Pandemic. *J Park Dis*. 2018;8(s1):S3-S8. doi:10.3233/JPD-181474
2. Bhidayasiri R, Sringean J, Phumphid S, et al. The rise of Parkinson's disease is a global challenge, but efforts to tackle this must begin at a national level: a protocol for national digital screening and "eat, move, sleep" lifestyle interventions to prevent or slow the rise of non-communicable diseases in Thailand. *Front Neurol*. 2024;15. doi:10.3389/fneur.2024.1386608
3. Xia R, Mao ZH. Progression of motor symptoms in Parkinson's disease. *Neurosci Bull*. 2012;28(1):39-48. doi:10.1007/s12264-012-1050-z
4. Mazzoni P, Shabbott B, Cortés JC. Motor Control Abnormalities in Parkinson's Disease. *Cold Spring Harb Perspect Med*. 2012;2(6):a009282. doi:10.1101/cshperspect.a009282
5. Doyon J. Motor sequence learning and movement disorders. *Curr Opin Neurol*. 2008;21(4):478-483. doi:10.1097/WCO.0b013e328304b6a3
6. Wu T, Hallett M, Chan P. Motor automaticity in Parkinson's disease. *Neurobiol Dis*. 2015;82:226-234. doi:10.1016/j.nbd.2015.06.014
7. Marinelli L, Quartarone A, Hallett M, Frazzitta G, Ghilardi MF. The many facets of motor learning and their relevance for Parkinson's disease. *Clin Neurophysiol*. 2017;128(7):1127-1141. doi:10.1016/j.clinph.2017.03.042
8. Vasu D, Hui LM, Fong W, Choong P, Chou LW. Evidence-Based Physiotherapeutic Interventions Enhancing Hand Dexterity, Activities of Daily Living and Quality of Life of Parkinson's Disease Patients: A Systematic Review. *Can J Neurol Sci*.

2024;1(13). doi:10.1017/cjn.2024.53

9. Rahman S, Griffin HJ, Quinn NP, Jahanshahi M. Quality of life in Parkinson's disease: The relative importance of the symptoms. *Mov Disord.* 2008;23(10):1428-1434. doi:10.1002/mds.21667
10. Prell T, Schöenberg A, Heimrich KG. The impact of loneliness on quality of life in people with Parkinson's disease: results from the Survey of Health, Ageing and Retirement in Europe. *Front Med.* 2023;10. doi:10.3389/fmed.2023.1183289
11. Vardanyan R, König HH, Hajek A. Association between Parkinson's Disease and Psychosocial Factors: Results of the Nationally Representative German Ageing Survey. *J Clin Med.* 2022;11(15):4569. doi:10.3390/jcm11154569
12. Rosenbaum DA. *Human Motor Control.* Academic Press; 2009.
13. Diedrichsen J, Kornysheva K. Motor skill learning between selection and execution. *Trends Cogn Sci.* 2015;19(4):227-233. doi:10.1016/j.tics.2015.02.003
14. Giszter SF. MOTOR PRIMITIVES - New Data and Future Questions. *Curr Opin Neurobiol.* 2015;33:156-165. doi:10.1016/j.conb.2015.04.004
15. Sakai K, Kitaguchi K, Hikosaka O. Chunking during human visuomotor sequence learning. *Exp Brain Res.* 2003;152(2):229-242. doi:10.1007/s00221-003-1548-8
16. Rosenbaum DA, Kenny SB, Derr MA. Hierarchical control of rapid movement sequences. *J Exp Psychol Hum Percept Perform.* 1983;9(1):86-102. doi:10.1037/0096-1523.9.1.86
17. Balleine BW, Dezfouli A, Ito M, Doya K. Hierarchical control of goal-directed action in the cortical-basal ganglia network. *Curr Opin Behav Sci.* 2015;5:1-7. doi:10.1016/j.cobeha.2015.06.001

18. Jin X, Tecuapetla F, Costa RM. Basal ganglia subcircuits distinctively encode the parsing and concatenation of action sequences. *Nat Neurosci*. 2014;17(3):423-430. doi:10.1038/nn.3632
19. Aldridge JW, Berridge KC. Coding of serial order by neostriatal neurons: a “natural action” approach to movement sequence. *J Neurosci Off J Soc Neurosci*. 1998;18(7):2777-2787.
20. Jin X, Costa RM. Start/stop signals emerge in nigrostriatal circuits during sequence learning. *Nature*. 2010;466(7305):457-462. doi:10.1038/nature09263
21. Shima K, Tanji J. Both Supplementary and Presupplementary Motor Areas Are Crucial for the Temporal Organization of Multiple Movements. *J Neurophysiol*. 1998;80(6):3247-3260. doi:10.1152/jn.1998.80.6.3247
22. Tanji J, Shima K. Role for supplementary motor area cells in planning several movements ahead. *Nature*. 1994;371(6496):413-416. doi:10.1038/371413a0
23. Rothwell PE, Hayton SJ, Sun GL, Fuccillo MV, Lim BK, Malenka RC. Input- and Output-Specific Regulation of Serial Order Performance by Corticostriatal Circuits. *Neuron*. 2015;88(2):345-356. doi:10.1016/j.neuron.2015.09.035
24. Roth RH, Ding JB. Cortico-basal ganglia plasticity in motor learning. *Neuron*. 2024;112(15):2486-2502. doi:10.1016/j.neuron.2024.06.014
25. Lemon RN. Descending Pathways in Motor Control. *Annu Rev Neurosci*. 2008;31(Volume 31, 2008):195-218. doi:10.1146/annurev.neuro.31.060407.125547
26. Kuypers HGJM. Anatomy of the Descending Pathways. In: *Comprehensive Physiology*. John Wiley & Sons, Ltd; 2011:597-666. doi:10.1002/cphy.cp010213
27. Taricotti L, Mattioli L, Viganò L, et al. Object-oriented hand dexterity and grasping

- abilities, from the animal quarters to the neurosurgical OR: a systematic review of the underlying neural correlates in non-human, human primate and recent findings in awake brain surgery. *Front Integr Neurosci.* 2024;18. doi:10.3389/fnint.2024.1324581
28. Vesia M, Crawford JD. Specialization of reach function in human posterior parietal cortex. *Exp Brain Res.* 2012;221(1):1-18. doi:10.1007/s00221-012-3158-9
29. Wey HY, Phillips KA, McKay DR, et al. Multi-region hemispheric specialization differentiates human from nonhuman primate brain function. *Brain Struct Funct.* 2014;219(6):2187-2194. doi:10.1007/s00429-013-0620-9
30. Lemon RN, Griffiths J. Comparing the function of the corticospinal system in different species: Organizational differences for motor specialization? *Muscle Nerve.* 2005;32(3):261-279. doi:10.1002/mus.20333
31. Verendeev A, Sherwood CC, Hopkins WD. Organization and Evolution of the Neural Control of the Hand in Primates: Motor Systems, Sensory Feedback, and Laterality. In: Kivell TL, Lemelin P, Richmond BG, Schmitt D, eds. *The Evolution of the Primate Hand: Anatomical, Developmental, Functional, and Paleontological Evidence.* Springer; 2016:131-153. doi:10.1007/978-1-4939-3646-5\_6
32. van Duinen H, Gandevia SC. Constraints for control of the human hand. *J Physiol.* 2011;589(23):5583-5593. doi:10.1113/jphysiol.2011.217810
33. Orban GA, Caruana F. The neural basis of human tool use. *Front Psychol.* 2014;5. doi:10.3389/fpsyg.2014.00310
34. Natraj N, Silversmith DB, Chang EF, Ganguly K. Compartmentalized dynamics within a common multi-area mesoscale manifold represent a repertoire of human

- hand movements. *Neuron*. 2022;110(1):154-174.e12.  
doi:10.1016/j.neuron.2021.10.002
35. Kubánek J, Miller KJ, Ojemann JG, Wolpaw JR, Schalk G. Decoding flexion of individual fingers using electrocorticographic signals in humans. *J Neural Eng*. 2009;6(6):066001. doi:10.1088/1741-2560/6/6/066001
36. Liao K, Xiao R, Gonzalez J, Ding L. Decoding Individual Finger Movements from One Hand Using Human EEG Signals. *PLOS ONE*. 2014;9(1):e85192. doi:10.1371/journal.pone.0085192
37. Boillat Y, Bazin PL, van der Zwaag W. Whole-body somatotopic maps in the cerebellum revealed with 7T fMRI. *NeuroImage*. 2020;211:116624. doi:10.1016/j.neuroimage.2020.116624
38. Maillard L, Ishii K, Bushara K, Waldvogel D, Schulman AE, Hallett M. Mapping the basal ganglia. *Neurology*. 2000;55(3):377-383. doi:10.1212/WNL.55.3.377
39. Pinsard B, Boutin A, Gabitov E, Lungu O, Benali H, Doyon J. Consolidation alters motor sequence-specific distributed representations. *eLife*. 2019;8. doi:10.7554/eLife.39324
40. Hardwick RM, Rottschy C, Miall RC, Eickhoff SB. A quantitative meta-analysis and review of motor learning in the human brain. *NeuroImage*. 2013;67:283-297. doi:10.1016/j.neuroimage.2012.11.020
41. Errante A, Fogassi L. Activation of cerebellum and basal ganglia during the observation and execution of manipulative actions. *Sci Rep*. 2020;10(1):12008. doi:10.1038/s41598-020-68928-w
42. Andersen KW, Madsen KH, Siebner HR. Discrete finger sequences are widely



- represented in human striatum. *Sci Rep.* 2020;10(1):13189.  
doi:10.1038/s41598-020-69923-x
43. Yokoi A, Arbuckle SA, Diedrichsen J. Does human primary motor cortex represent sequences of finger movements? *bioRxiv*. Published online June 29, 2017:157438.  
doi:10.1101/157438
44. Gordon EM, Chauvin RJ, Van AN, et al. A somato-cognitive action network alternates with effector regions in motor cortex. *Nature*. 2023;617(7960):351-359.  
doi:10.1038/s41586-023-05964-2
45. Deo DR, Okorokova EV, Pritchard AL, et al. A mosaic of whole-body representations in human motor cortex. Published online September 16, 2024:2024.09.14.613041.  
doi:10.1101/2024.09.14.613041
46. Lungu O, Monchi O, Albouy G, et al. Striatal and hippocampal involvement in motor sequence chunking depends on the learning strategy. *PloS One*. 2014;9(8):e103885. doi:10.1371/journal.pone.0103885
47. Wymbs NF, Bassett DS, Mucha PJ, Porter MA, Grafton ST. Differential Recruitment of the Sensorimotor Putamen and Frontoparietal Cortex during Motor Chunking in Humans. *Neuron*. 2012;74(5):936-946. doi:10.1016/j.neuron.2012.03.038
48. Yokoi A, Diedrichsen J. Neural Organization of Hierarchical Motor Sequence Representations in the Human Neocortex. *Neuron*. 2019;103(6):1178-1190.e7.  
doi:10.1016/j.neuron.2019.06.017
49. Lehericy S, Benali H, Moortele PFV de, et al. Distinct basal ganglia territories are engaged in early and advanced motor sequence learning. *Proc Natl Acad Sci*. 2005;102(35):12566-12571. doi:10.1073/pnas.0502762102

50. Doyon J, Benali H. Reorganization and plasticity in the adult brain during learning of motor skills. *Curr Opin Neurobiol.* 2005;15(2):161-167. doi:10.1016/j.conb.2005.03.004
51. Gabitov E, Lungu O, Albouy G, Doyon J. Weaker Inter-hemispheric and Local Functional Connectivity of the Somatomotor Cortex During a Motor Skill Acquisition Is Associated With Better Learning. *Front Neurol.* 2019;10:1242. doi:10.3389/fneur.2019.01242
52. Anwar AR, Muthalib M, Perrey S, et al. Effective Connectivity of Cortical Sensorimotor Networks During Finger Movement Tasks: A Simultaneous fNIRS, fMRI, EEG Study. *Brain Topogr.* 2016;29(5):645-660. doi:10.1007/s10548-016-0507-1
53. Heitger MH, Ronsse R, Dhollander R, Dupont P, Caeyenberghs K, Swinnen SP. Motor learning-induced changes in functional brain connectivity as revealed by means of graph-theoretical network analysis. *NeuroImage.* 2012;61(3):633-650. doi:https://doi.org/10.1016/j.neuroimage.2012.03.067
54. Debas K, Carrier J, Barakat M, et al. Off-line consolidation of motor sequence learning results in greater integration within a cortico-striatal functional network. *NeuroImage.* 2014;99:50-58. doi:10.1016/j.neuroimage.2014.05.022
55. Adam JJ, Van Veggel LM. Discrete Finger Response Latencies in a Simple Reaction Time Task. *Percept Mot Skills.* 1991;73(3):863-866. doi:10.2466/pms.1991.73.3.863
56. Martin JA, Zimmermann N, Scheef L, et al. Disentangling motor planning and motor execution in unmedicated de novo Parkinson's disease patients: An fMRI study. *NeuroImage Clin.* 2019;22:101784. doi:10.1016/j.nicl.2019.101784

57. Meule A. Reporting and Interpreting Task Performance in Go/No-Go Affective Shifting Tasks. *Front Psychol.* 2017;8. doi:10.3389/fpsyg.2017.00701
58. Tyburski E, Kerestey M, Kerestey P, Radoń S, Mueller ST. Assessment of Motor Planning and Inhibition Performance in Non-Clinical Sample—Reliability and Factor Structure of the Tower of London and Go/No Go Computerized Tasks. *Brain Sci.* 2021;11(11):1420. doi:10.3390/brainsci11111420
59. Narmashiri A. Effects of stimulus onset asynchrony on cognitive control in healthy adults. *PLOS ONE.* 2024;19(7):e0306609. doi:10.1371/journal.pone.0306609
60. Simmonds DJ, Pekar JJ, Mostofsky SH. Meta-analysis of Go/No-go tasks demonstrating that fMRI activation associated with response inhibition is task-dependent. *Neuropsychologia.* 2008;46(1):224-232. doi:10.1016/j.neuropsychologia.2007.07.015
61. Ariani G, Diedrichsen J. Sequence learning is driven by improvements in motor planning. *J Neurophysiol.* 2019;121(6):2088-2100. doi:10.1152/jn.00041.2019
62. Ariani G, Kordjazi N, Pruszynski JA, Diedrichsen J. The Planning Horizon for Movement Sequences. *eneuro.* 2021;8(2):ENEURO.0085-21.2021. doi:10.1523/ENEURO.0085-21.2021
63. Verwey WB, Shea CH, Wright DL. A cognitive framework for explaining serial processing and sequence execution strategies. *Psychon Bull Rev.* 2015;22(1):54-77. doi:10.3758/s13423-014-0773-4
64. Wong AL, Haith AM, Krakauer JW. Motor Planning. *The Neuroscientist.* 2015;21(4):385-398. doi:10.1177/1073858414541484
65. Verwey WB. Evidence for the development of concurrent processing in a sequential

- keypressing task. *Acta Psychol (Amst)*. 1994;85(3):245-262.  
doi:10.1016/0001-6918(94)90038-8
66. Zhang Y, Larcher KMH, Misic B, Dagher A. Anatomical and functional organization of the human substantia nigra and its connections. Johansen-Berg H, ed. *eLife*. 2017;6:e26653. doi:10.7554/eLife.26653
67. Fasano A, Mazzoni A, Falotico E. Reaching and Grasping Movements in Parkinson's Disease: A Review. *J Park Dis*. 2022;12(4):1083-1113. doi:10.3233/JPD-213082
68. Avanzino L, Pelosin E, Martino D, Abbruzzese G. Motor Timing Deficits in Sequential Movements in Parkinson Disease Are Related to Action Planning: A Motor Imagery Study. *PLOS ONE*. 2013;8(9):e75454. doi:10.1371/journal.pone.0075454
69. Ruitenbergh MFL, Duthoo W, Santens P, Notebaert W, Abrahamse EL. Sequential movement skill in Parkinson's disease: A state-of-the-art. *Cortex*. 2015;65:102-112. doi:10.1016/j.cortex.2015.01.005
70. Agostino R, Currà A, Giovannelli M, Modugno N, Manfredi M, Berardelli A. Impairment of individual finger movements in Parkinson's disease. *Mov Disord*. 2003;18(5):560-565. doi:10.1002/mds.10313
71. Lee MS, Lyoo CH, Lee MJ, Sim J, Cho H, Choi YH. Impaired finger dexterity in patients with parkinson's disease correlates with discriminative cutaneous sensory dysfunction. *Mov Disord*. 2010;25(15):2531-2535. doi:10.1002/mds.23304
72. Foki T, Pirker W, Geißler A, et al. Finger dexterity deficits in Parkinson's disease and somatosensory cortical dysfunction. *Parkinsonism Relat Disord*.

2015;21(3):259-265. doi:10.1016/j.parkreldis.2014.12.025

73. Vanbellinghen T, Kersten B, Bellion M, et al. Impaired finger dexterity in Parkinson's disease is associated with praxis function. *Brain Cogn.* 2011;77(1):48-52. doi:10.1016/j.bandc.2011.06.003
74. Uzochukwu JC, Stegemöller EL. Repetitive Finger Movement and Dexterity Tasks in People With Parkinson's Disease. *Am J Occup Ther.* 2019;73(3):7303205090p1-7303205090p8. doi:10.5014/ajot.2019.028738
75. Gebhardt A, Vanbellinghen T, Baronti F, Kersten B, Bohlhalter S. Poor dopaminergic response of impaired dexterity in Parkinson's disease: Bradykinesia or limb kinetic apraxia? *Mov Disord.* 2008;23(12):1701-1706. doi:10.1002/mds.22199
76. Fama R, Sullivan EV. Motor Sequencing in Parkinson's Disease: Relationship to Executive Function and Motor Rigidity. *Cortex.* 2002;38(5):753-767. doi:10.1016/S0010-9452(08)70042-X
77. Harrington DL, Haaland KY. Sequencing in Parkinson's Disease: Abnormalities in programming and controlling movement. *Brain.* 1991;114A(1):99-115. doi:10.1093/oxfordjournals.brain.a101870
78. McGregor MM, Nelson AB. Circuit Mechanisms of Parkinson's Disease. *Neuron.* 2019;101(6):1042-1056. doi:10.1016/j.neuron.2019.03.004
79. Singh A. Oscillatory activity in the cortico-basal ganglia-thalamic neural circuits in Parkinson's disease. *Eur J Neurosci.* 2018;48(8):2869-2878. doi:10.1111/ejn.13853
80. Jenkinson N, Brown P. New insights into the relationship between dopamine, beta oscillations and motor function. *Trends Neurosci.* 2011;34(12):611-618. doi:10.1016/j.tins.2011.09.003

81. Engel AK, Fries P. Beta-band oscillations — signalling the status quo? *Curr Opin Neurobiol.* 2010;20(2):156-165. doi:10.1016/j.conb.2010.02.015
82. Johari K, Behroozmand R. Neural correlates of speech and limb motor timing deficits revealed by aberrant beta band desynchronization in Parkinson's disease. *Clin Neurophysiol.* 2021;132(10):2711-2721. doi:10.1016/j.clinph.2021.06.022
83. Kühn AA, Williams D, Kupsch A, et al. Event-related beta desynchronization in human subthalamic nucleus correlates with motor performance. *Brain.* 2004;127(4):735-746. doi:10.1093/brain/awh106
84. Yin Z, Zhu G, Zhao B, et al. Local field potentials in Parkinson's disease: A frequency-based review. *Neurobiol Dis.* 2021;155:105372. doi:10.1016/j.nbd.2021.105372
85. Leblois A, Meissner W, Bioulac B, Gross CE, Hansel D, Boraud T. Late emergence of synchronized oscillatory activity in the pallidum during progressive parkinsonism. *Eur J Neurosci.* 2007;26(6):1701-1713. doi:10.1111/j.1460-9568.2007.05777.x
86. Bocci T, Prenassi M, Arlotti M, et al. Eight-hours conventional versus adaptive deep brain stimulation of the subthalamic nucleus in Parkinson's disease. *Npj Park Dis.* 2021;7(1):1-6. doi:10.1038/s41531-021-00229-z
87. An Q, Yin Z, Ma R, et al. Adaptive deep brain stimulation for Parkinson's disease: looking back at the past decade on motor outcomes. *J Neurol.* 2023;270(3):1371-1387. doi:10.1007/s00415-022-11495-z
88. Evarts EV, Teräväinen H, Calne DB. Reaction time in Parkinson's disease. *Brain J Neurol.* 1981;104(Pt 1):167-186. doi:10.1093/brain/104.1.167
89. Oehrns CR, Cernera S, Hammer LH, et al. Chronic adaptive deep brain stimulation

- versus conventional stimulation in Parkinson's disease: a blinded randomized feasibility trial. *Nat Med*. Published online August 19, 2024:1-12. doi:10.1038/s41591-024-03196-z
90. Lemke SM, Ramanathan DS, Guo L, Won SJ, Ganguly K. Emergent modular neural control drives coordinated motor actions. *Nat Neurosci*. 2019;22(7):1122-1131. doi:10.1038/s41593-019-0407-2
91. Sharpe MH, Cermak SA, Sax DS. Motor planning in Parkinson patients. *Neuropsychologia*. 1983;21(5):455-462. doi:10.1016/0028-3932(83)90002-7
92. Wu T, Hallett M. A functional MRI study of automatic movements in patients with Parkinson's disease. *Brain J Neurol*. 2005;128(Pt 10):2250-2259. doi:10.1093/brain/awh569
93. Caproni S, Muti M, Principi M, et al. Complexity of Motor Sequences and Cortical Reorganization in Parkinson's Disease: A Functional MRI Study. *PLOS ONE*. 2013;8(6):e66834. doi:10.1371/journal.pone.0066834
94. Udupa K, Chen R. Motor Cortical Plasticity in Parkinson's Disease. *Front Neurol*. 2013;4. doi:10.3389/fneur.2013.00128
95. Boon LI, Geraedts VJ, Hillebrand A, et al. A systematic review of MEG-based studies in Parkinson's disease: The motor system and beyond. *Hum Brain Mapp*. 2019;40(9):2827-2848. doi:10.1002/hbm.24562
96. Wu T, Chan P, Hallett M. Effective connectivity of neural networks in automatic movements in Parkinson's disease. *NeuroImage*. 2010;49(3):2581-2587. doi:10.1016/j.neuroimage.2009.10.051
97. Nackaerts E, D'Cruz N, Dijkstra BW, Gilat M, Kramer T, Nieuwboer A. Towards

- understanding neural network signatures of motor skill learning in Parkinson's disease and healthy aging. *Br J Radiol.* 2019;92(1101):20190071. doi:10.1259/bjr.20190071
98. Cristini J, Parwanta Z, De las Heras B, et al. Motor Memory Consolidation Deficits in Parkinson's Disease: A Systematic Review with Meta-Analysis. *J Park Dis.* 2023;13(6):865-892. doi:10.3233/JPD-230038
99. Dan X, King BR, Doyon J, Chan P. Motor Sequence Learning and Consolidation in Unilateral De Novo Patients with Parkinson's Disease. *PloS One.* 2015;10(7):e0134291. doi:10.1371/journal.pone.0134291
100. Ramirez-Zamora A, Ostrem JL. Globus Pallidus Interna or Subthalamic Nucleus Deep Brain Stimulation for Parkinson Disease: A Review. *JAMA Neurol.* 2018;75(3):367-372. doi:10.1001/jamaneurol.2017.4321
101. Eisinger RS, Cernera S, Gittis A, Gunduz A, Okun MS. A review of basal ganglia circuits and physiology: Application to deep brain stimulation. *Parkinsonism Relat Disord.* 2019;59:9-20. doi:10.1016/j.parkreldis.2019.01.009
102. Carbon M, Eidelberg D. Functional imaging of sequence learning in Parkinson's disease. *J Neurol Sci.* 2006;248(1):72-77. doi:10.1016/j.jns.2006.05.005
103. Muehlberg C, Fricke C, Wegscheider M, et al. Motor learning is independent of effects of subthalamic deep brain stimulation on motor execution. *Brain Commun.* 2023;5(2):fcad070. doi:10.1093/braincomms/fcad070
104. Ingram LA, Carroll VK, Butler AA, Brodie MA, Gandevia SC, Lord SR. Quantifying upper limb motor impairment in people with Parkinson's disease: a physiological profiling approach. *PeerJ.* 2021;9:e10735. doi:10.7717/peerj.10735



105. Teixeira NB, Alouche SR. The dual task performance in Parkinson's disease. *Braz J Phys Ther.* 2007;11:127-132. doi:10.1590/S1413-35552007000200007
106. Park JE. Apraxia: Review and Update. *J Clin Neurol.* 2017;13(4):317-324. doi:10.3988/jcn.2017.13.4.317
107. Heilman KM. Chapter 24 - Action programming disorders associated with Parkinson's disease. In: Martin CR, Preedy VR, eds. *Genetics, Neurology, Behavior, and Diet in Parkinson's Disease.* Academic Press; 2020:377-393. doi:10.1016/B978-0-12-815950-7.00024-2
108. Kumari LS, Kouzani AZ. Phase-Dependent Deep Brain Stimulation: A Review. *Brain Sci.* 2021;11(4):414. doi:10.3390/brainsci11040414
109. Khanna P, Totten D, Novik L, Jeffrey Roberts, Morecraft RJ, Ganguly K. Low-frequency stimulation enhances ensemble co-firing and dexterity after stroke. *Cell.* 2021;184(4):912-930.e20. doi:10.1016/j.cell.2021.01.023
110. Ganguly K, Carmena JM. Emergence of a Stable Cortical Map for Neuroprosthetic Control. *PLOS Biol.* 2009;7(7):e1000153. doi:10.1371/journal.pbio.1000153
111. Peters AJ, Chen SX, Komiyama T. Emergence of reproducible spatiotemporal activity during motor learning. *Nature.* 2014;510(7504):263-267. doi:10.1038/nature13235
112. Rostami V, Rost T, Schmitt FJ, Albada SJ van, Riehle A, Nawrot MP. Spiking attractor model of motor cortex explains modulation of neural and behavioral variability by prior target information. Published online March 5, 2024:2020.02.27.968339. doi:10.1101/2020.02.27.968339

113. Guo L, Kondapavulur S, Lemke SM, Won SJ, Ganguly K. Coordinated increase of reliable cortical and striatal ensemble activations during recovery after stroke. *Cell Rep.* 2021;36(2):109370. doi:10.1016/j.celrep.2021.109370
114. Ganguly K, Khanna P, Morecraft RJ, Lin DJ. Modulation of neural co-firing to enhance network transmission and improve motor function after stroke. *Neuron.* 2022;110(15):2363-2385. doi:10.1016/j.neuron.2022.06.024
115. Carrillo-Reid L. Neuronal ensembles in memory processes. *Semin Cell Dev Biol.* 2022;125:136-143. doi:10.1016/j.semcdb.2021.04.004
116. Lu X, Ashe J. Anticipatory activity in primary motor cortex codes memorized movement sequences. *Neuron.* 2005;45(6):967-973. doi:10.1016/j.neuron.2005.01.036
117. Hatsopoulos NG, Paninski L, Donoghue JP. Sequential movement representations based on correlated neuronal activity. *Exp Brain Res.* 2003;149:478-486. doi:10.1007/s00221-003-1385-9
118. Hahn G, Ponce-Alvarez A, Deco G, Aertsen A, Kumar A. Portraits of communication in neuronal networks. *Nat Rev Neurosci.* 2019;20(2):117-127. doi:10.1038/s41583-018-0094-0
119. Mazzoni A, Whittingstall K, Brunel N, Logothetis NK, Panzeri S. Understanding the relationships between spike rate and delta/gamma frequency bands of LFPs and EEGs using a local cortical network model. *NeuroImage.* 2010;52(3):956-972. doi:10.1016/j.neuroimage.2009.12.040
120. Schroeder CE, Lakatos P. Low-frequency neuronal oscillations as instruments of sensory selection. *Trends Neurosci.* 2009;32(1):10.1016/j.tins.2008.09.012.

doi:10.1016/j.tins.2008.09.012

121. Lakatos P, Karmos G, Mehta AD, Ulbert I, Schroeder CE. Entrainment of neuronal oscillations as a mechanism of attentional selection. *Science*. 2008;320(5872):110-113. doi:10.1126/science.1154735
122. Muller L, Chavane F, Reynolds J, Sejnowski TJ. Cortical travelling waves: mechanisms and computational principles. *Nat Rev Neurosci*. 2018;19(5):255-268. doi:10.1038/nrn.2018.20
123. Whittingstall K, Logothetis NK. Frequency-band coupling in surface EEG reflects spiking activity in monkey visual cortex. *Neuron*. 2009;64(2):281-289. doi:10.1016/j.neuron.2009.08.016
124. Hamel-Thibault A, Thénault F, Whittingstall K, Bernier PM. Delta-Band Oscillations in Motor Regions Predict Hand Selection for Reaching. *Cereb Cortex*. 2018;28(2):574-584. doi:10.1093/cercor/bhw392
125. Ferreri F, Vecchio F, Ponzio D, Pasqualetti P, Rossini PM. Time-varying coupling of EEG oscillations predicts excitability fluctuations in the primary motor cortex as reflected by motor evoked potentials amplitude: An EEG-TMS study. *Hum Brain Mapp*. 2014;35(5):1969-1980. doi:10.1002/hbm.22306
126. Brown P. Oscillatory nature of human basal ganglia activity: Relationship to the pathophysiology of Parkinson's disease. *Mov Disord*. 2003;18(4):357-363. doi:10.1002/mds.10358
127. Meissner SN, Krause V, Südmeyer M, Hartmann CJ, Pollok B. Pre-stimulus beta power modulation during motor sequence learning is reduced in 'Parkinson's disease. *NeuroImage Clin*. 2019;24:102057. doi:10.1016/j.nicl.2019.102057

128. Rockhill AP, Mantovani A, Stedelin B, Nerison CS, Raslan AM, Swann NC. Stereo-EEG recordings extend known distributions of canonical movement-related oscillations. *J Neural Eng.* 2023;20(1):016007. doi:10.1088/1741-2552/acae0a
129. Mäki H, Ilmoniemi RJ. EEG oscillations and magnetically evoked motor potentials reflect motor system excitability in overlapping neuronal populations. *Clin Neurophysiol.* 2010;121(4):492-501. doi:10.1016/j.clinph.2009.11.078
130. Schutter DJLG, Hortensius R. Brain oscillations and frequency-dependent modulation of cortical excitability. *Brain Stimulat.* 2011;4(2):97-103. doi:10.1016/j.brs.2010.07.002
131. Berger B, Minarik T, Liuzzi G, Hummel FC, Sauseng P. EEG Oscillatory Phase-Dependent Markers of Corticospinal Excitability in the Resting Brain. *BioMed Res Int.* 2014;2014(1):936096. doi:10.1155/2014/936096
132. Bhatt MB, Bowen S, Rossiter HE, et al. Computational modelling of movement-related beta-oscillatory dynamics in human motor cortex. *NeuroImage.* 2016;133:224-232. doi:10.1016/j.neuroimage.2016.02.078
133. Kaufman MT, Churchland MM, Ryu SI, Shenoy KV. Cortical activity in the null space: permitting preparation without movement. *Nat Neurosci.* 2014;17(3):440-448. doi:10.1038/nn.3643
134. Churchland MM, Shenoy KV. Preparatory activity and the expansive null-space. *Nat Rev Neurosci.* 2024;25(4):213-236. doi:10.1038/s41583-024-00796-z
135. Chang EF. Towards Large-Scale, Human-Based, Mesoscopic Neurotechnologies. *Neuron.* 2015;86(1):68-78. doi:10.1016/j.neuron.2015.03.037
136. Abrahamse E, Ruitenberg M, De Kleine E, Verwey WB. Control of automated

- behavior: insights from the discrete sequence production task. *Front Hum Neurosci.* 2013;7. doi:10.3389/fnhum.2013.00082
137. VanRullen R. How to Evaluate Phase Differences between Trial Groups in Ongoing Electrophysiological Signals. *Front Neurosci.* 2016;10:426. doi:10.3389/fnins.2016.00426
138. Lachaux JP, Rodriguez E, Martinerie J, Varela FJ. Measuring phase synchrony in brain signals. *Hum Brain Mapp.* 1999;8(4):194-208. doi:10.1002/(SICI)1097-0193(1999)8:4<194::AID-HBM4>3.0.CO;2-C
139. Vinck M, van Wingerden M, Womelsdorf T, Fries P, Pennartz CMA. The pairwise phase consistency: A bias-free measure of rhythmic neuronal synchronization. *NeuroImage.* 2010;51(1):112-122. doi:10.1016/j.neuroimage.2010.01.073
140. Nolte G, Ziehe A, Nikulin VV, et al. Robustly Estimating the Flow Direction of Information in Complex Physical Systems. *Phys Rev Lett.* 2008;100(23):234101. doi:10.1103/PhysRevLett.100.234101
141. Taylor JA, Ivry RB. Flexible Cognitive Strategies during Motor Learning. *PLOS Comput Biol.* 2011;7(3):e1001096. doi:10.1371/journal.pcbi.1001096
142. Wulf G. Attentional focus and motor learning: a review of 15 years. *Int Rev Sport Exerc Psychol.* 2013;6(1):77-104. doi:10.1080/1750984X.2012.723728
143. Song JH. The role of attention in motor control and learning. *Curr Opin Psychol.* 2019;29:261-265. doi:10.1016/j.copsyc.2019.08.002
144. Clark D, Ivry RB. Multiple systems for motor skill learning. *Wiley Interdiscip Rev Cogn Sci.* 2010;1(4):461-467. doi:https://doi.org/10.1002/wcs.56
145. Serrien DJ, Ivry RB, Swinnen SP. The missing link between action and cognition.

*Prog Neurobiol.* 2007;82(2):95-107. doi:10.1016/j.pneurobio.2007.02.003

146. Goetz CG, Tilley BC, Shaftman SR, et al. Movement Disorder Society-sponsored revision of the Unified Parkinson's Disease Rating Scale (MDS-UPDRS): Scale presentation and clinimetric testing results. *Mov Disord.* 2008;23(15):2129-2170. doi:10.1002/mds.22340
147. Saleh M, Reimer J, Penn R, Ojakangas CL, Hatsopoulos NG. Fast and Slow Oscillations in Human Primary Motor Cortex Predict Oncoming Behaviorally Relevant Cues. *Neuron.* 2010;65(4):461-471. doi:10.1016/j.neuron.2010.02.001
148. Crone NE, Miglioretti DL, Gordon B, Lesser RP. Functional mapping of human sensorimotor cortex with electrocorticographic spectral analysis. II. Event-related synchronization in the gamma band. *Brain.* 1998;121(12):2301-2315. doi:10.1093/brain/121.12.2301
149. Herrojo Ruiz M, Brücke C, Nikulin VV, Schneider GH, Kühn AA. Beta-band amplitude oscillations in the human internal globus pallidus support the encoding of sequence boundaries during initial sensorimotor sequence learning. *NeuroImage.* 2014;85:779-793. doi:10.1016/j.neuroimage.2013.05.085
150. Herrojo Ruiz M, Rusconi M, Brücke C, Haynes JD, Schönecker T, Kühn AA. Encoding of sequence boundaries in the subthalamic nucleus of patients with Parkinson's disease. *Brain J Neurol.* 2014;137(Pt 10):2715-2730. doi:10.1093/brain/awu191
151. Jenkinson N, Kühn AA, Brown P. Gamma oscillations in the human basal ganglia. *Exp Neurol.* 2013;245:72-76. doi:10.1016/j.expneurol.2012.07.005
152. Muralidharan V, Aron AR. Behavioral Induction of a High Beta State in

- Sensorimotor Cortex Leads to Movement Slowing. *J Cogn Neurosci*. 2021;33(7):1311-1328. doi:10.1162/jocn\_a\_01717
153. Torrecillos F, Tinkhauser G, Fischer P, et al. Modulation of Beta Bursts in the Subthalamic Nucleus Predicts Motor Performance. *J Neurosci*. 2018;38(41):8905-8917. doi:10.1523/JNEUROSCI.1314-18.2018
154. Pascual-Leone A, Valls-Solé J, Brasil-Neto JP, Cohen LG, Hallett M. Akinesia in Parkinson's disease. I. Shortening of simple reaction time with focal, single-pulse transcranial magnetic stimulation. *Neurology*. 1994;44(5):884-884. doi:10.1212/WNL.44.5.884
155. Combrisson E, Perrone-Bertolotti M, Soto JL, et al. From intentions to actions: Neural oscillations encode motor processes through phase, amplitude and phase-amplitude coupling. *NeuroImage*. 2017;147:473-487. doi:10.1016/j.neuroimage.2016.11.042
156. Attaheri A, Choisdealbha ÁN, Di Liberto GM, et al. Delta- and theta-band cortical tracking and phase-amplitude coupling to sung speech by infants. *NeuroImage*. 2022;247:118698. doi:10.1016/j.neuroimage.2021.118698
157. Ramanathan DS, Guo L, Gulati T, et al. Low-frequency cortical activity is a neuromodulatory target that tracks recovery after stroke. *Nat Med*. 2018;24(8):1257-1267. doi:10.1038/s41591-018-0058-y
158. Pal A, Pegwal N, Behari M, Sharma R. High delta and gamma EEG power in resting state characterise dementia in Parkinson's patients. *Biomark Neuropsychiatry*. 2020;3:100027. doi:10.1016/j.bionps.2020.100027
159. Ponsen MM, Stam CJ, Bosboom JLW, Berendse HW, Hillebrand A. A three

- dimensional anatomical view of oscillatory resting-state activity and functional connectivity in Parkinson's disease related dementia: An MEG study using atlas-based beamforming. *NeuroImage Clin.* 2013;2:95-102. doi:10.1016/j.nicl.2012.11.007
160. Rucco R, Lardone A, Liparoti M, et al. Brain Networks and Cognitive Impairment in Parkinson's Disease. *Brain Connect.* 2022;12(5):465-475. doi:10.1089/brain.2020.0985
161. Ray S, Crone NE, Niebur E, Franaszczuk PJ, Hsiao SS. Neural Correlates of High-Gamma Oscillations (60–200 Hz) in Macaque Local Field Potentials and Their Potential Implications in Electrocorticography. *J Neurosci.* 2008;28(45):11526-11536. doi:10.1523/JNEUROSCI.2848-08.2008
162. Rusu SI, Pennartz CMA. Learning, memory and consolidation mechanisms for behavioral control in hierarchically organized cortico-basal ganglia systems. *Hippocampus.* 2020;30(1):73-98. doi:10.1002/hipo.23167
163. Caligiore D, Arbib MA, Miall RC, Baldassarre G. The super-learning hypothesis: Integrating learning processes across cortex, cerebellum and basal ganglia. *Neurosci Biobehav Rev.* 2019;100:19-34. doi:10.1016/j.neubiorev.2019.02.008
164. Simonyan K. Recent advances in understanding the role of the basal ganglia. *F1000Research.* 2019;8:F1000 Faculty Rev-122. doi:10.12688/f1000research.16524.1
165. Klaus A, Silva JA da, Costa RM. What, If, and When to Move: Basal Ganglia Circuits and Self-Paced Action Initiation. *Annu Rev Neurosci.* 2019;42(Volume 42, 2019):459-483. doi:10.1146/annurev-neuro-072116-031033



166. Milardi D, Quartarone A, Bramanti A, et al. The Cortico-Basal Ganglia-Cerebellar Network: Past, Present and Future Perspectives. *Front Syst Neurosci.* 2019;13. doi:10.3389/fnsys.2019.00061
167. Toni I, Rowe J, Stephan KE, Passingham RE. Changes of Cortico-striatal Effective Connectivity during Visuomotor Learning. *Cereb Cortex.* 2002;12(10):1040-1047. doi:10.1093/cercor/12.10.1040
168. Doyon J, Penhune V, Ungerleider LG. Distinct contribution of the cortico-striatal and cortico-cerebellar systems to motor skill learning. *Neuropsychologia.* 2003;41(3):252-262. doi:10.1016/S0028-3932(02)00158-6
169. Sun H, Blakely TM, Darvas F, et al. Sequential activation of premotor, primary somatosensory and primary motor areas in humans during cued finger movements. *Clin Neurophysiol.* 2015;126(11):2150-2161. doi:10.1016/j.clinph.2015.01.005
170. Canavier CC. Phase-resetting as a tool of information transmission. *Curr Opin Neurobiol.* 2015;31:206-213. doi:10.1016/j.conb.2014.12.003
171. Harmony T. The functional significance of delta oscillations in cognitive processing. *Front Integr Neurosci.* 2013;7. doi:10.3389/fnint.2013.00083
172. Voloh B, Womelsdorf T. A Role of Phase-Resetting in Coordinating Large Scale Neural Networks During Attention and Goal-Directed Behavior. *Front Syst Neurosci.* 2016;10. doi:10.3389/fnsys.2016.00018
173. Miyachi S, Hikosaka O, Miyashita K, Kárádi Z, Rand MK. Differential roles of monkey striatum in learning of sequential hand movement. *Exp Brain Res.* 1997;115(1):1-5. doi:10.1007/PL00005669
174. Johansson ME, Toni I, Kessels RPC, Bloem BR, Helmich RC. Clinical severity in

- Parkinson's disease is determined by decline in cortical compensation. *Brain*. 2024;147(3):871-886. doi:10.1093/brain/awad325
175. Burciu RG, Vaillancourt DE. Imaging of Motor Cortex Physiology in Parkinson's Disease. *Mov Disord*. 2018;33(11):1688-1699. doi:10.1002/mds.102
176. Levy R, Ashby P, Hutchison WD, Lang AE, Lozano AM, Dostrovsky JO. Dependence of subthalamic nucleus oscillations on movement and dopamine in Parkinson's disease. *Brain*. 2002;125(6):1196-1209. doi:10.1093/brain/awf128
177. Zhuang P, Hallett M, Meng D, Zhang Y, Li Y. Characteristics of oscillatory activity in the globus pallidus internus in patients with Parkinson's disease (P1.8-028). *Neurology*. 2019;92(15 Supplement). doi:10.1212/WNL.92.15\_supplement.P1.8-028
178. Whalen TC, Willard AM, Rubin JE, Gittis AH. Delta oscillations are a robust biomarker of dopamine depletion severity and motor dysfunction in awake mice. *J Neurophysiol*. 2020;124(2):312-329. doi:10.1152/jn.00158.2020
179. Tosin MHS, Stebbins GT, Comella C, Patterson CG, Hall DA, SPARX Study Group. Does MDS-UPDRS Provide Greater Sensitivity to Mild Disease than UPDRS in De Novo Parkinson's Disease? *Mov Disord Clin Pract*. 2021;8(7):1092-1099. doi:10.1002/mdc3.13329
180. Dann B, Michaels JA, Schaffelhofer S, Scherberger H. Uniting functional network topology and oscillations in the fronto-parietal single unit network of behaving primates. Stephan KE, ed. *eLife*. 2016;5:e15719. doi:10.7554/eLife.15719
181. Wyart V, de Gardelle V, Scholl J, Summerfield C. Rhythmic fluctuations in evidence accumulation during decision making in the human brain. *Neuron*. 2012;76(4):847-858. doi:10.1016/j.neuron.2012.09.015

182. Riddle J, McFerren A, Frohlich F. Causal role of cross-frequency coupling in distinct components of cognitive control. *Prog Neurobiol.* 2021;202:102033. doi:10.1016/j.pneurobio.2021.102033
183. Kleen JK, Testorf ME, Roberts DW, et al. Oscillation Phase Locking and Late ERP Components of Intracranial Hippocampal Recordings Correlate to Patient Performance in a Working Memory Task. *Front Hum Neurosci.* 2016;10. doi:10.3389/fnhum.2016.00287
184. Gaidica M, Hurst A, Cyr C, Leventhal DK. Interactions Between Motor Thalamic Field Potentials and Single-Unit Spiking Are Correlated With Behavior in Rats. *Front Neural Circuits.* 2020;14. doi:10.3389/fncir.2020.00052
185. Fleischer P, Abbasi A, Fealy AW, et al. Emergent Low-Frequency Activity in Cortico-Cerebellar Networks with Motor Skill Learning. *eNeuro.* 2023;10(2). doi:10.1523/ENEURO.0011-23.2023
186. Hall TM, de Carvalho F, Jackson A. A common structure underlies low-frequency cortical dynamics in movement, sleep, and sedation. *Neuron.* 2014;83(5):1185-1199. doi:10.1016/j.neuron.2014.07.022
187. Haberly LB, Shepherd GM. Current-density analysis of summed evoked potentials in opossum prepyriform cortex. *J Neurophysiol.* 1973;36(4):789-802. doi:10.1152/jn.1973.36.4.789
188. Rebert CS. Slow potential correlates of neuronal population responses in the cat's lateral geniculate nucleus. *Electroencephalogr Clin Neurophysiol.* 1973;35(5):511-515. doi:10.1016/0013-4694(73)90027-8
189. Mitzdorf U. Current source-density method and application in cat cerebral cortex:

- investigation of evoked potentials and EEG phenomena. *Physiol Rev.* 1985;65(1):37-100. doi:10.1152/physrev.1985.65.1.37
190. Parker A, Derrington A, Blakemore C, Logothetis NK. The neural basis of the blood–oxygen–level–dependent functional magnetic resonance imaging signal. *Philos Trans R Soc Lond B Biol Sci.* 2002;357(1424):1003-1037. doi:10.1098/rstb.2002.1114
191. Roller ML, Lazaro RT, Byl NN, Umphred DA. Contemporary issues and theories of motor control, motor learning, and neuroplasticity. In: *Umphred's Neurological Rehabilitation.* ; 2013:69-98. doi:10.1016/B978-0-323-07586-2.00013-3
192. Merel J, Botvinick M, Wayne G. Hierarchical motor control in mammals and machines. *Nat Commun.* 2019;10. doi:10.1038/s41467-019-13239-6
193. Proud EL, Morris ME. Skilled Hand Dexterity in Parkinson's Disease: Effects of Adding a Concurrent Task. *Arch Phys Med Rehabil.* 2010;91(5):794-799. doi:10.1016/j.apmr.2010.01.008
194. Rahimpour S, Rajkumar S, Hallett M. The Supplementary Motor Complex in Parkinson's Disease. *J Mov Disord.* 2022;15(1):21-32. doi:10.14802/jmd.21075

## Publishing Agreement

It is the policy of the University to encourage open access and broad distribution of all theses, dissertations, and manuscripts. The Graduate Division will facilitate the distribution of UCSF theses, dissertations, and manuscripts to the UCSF Library for open access and distribution. UCSF will make such theses, dissertations, and manuscripts accessible to the public and will take reasonable steps to preserve these works in perpetuity.

I hereby grant the non-exclusive, perpetual right to The Regents of the University of California to reproduce, publicly display, distribute, preserve, and publish copies of my thesis, dissertation, or manuscript in any form or media, now existing or later derived, including access online for teaching, research, and public service purposes.

DocuSigned by:

*Kara Presbrey*

421DA5F71880487...

Author Signature

11/28/2024

Date